TECHNISCHE UNIVERSITÄT WIEN
Vienna University of Technology

DIPLOMARBEIT

Simulation of Sound Pressure Levels in Urban Canyons

unter der Leitung von

Univ.-Prof. DI Dr. Ardeshir Mahdavi

E 259-3 Abteilung für Bauphysik und Bauökologie

Institut für Architekturwissenschaften

eingereicht an der

Technische Universität Wien

Fakultät für Architektur und Raumplanung

von

Anna Eszter Engedy

01527463

Wien, März 2018

KURZFASSUNG

Probleme im Zusammenhang mit einer erhöhten Lärmbelastung, insbesondere aufgrund des Straßenverkehrs im städtischen Kontext, sind allgemein bekannt. Obwohl theoretisches Wissen über Schallausbreitung und Simulationssoftware für die Raumakustik bereits verfügbar sind, jedoch die akustische Planung von städtischen öffentlichen Räumen und das Potential der Simulation stehen immer noch nicht im Fokus des Interesses. In diesem Zusammenhang konzentriert sich der vorliegende Beitrag auf Straßenschluchten, in den gemessene und simulierte Schallpegeln verglichen wurden. Zu diesem Zweck wurde eine kommerziell erhältliche raumakustische Simulationssoftware eingesetzt, um zwei innerstädtischer Bereiche in der Stadt Wien, Österreich zu modellieren. Dabei wurden geometrische Daten von einer öffentlich zugänglichen Quelle abgerufen und anschließend an die Anforderungen der ausgewählten Anwendung angepasst. Darüber hinaus wurden mehrere Informationsquellen recherchiert, um z.B.: die Schallabsorptions-koeffizienten der relevanten Oberflächen zu spezifizieren. Ebenso wurden Annahmen bezüglich der Schallleistung relevanter Quellen basierend auf geltenden Normen und Beobachtungen vor Ort getroffen. Infolge kann die Abweichung zwischen simulierten und gemessenen Werten als zulässig beurteilt werden. Der Beitrag enthält auch eine Empfindlichkeitsanalyse, die berücksichtigt verschiedene Modellannahmen wie z.B.: Oberflächeneigenschaften, Verkehrsfluss, Position des Mikrofons, und softwarebezogene Einstellungen. Dadurch kann die Kalibrierungsfähigkeit von akustischen Simulationssoftware in Stadtplanungsanwendungen erforscht werden.

ABSTRACT

Problems associated with increased noise exposure – especially due to road traffic in the urban context – are well known. Theoretical knowledge about sound propagation and acoustical simulation software are already available, however, the acoustic planning of outdoor urban areas and the potential of simulation still does not receive sufficient attention. In this context, the present contribution focuses on urban canyons via comparison of measured and simulated sound levels. Toward this end, a commercially available room acoustic simulation tool was deployed to model two inner-city areas in the city of Vienna, Austria. Thereby, geometric data was obtained from an existing repository and subsequently adjusted to fit the input requirements of the selected application. Furthermore, multiple sources of information were consulted to specify material properties such as the absorption coefficients of the relevant surfaces. Likewise, assumptions pertaining to the sound power of pertinent sources were made based on applicable standards and in-situ observations. Thereby, the agreement between simulations and measurements can be qualified as satisfactory. The contribution includes also a sensitivity analysis that takes into account variations in model assumptions, including factors such as surface characteristics, traffic flow, receiver positions, and the simulation tool's settings. Thus, the calibration potential of acoustical simulation tools in urban planning applications can be explored.

Keywords

microscale, urban acoustics, room acoustic simulation, urban canyon, Odeon, traffic noise prediction, CNOSSOS, multiple reflections, surface absorption, scattering, sound pressure level

ACKNOWLEDGEMENTS

First I would like to express my recognition to all colleagues of the Department of Building Physics and Building Ecology for the motivating atmosphere of the Building Science and Technology master program. The obtained knowledge, skills and acquaintances remain a defining experience for the whole life.

My special thanks goes to Prof. Ardeshir Mahdavi, my supervisor, whose expertise, and useful remarks always pointed out the right direction of my thesis.

Also, this work would not have been completed without the generous and tireless support and infinite patience of my co-supervisor, Josef Lechleitner. Also, I am very grateful to Marco Fiedler for his measurements, which form an essential part of my contribution.

Finally, I want to say thanks for my family who provide me a solid background in life, and above all, to my brother whose curiosity and energetic spirit always gives me encouragement.

CONTENTS

1 INTRODUCTION

1.1 Overview

Before the era of motorization, by lower population densities, organically grown city structures, traditional building methods and materials there was no need for specific acoustic planning of open spaces. Due to urbanization processes, however, the density of building stock and population rises and accordingly does traffic noise. Elevated sound levels are listed under environmental stressors together with inadequate temperatures, over-illumination, air pollution and overcrowding. Noise exposure in cities is increasing, which results in a series of health implications both physiological and psychological in nature (WHO-JRC, 2011). Common urban areas belong to “nobody” and their sound environment is not a primary concern neither for architects nor for urban designers, unlike public lighting on streets.

Similarly to thermal and visual comfort simulations, the demand of keeping urban sound environments under control requires a science-based planning approach. Computational modelling has the power to predict sound field scenarios with a sufficient precision according to the applied simulation method (Hornikx, 2016). In case of closed urban canyons typical in city centres room acoustic software – namely Odeon – was already used in practice (Odeon, 2016), and measurements on physical scale model of urban canyon were recorded (Hornikx, 2009). This suggests that the role of computer simulations will gain importance in the fields of urban acoustics in future.

The main scope of this work was to detect the level of impact of the sound source and the field of sound propagation on sound pressure levels (SPLs) with regard to receivers at different heights. As most important factors the flow, the speed and the composition of road traffic were considered. In the meanwhile, the materials of the model surfaces were characterized by their sound absorption and scattering properties. Further tests were pursued on simulation settings, the medium of sound propagation, and receiver positions. In addition, the impact of modelling considerations as the representation of the sky and the cut off surfaces of streets` cross section were explored. On the other hand, a comparative analysis between the simulated SPLs and the on-site measurements provided information about the potential and uncertainties of such room acoustic models.

In order to evaluate the impact of input parameters and the agreement between computer simulation and measurements, two case studies, both of which located in

Vienna, were set up in the room acoustic simulation software Odeon. The workflow included the implementation of the real locations with best possible first approximations on geometry and other input data. The estimation of material properties was based on literature research, while traffic metering was performed on-site. The results of the baseline simulation model were compared with the on-site measurements, and therefore, the validity of the model could be assessed. Thereafter, the baseline model was used to develop scenarios with regard to input parameters such as traffic, surface properties, simulation settings, etc. The level of impact of single input variables on SPLs was analysed in the frequency range of 63 Hz – 8 kHz. The findings give information about the validity of the two room acoustic models and provide a more general knowledge on the impact of input data. Finally, a systematic overview is given about the most important results of this contribution, and potential fields of future research are proposed.

1.2 Motivation

Our cities get noisier due to increased traffic, the change of building stock both in size and applied materials, and the reduction of green areas. With the increase of noise in urban spaces the sound insulation of the building envelope gains more importance. According to the Environmental Noise Directive 2002/49/EC (European Commission, 2002) the completion of noise maps of highly populated areas and surroundings of busy transportation lines is mandatory for member states in each five years. Conflict maps indicate areas with exceeded threshold levels in terms of L_{den} and L_n. Furthermore, urban noise maps form the basis of action plans to reduce SPLs. However, they give an indicative value of the burden from noise at a reference height, and thus, they are not sufficient to evaluate the sound field at different floor levels and frequencies. Nevertheless, reliable information on SPLs in the urban canyon is needed to derive the required minimum level of sound insulation for building components. These values are calculated based on the burden of noise outside and the maximum acceptable SPLs within the protected room. However, the external SPLs from urban noise map simulations or in-situ measurements fail to account for the final sound environment of the location.

Apart from building acoustics, room acoustic design is a growing concern especially in public buildings with big indoor spaces and special needs. At the same time no such attention is given to outdoor spaces with the same scales and similar sound propagation characteristics including closed urban canyons. A better understanding

of the influencing factors of SPLs in open air urban spaces could help to take targeted actions and achieve pleasant sound environments. The benefits of limited SPLs would be most evident for hearing-, and visually impaired people. In the latter case, while having a limited or no eye-sight at all, the audible sensation of the surroundings becomes more important. This is made obvious to the broad public too by thematic exhibitions (e.g. Dialog im Dunkeln in Vienna and Hamburg, and Invisible Exhibition in Prague, Warsaw, Budapest and Stockholm). Furthermore, pleasant acoustic environments and low SPLs in public spaces have multiple benefits on the broad range of the society. It affects the health of people positively, results in lower expenses of the health care system and improved productivity of people. Moreover, enhanced sonic environment in urban areas would allow a more extended use of natural ventilation. It would result in reduced energy consumption and costs both for residential and commercial buildings, especially during the summer season when buildings have high cooling loads. Moreover, while dwellings on higher floors usually benefit from abundant daylight, and sold at a higher price, they may suffer from higher noise levels, as the shading effect of surrounding buildings and vegetation reduces.

Until today no regulation or guideline exists that would keep the acoustic characteristics of urban environments under control, unlike to visual aspects with regard to minimum illuminance levels on streets. The sound emission of road traffic is controlled only to a small extent (e.g. by speed limits) and the acoustic behaviour of buildings both in terms of geometry and materials is ignored.

1.3 Background

1.3.1 Overview

This chapter gives an overview about the theoretical background of the research field of the thesis. It includes chapters about the modelling techniques in virtual acoustics, especially on ray-based methods and the calculation process of the room acoustic software Odeon. The input data of a room acoustic model is also discussed and with regard to Odeon the level of impact of input data was studied in the literature.

1.3.2 Modelling techniques in virtual acoustics

Virtual acoustics became a common tool to assess the acoustic performance of indoor spaces and there is an increasing demand to expand the field of application on outdoor spaces as well. This section gives an overview about the urban propagation effects and urban scales, furthermore, the different modelling techniques of the impulse response simulation.

In the area of urban acoustics micro-, and macroscale levels are defined. The microscale is concerned with sound fields comparable to streets, squares and courtyards. Aspects that play an important role in sound propagation at this level are the height-width ratio, façade irregularities, absorption properties, the rate of openings, roof shapes, materials and in case of distant noise sources even meteorological effects. On the other hand, macroscale level is interested in sound levels of wider areas where aspects of building-, and population density, compactness of buildings, ratio of open spaces, etc. are taken into account. The sources are characterized by their sound power, spectral distribution, and directivity pattern (Hornikx, 2016).

The sound propagation from source to receiver is a function of space geometry, applied boundary materials and characteristics of the medium. The sound energy is carried by pressure difference in the air as longitudinal wave, and surface reflections modify its path. In real sound fields each reflection has both a specular and a diffuse part. The sound that reaches the receiver consists of three components depending of their time of arrival: direct sound, early reflections and late reverberation (Savioja, 1999). The earliest, the *direct* part reaches the listener due to straight-line sound propagation from the source without any obstacles or disturbance. The *early reflections* are those that develop in the first 80-100 ms due to early surface reflections when the sound still carries a high level of energy. Therefore, they appear as distinct

strengthenings in the impulse response length measurements. In the meanwhile, due to the diffusely reflected part the diffuse component of the sound field is increasing with time. The part above the 2 s is the *late reverberation* when the sound field is already considered as diffuse (Savioja, 1999). The impulse response of a concert hall is shown in Figure 1 indicating the early and late reflection phases.

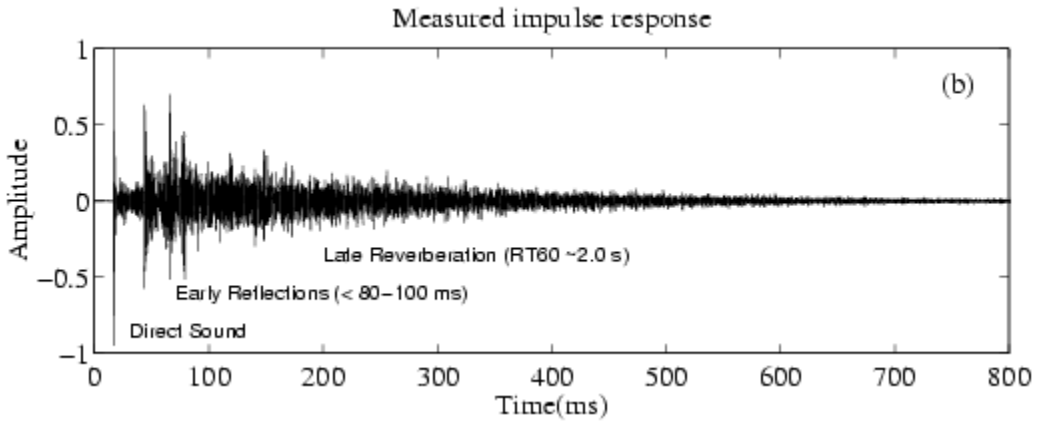

Figure 1 Imitated room impulse response of a concert hall. Direct sound, early reflections and late reverberation. (source: (Savioja, et al., 1999))

Sound propagation is described by the Helmholtz equation, however, it cannot be solved in analytic form (Savioja, 1999). There are different types of calculation methods in virtual acoustics to gain an impulse response, those of *wave-based methods, ray-based methods, diffuse field method,* and *statistical models* (Hornikx, 2016 and Savioja, 1999).

The *wave-based* methods are either finite element methods (FEM), boundary element methods (BEM) or finite-difference time-domain (FDTD) methods that solve the wave equations and therefore require a high computational load (Savioja, 1999), especially at high frequencies (Hornikx, 2016). On the other hand, wave-based methods include all wave propagation phenomena implicitly that makes them applicable at small scales at a high precision (Hornikx, 2016). Therefore, in the future they will gain importance at the simulation of inner city environments such as urban streets, squares and inner courtyards.

The *diffuse field methods* consider the sound energy propagating through a volumetric grid. The calculation cost is lower than that of ray-based methods and it is applicable if the sound space is diffuse, which mostly occurs in indoor spaces and inner city scenarios (Hornikx, 2016).

The *statistical methods* are based on the statistical analysis of sound energy (SEA). They are used for predicting the transmission of sound and vibration, however, they do not consider the time aspect of the sound field (Savioja, 1999).

1.3.3 Ray-based methods

Primarily, *ray-based methods* were developed and used until today for noise mapping purposes covering larger areas, and the room acoustics software Odeon is based on this principle too. Ray-based methods provide a good accuracy at a low computational cost (Hornikx, 2016). Also referenced as geometrical acoustics or engineering method, the sound wave is replaced by the propagation direction of the wavefront and considered as a ray that interacts with the boundary surfaces (Hornikx, 2016). The sound ray is determined by its *directivity*, its *wavelength* (i.e. frequency that stands for the pitch of the sound) and the *amplitude* of the sound wave (i.e. the degree of change in atmospheric pressure that is responsible for the perceived loudness).

The ray-based approach is applicable if the wavelength of the sound is smaller than the size of boundary surfaces, but larger than the roughness of them (Savioja, 1999). The wavelengths of interest in room acoustics fall between 63 Hz and 8000 Hz corresponding to ca. 5.5 m and 4 cm respectively. The typical surface sizes are above these values and even the roughness of the coarsest surface does not exceed 4 cm. Thus, the criteria for the application of ray-based methods are met, especially at higher frequencies, for instance 500 Hz that corresponds to 68 cm.

Geometrical acoustics handles the ray–surface interactions in an explicit way (Hornikx, 2016). Interaction between the sound wave and the boundary surfaces are: reflection, diffraction and scattering. *Reflection* is the redirection of the sound wave, while *diffraction* stands for the disturbance and the spatial redistribution of the sound wave due to an obstacle (e.g. surface edge). Finally, by *scattering* is meant the modification of wave propagation due to obstacles or fluctuations of the medium if the wavelength is of the same order as the size of the obstacle.

Below the two ray-based methods applied in Odeon are presented.

Image-source method

In the image-source method the sound source is mirrored to the surface and hereinafter the resulting image source represents the reflection path. By mirroring the image source to further surfaces, higher order image sources are discovered. The

direct path starting from the image source is identical to the reflected path from the original source. If the path between the listener and the image source is without obstacles then the image source is visible from that listener, however, it may be invisible from another listener position. The image source tree (i.e. the sequence of image sources by reflection orders) is independent from the listener(s) position. The image source tree is also independent from the number and directivity of the rays emitted from the source, alone the position of the source and the room surfaces that matter. Therefore, the same image tree can be used by different directivity patterns of the same sound source. The principle of image source method is shown in Figure 2.

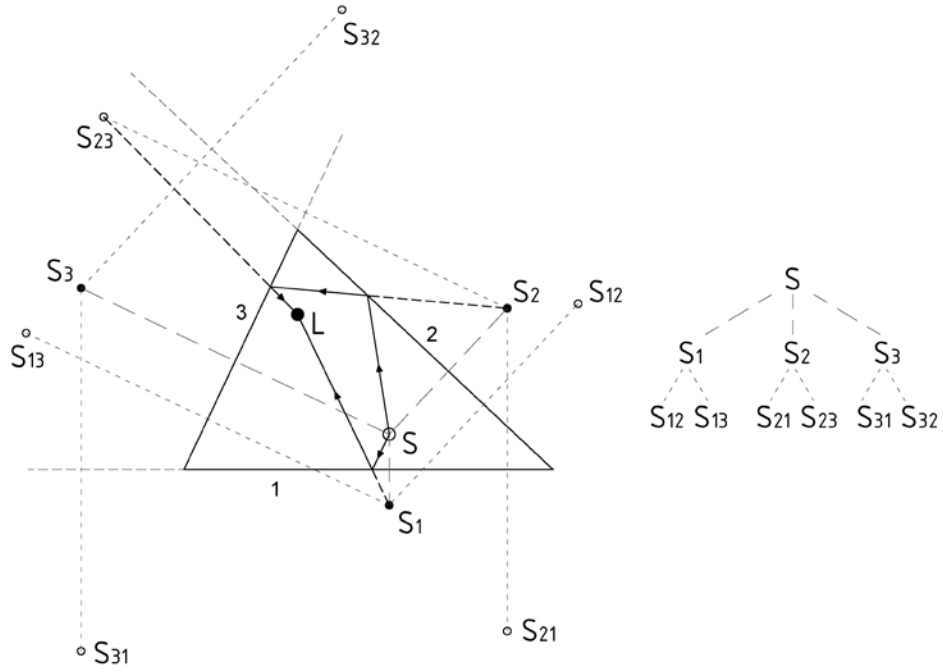

Figure 2 Image source method and image source tree

The number of image sources increases exponentially by the increase of reflection order. The number of new image sources at the i^{th} reflection order is calculated according to Equation 1.

$$N = n(n-1)^{i-1} \qquad 1$$

Where

N number of new image sources at the ith reflection order,

n number of boundary surfaces of the room, and

i reflection order.

The computational cost of this method depends of the number of room surfaces and the reflection order. Although this method tracks down reflection paths accurately, finding higher order reflections is computationally very expensive. Therefore, this method is used only in case of early reflections, which carry high amounts of sound energy (Savioja, 1999).

Ray-tracing method

In ray-tracing method the rays emitted from the source are followed one by one. The rays are reflected at the room surfaces either by following the rule of specular reflection or by taking into consideration the scattering phenomenon too. The scattering effects are handled according to Lambert distribution in Odeon. Sources assumed to distribute rays over a sphere uniformly, or according to a predefined pattern.

The computational cost of this method depends of the *number of rays* emitted from source, the *algorithm of reflection* applied and the *order of reflections* considered. On the other hand, the calculation cost is independent from the number of room surfaces and the position of the source and listener as the actual path of rays is followed.

Although the calculation cost of ray-tracing method also increases by the reflection order, the rate of increase is linear and not exponential like in case of image-source method. Therefore, it is used to account for late reflections in room acoustic models. The drawback of the method is that not all rays that are randomly emitted and followed have a contribution to the sound field at the receiver's position, only those that are close. The principle of the ray-tracing method is shown in Figure 3.

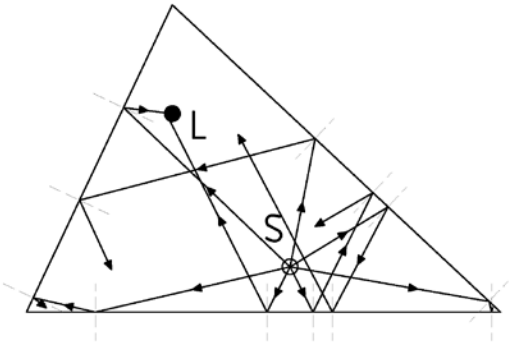

Figure 3 Ray–tracing method

Both image-source and ray-tracing method have their advantages and disadvantages, and therefore hybrid methods were developed to exploit the potential of both of them. In order to account for accurate ray paths in the early reflection phase the image-source method is more favourable, while ray-tracing is more practical for the late part of the calculation (Savioja, 1999).

1.3.4 Calculation process of Odeon

The calculation process of Odeon 11.0 consists of three steps. The software uses *ray-tracing* for the mapping of the room geometry, *image-source* method for the generation of early reflections and so-called *secondary source* method for the generation of late reflections. The transition criterion between the generation of early and late reflections is the reflection order and named as transition order. Although within the framework of this work only line sources are used, to which the transition order is automatically set to 0, all steps of the calculation process are explained below. All methods are based on energy variables and no filtering is used in the process.

First stage: Ray tracing

Ray tracing is used to explore the geometry of the room. Two assumptions are made in this phase. Namely, that *surfaces are plane,* and *reflections are specular until the transition criterion holds.* The transition criterion is the reflection order in Odeon, but the limit could be path length or that the ray hits a diffuser. After the transition criterion fails, the reflections are no more specular, but their directionality and distribution is based on the diffusion coefficient of the surface and probabilistic methods. The

diffusion coefficient informs about how uniformly the reflected energy is distributed for a given angle of incidence. The ray path is dependent of *room geometry*, *diffusion coefficients*, and *source position*, and therefore, the same ray tracing history can be used for different *receiver positions*, *absorption scenarios* and *source directivity patterns*. The files containing the ray tracing history can be very large.

Second stage: Early reflections – image source method

Every time a ray is reflected, an image source is generated, which is potential source of early reflection. However, this image source contributes to the response at the receiver position only if it is visible from the receiver, therefore, this criterion must be checked for all image sources generated. If this criterion holds then the image source becomes the part of the image tree. One valid image source is counted only once. The reflections follow the rules of geometrical acoustics. That means the rays are reflected specularly and the intensity of the reflected ray equals to the product of the source intensity in the given direction and the reflection coefficient of the wall. The time of arrival of an early reflection is derived from the path length of the sound ray.

Third stage: Late reflections – secondary source method

In Odeon 1.0 version the method used for finding sources of late reflections also followed the rules of image source method, however, these late sources were treated differently. As a transition criterion the time limit was used, and therefore image sources above a certain distance from the source took part in the generation of late reflections. However, the applicability of this method was limited with regard to the reliability of responses, and therefore, only convex rooms with well mixing geometries and without coupled spaces could be simulated.

Up from Odeon 2.0 the *secondary source* method is applied to model the sources of late reflections. As transition criterion the reflection order is used, that means, above a pre-defined reflection order late reflections are generated.

Overall, the room response has three phases along the time. In the first part only early reflections are present, while in the second phase – in the transition zone – the late reflections start to appear and gradually overtake the early reflections in number. In the final phase the space is dominated by late reflections.

At each reflection above the transition order a secondary source is generated that radiates the energy into the space distributed by a hemisphere. According to a

radiosity model at each secondary source a high number of rays would be emitted, and each of them would create new secondary sources. However, the number of secondary sources would increase exponentially and therefore the computational cost would be enormous. In contrast, the reflection from secondary sources is simulated as a single ray according to *Lambert*, *Lambert oblique* or *uniform* directivity, and has the potential to generate further secondary sources.

As a consequence, the number of rays does not increase, nor the reflection density unlike to reality. The average density of late reflections follows the rate of potential image source generation according to Equation 2.

$$I_m = \frac{cN}{\bar{l}} \qquad 2$$

Where

I_m rate of potential image generation,

c speed of sound,

N number of rays emitted from the source, and

$\bar{l}$ mean free path.

The energy from the j[th] order secondary source radiated into the room is calculated by the Equation 3 (Naylor, 1992).

$$E_j = \frac{E_s}{N}\prod_{i=1}^{j}(1-\alpha_i) \qquad 3$$

Where

E_j energy of the j[th] order secondary source radiated into a hemisphere,

E_s energy of the source,

N number of rays emitted from the source,

α_i absorption coefficient of the i[th] surface, and

$(1-\alpha_i)$ reflectivity of the i[th] surface.

The time of arrival of late reflection is determined by the path length. It consists of the section from primary source to the secondary source, during which reflections occur, and the distance between secondary source and receiver. The intensity at a receiver from a secondary source is calculated according to Equation 4 (Naylor, 1992), and it is shown in Figure 4. Air absorption according to the path length is also taken into account.

$$I = \frac{P}{N}\prod_{i=1}^{n}(1-\alpha_i)\,\frac{2cos\,\theta}{2\pi r^2} \qquad 4$$

Where

P intensity of the primary source in the relevant direction,

N number of rays emitted from the primary source,

θ angle between the surface normal and the vector from the secondary source to the receiver,

$2\pi r^2$ surface area of a hemisphere,

α_i absorption coefficient of the i[th] surface, and

$(1-\alpha_i)$ reflectivity of the i[th] surface.

(2- in the nominator – normalization)

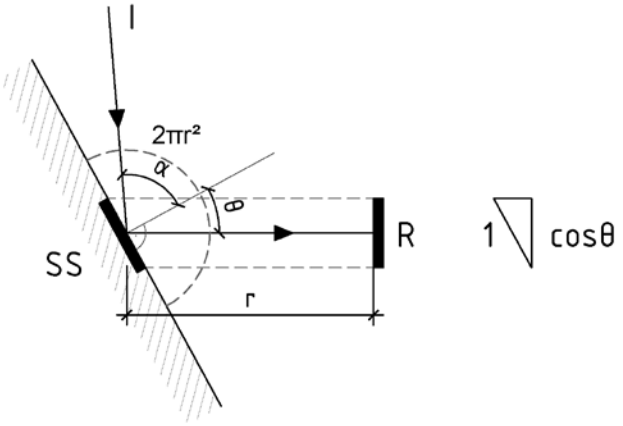

Figure 4 Intensity at a receiver from a secondary source according to Equation 4.

Odeon combines the image source method and the secondary source method that are together often referenced as a *hybrid method*. The re-radiation of the energy from the secondary source is not specular but has a directivity characteristic and this mixing of the rays models the diffuse transport of energy. As a result, the calculation process is not sensitive to the room geometry unlike to Odeon 1.0.

Figure 5 shows the transition between the early and late reflections. Until the transition order of two is not exceeded the reflections are specular, and by each hit of a surface an image source is generated (e.g. S1).

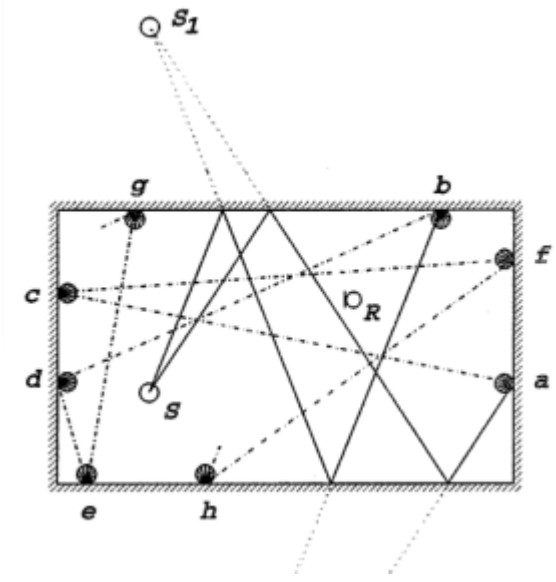

Figure 5 Paths of early and late reflections at transition order set to 2 (source: User Manual Odeon 11.0)

Above the transition order, however, secondary sources are created, from which the reflections are no longer specular, but calculated according to the *reflection based scattering* method.

The reflection based scattering method takes into account scattering from *geometrical properties* (i.e. surface size, edge diffraction, angle of incidence and path length). Therefore, if it is activated under the Room Setup settings in Odeon then the surface scattering coefficients should exceptionally refer to scattering due to surface roughness. However, if scattering due to geometrical properties is included in the material based scattering coefficients, this option should be avoided. The angle of incidence and the path length are unknown until the source and receiver are defined. Both the scattering due to surface roughness and edge diffraction is a function of frequency as explained in more detail under the chapters *Scattering* and *Diffraction.*

The reflection based scattering coefficient s_r that is used by Odeon 11.0 is calculated according to Equation 5.

$$s_r = 1 - (1 - s_d)(1 - s_s) \qquad 5$$

Where

s_d	scattering coefficient due to diffraction,
s_s	scattering coefficient due to surface quality, and
$(1 - s_d)(1 - s_s)$	specularly reflected part.

At any *s* value of scattering coefficient the method results in a single reflected ray, which is the geometrical average of the specular and the scattered rays. The directivity of the specularly reflected ray follows Snell's law (i.e. the angle of incident and reflected rays are equal) and its magnitude corresponds to the non-scattered part of the incident intensity *I*, namely *I(1-s),* if the surface absorptance is taken to zero. The direction of the scattered ray is randomly chosen by Lambert distribution, and its size is proportional to *s*. If *s* = 0 then the reflection is specular, while in case of *s* = 1 the total incident sound energy is reflected into a random direction. The procedure is shown in Figure 6 below.

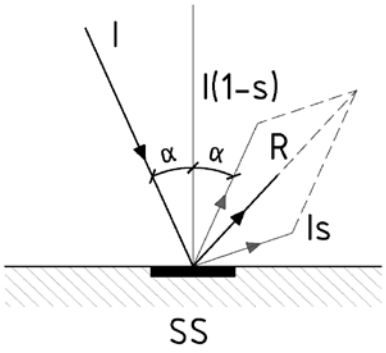

Figure 6 Reflection based scattering method – I incident ray, R – reflected ray, s – reflection based scattering coefficient (adapted, based on: User Manual Odeon 11.0 (Christensen, 2011))

The advantage of the secondary source method is that without the increase of reflection density a large number of secondary sources are generated, and therefore, the required level of reflections at the receiver can be achieved. This enables a low calculation time and a high level of reliability even for complex room geometries.

On the other hand, the disadvantage of the secondary source model is that even reflection directions that have low probability according to the Lambert distribution may appear and transfer unrealistic energy contributions to the receiver, causing local jumps in the decay curves.

The process described above with regard to the generation of early and late reflections, however, stands only for point sources in Odeon. In case of line and surface sources the image source method of the early reflections is left behind, and solely the secondary source method is used. As a consequence, transition order is always zero, and therefore, this approach complies rather with a ray-tracing process.

1.3.5 Impact analysis of input data and calculation parameters

In a room acoustics model the room geometry and the frequency dependent absorption coefficients are the two main input data to characterize the room. On the other hand, the results may depend of the calculation parameters to a great extent. Naylor and Rindel (1992) have investigated the level of impact of the room data and settings in Odeon 2.0. The indices of their analysis were the level of difference between measured and simulated values with regard to results and simulation time. It was found, if the *absorption coefficients* of large surfaces are well estimated then

neither small variations in these values nor the absorption of small surfaces have notable effect on indices.

With regard to *geometry*, a higher number of surfaces contribute to increasing simulation time during the image-source method used in the early reflections phase. Therefore, too many small surfaces should be avoided and simplifications to the original geometry data may be necessary.

Concerning the calculation parameters the *number of rays* and the *transition order from early to late reflections* were investigated. The number of rays should be at least 25-100 times higher than those of surfaces, nevertheless, the results are not affected remarkably. The impact of *transition order* on end result depends from the geometry to a great extent. Image sources from multiple small surfaces increase the simulation time unnecessarily, because only a small amount of energy is reflected from their combination. Therefore transition order should be kept low if the geometry is more complex and favourably not exceed two. Nonetheless, in case of line sources the value of zero is assigned by the software, and thus, no image-source method is used in the calculation.

Measured and calculated indices may differ due to uncertainties on both sides. The difference between measured values of the same scenario can be the result of the lack of *reproducibility* of the sound sources and listeners, but it may change also due to different *measurement systems*. In comparison with the simulated results a variation in the simulated indices can occur from the imprecise *positioning* of the sources and the receiver, the *simplification of the geometry* and the *properties of surfaces* close to the sources and receivers. Furthermore, the energy based *calculation method* of the simulation tool simplifies the real wave phenomenon (i.e. propagation of pressure difference in the air) and thus, excludes phenomenon as the interference of sound waves that causes strengthenings and attenuations.

Naylor and Rindel (1992) compared measured and simulated room acoustic indices of the Royal Festival Hall in London using Odeon 2.0. They reported that the worst error between measured and simulated sound pressure levels using 5000 rays and considering the results at 1000 Hz was within the range of 1.5 dB for all source – receiver combinations. The applied transition order of one is justified by the small number of large surfaces that alone give image-sources of great importance. The findings have also shown that the increase of transition order resulted in a smaller agreement between measured and simulated data. The general conclusion was that the less big specularly reflecting surfaces are present in the room, the faster (i.e. at a low number of reflections) the space becomes diffuse field, and therefore a smaller

transition order is appropriate. The experiment has also shown that already a relatively low number of rays and transition order returns values close to the measured ones, and therefore a sufficiently precise result is available at a low computational cost. However, it was also shown that the ideal parameter settings to obtain the best fitting values to those of measured values may vary by indices.

The further sections give an overview about the theoretical background of the specific room acoustic input data. Basic theoretical knowledge, software related information as well as findings of recent researches both in terms of methodology and numeric data are presented. Input datasets used in the simulation are presented under *Method / Room acoustic simulation* chapter.

1.3.6 Geometry

Generally, the three-dimensional data for room acoustics simulation is derived from other applications such as architectural models or GIS databases. However, these models are not always ideal as they may include too much or too little details. A model with a high level of details might require excessive simulation times. On the contrary, a coarse model may fail to account for important details, and therefore, return false results. The ideal level of details depends from the field of application. Although classic room acoustics simulation tasks need a rather high level of detail to account for reliable results, the same scale is not practical for urban acoustics, because simulation time would increase unnecessarily. In order to achieve the ideal geometry (i.e. a model that returns reliable outputs at a low simulation cost) simplifications, detailing or maybe both are needed. This chapter focuses on simplification methods in line with the needs of this work and gives an overview about geometry reduction algorithms (Siltanen, et al., 2008).

The reduction methods can be divided into *decimation* and *surface reconstruction* algorithms. The decimation algorithms are those of *vertex removal*, *vertex clustering*, *edge collapsing*, and *face removal*. While these methods have a local effect on the geometry, surface reconstruction algorithms affect the model globally and based on *re-meshing* or *volumetric approaches*.

Decimation algorithms operate with element removal that reduces the level of detail. However, at the same time the surroundings are affected and the computational cost of the modification can be high. The simplification process includes which type of element to remove, a criterion for when to remove the chosen element, and finally,

how to modify the surroundings. The algorithm is based on ranking and selection of the elements by error-value calculation. For instance, in case of *vertex removal* the error-value is a function of the distance from the surrounding polygons. With the elimination of the vertex the connecting faces also disappear, and the remaining hole has to be filled by triangulation procedure. This method has the benefit of representing details by less vertices, however, the labour-intensive triangulation step makes its use less practical for models with large flat surfaces.

The *vertex clustering* algorithm has a high potential of simplifying parts of the model that consist of many small surfaces (i.e. areas with a high density of vertices) by merging more vertices into one, and therefore, eliminate many small details close to each other. The process includes the sorting of vertices according to a grading criterion that is based on the density of vertices. Afterwards, a grid of clustering volumes are placed on the triangulated model, and vertices in the same box are replaced by their representative. The algorithm can cause the degeneration of triangles into edges or vertices.

Edge collapsing merges the end points of an edge into one, and thus, the triangles on its both sides degenerate into a line. The edge might be collapsed into one of this end points, the centre point, or else. The position of the new vertex is determined by a geometric criterion. By this one step the number of edges, triangles and vertices falls by 3, 2 and 1 respectively. There is no need of further triangulation, and therefore, this method handles even large scale models at a low calculation cost.

The algorithm of *face removal* can be described as a series of edge collapsing. In the method the selected triangle is eliminated and replaced by a new vertex. Consequently, its neighbouring triangles are removed too, and the resulting loop around the hole is triangulated by the new vertex. It is most useful in areas where polygons are almost in the same plane and if the model needs be reduced to a certain number of polygons.

Unlike decimation approaches, that try to reduce the complexity of the model by taking away elements one by one, the surface reconstruction methods deal with the entire model and aim to approximate an ideal surface. It is most useful, if there is a desired number of polygons as an end result, similarly to face removal.

In case of the *re-meshing* method the entire model is reconstructed as a higher detail model and a simplified one is derived from this. The advantage of the algorithm is the preservation of the topology at the reduction of polygons and vertices. It is optimal if a certain type of mesh is needed, however, at a high calculation cost.

Another instance of reconstruction methods is the *volumetric approach* that represents the mesh as volume elements and a new surface is created from this. Drastic simplifications and elimination of insignificant details are possible in this way.

Although the above presented methods are developed for computational purposes, this overview gives an impression about the workload and the outcomes of the algorithms. Therefore, the principles of the most practical ones can be utilized during the manual processing of the geometry.

1.3.7 Absorption

When building a digital room model for an existing room, the matching of the simulated model based on the measured room acoustic parameters (i.e. validation of the model) is necessary. The on-site measurement is regarded as a settled tool for evaluating a room, on the other hand, simulation results are very sensitive to input data. Data on surface materials is usually unknown, and therefore assumptions are made. In this section the focus is given to the acquisition of absorption coefficients of a room model. This approach, however, implicitly considers that the simulation of sound propagation is accurate and input data on the sound sources and receivers is precise.

Obtaining absorption data by classical methods includes *reverberation chamber* measurements that provide data for diffuse field scenarios, or *impedance tube* measurements that consider only normal incidence. These are standardized measurements carried out under controlled conditions according to ISO 354:2003 (ISO, 2003) and ISO-10534:1998 (ISO, 1998). In order to obtain reliable input data measurements should be performed on material samples from on-site, however, this is not realistic in most cases. Therefore, on-site methods were developed, for instance *PU-probe* that measures the local impedance using a pressure and velocity sensor. Further sources of input data may be *databases* of manufacturers or pre-set *material libraries* of the room acoustic software like Odeon and Raven. Recently also *inverse calculation* models gained importance with regard to the derivation of absorption data. This method replaces the manual calibration of absorption coefficients that is time consuming and doubtful whether a reasonable match can be achieved (Aspöck, et al., 2016). Absorption material data from different sources – measurements and databases – were compared with special interest to their impact on the simulation results (Aspöck, et al., 2016). Absorption coefficients of the same porous material resulting from different measuring methods, i.e. impedance tube method, in-situ PU-probe and dataset from manufacturer based on reverberation chamber measurement

were compared. The results have shown significant deviations in all frequency ranges and differences of 0.2 - 0.3 were observed without any trend.

In a further experiment three databases – one of which based on in-situ PU-probe measurement and another two that were obtained from software databases – were applied in room acoustic simulations. The deviance of room acoustic indicators from the measured values was investigated. It was found that the relative deviation exceed the level of JND (just noticeable difference to human ear) to a great extent. In case of T30 reverberation time the difference accounted to 10-80% to which the JND is determined as 5% in ISO 3382 standard. Using input data retrieved from inverse techniques resulted in better agreement between measured and simulated indices. The test has also shown that the degree of agreement is dependent of the index looked at. While the agreement of T30 [s] reverberation time was very poor, the C80 [dB] clarity index was acceptable (Aspöck, et al., 2016).

Odeon 13 introduced an inverse calculation model called Material Optimization Tool. The tool is based on a genetic algorithm (GA) that handles multi-variable problems with success. A short description of the method is given below.

In the evaluation process for each of the 8 octave bands an independent GA is run. The absorption coefficients correspond to the genes of an individual. For all materials 4 individuals are set. The individuals of the same evolutional stage form a generation. To each material for each frequency an initial value and a search range is set. The simulated room acoustic parameters are compared to the measured ones by a fitness function. This function returns a value that characterizes the difference between the simulated and the measured room acoustic parameters, meaning a smaller value stands for better agreement. After the normalization of the specific parameters to their JND levels various parameters can be combined into one fitness value. Values retrieved and averaged from a number of source – receiver combinations make them more reliable. The individuals are ranked according to their fitness values. A so called *elitist* selection process chooses the highest ranking individuals as parents of the next generation. Through genetic operators as crossover, inversion, mutation the next generation is created, and the GA starts from the beginning. The calibration process stops when the convergence criterion of the fitness value is met. The GA method was applied with success on a real lecture hall example, and the fitness of calibrated materials was improved to a great extent compared to original data sets. With the exception of low frequencies the errors of the best fitting results stayed below 1 JND. However, in case of a lecture hall size model with 11 different types of materials, 8 new generations, using 2000 rays and considering 10 source – receiver positions the

calculation time was ca. 30 minutes even with a rather strong processor (Intel CoreTM i7 CPU, 3.4 GHz, 4 cores) (Christensen, et al., 2014).

The acquisition of absorption data for urban scenarios faces the problem that some surface types are not available in the material libraries as they are not typical for interiors. Especially, surfaces with a high percentage of the total surface area or close to the sound source or receiver are in the focus of interest. For instance, ground surfaces in the vicinity of sound sources play an important role in the generation of early reflections. Some theoretical considerations may help in certain cases. In case of the sky the absorption coefficient can be set to 1 because it is similar to an open window in interior room acoustic model where no rays are bounced back from such a surface. This method was already applied in Odeon simulation of an atrium (Odeon, 2016) and in later versions a sky box placement is facilitated by a built-in function of the software.

The acoustic properties of different asphalt mixtures were studied widely in recent years due to the emerging need of urban noise mitigation. The topic of acoustical parameters of road surfaces and noise generation from the tire-pavement contact is strongly interrelated and usually investigated hand in hand. These experiments (Knabben et al. 2016, Raimundo et al. 2010 and Paje et al. 2008) give information on the characteristics of different asphalt mixtures with regard to their noise reduction potential. Concentrating solely to the absorption properties of the samples is not sufficient, because a mixture with a good noise absorption may also generate higher sound pressure levels due to its texture, and therefore, emits an overall higher level of close proximity noise (Paje et al. 2008). The core samples were either produced for the experiment with pre-determined characteristics (Raimundo et al. 2010), or cut out from actual street pavements (Paje et al. 2008). The measurements were carried out in impedance tube according to standard ISO 10534-2, which gives information about the normal incidence sound absorption. The impact of different material properties on sound absorption coefficient were studied according to granulometry (distribution of aggregate size), maximum aggregate size, composition and amount of binder, void volume (porosity), interconnected void volume and thickness of coating layer. According to the type of the granulometry of the aggregate the three main categories together with the porous mixture are listed in Table 1, and the difference in the surface pattern is indicated in Figure 7 and Figure 8.

Table 1 Type of asphalt mixtures and propertie (source: (Knabben et al. 2016, Raimundo et al. 2010, Paje et al. 2008))

Mixture	Granulometry	Binder content	Void volume	Interconnected void volume
Common dense graded	even distribution	normal	2-6 %	-
Gap graded (SMA – stone matrix asphalt)	no middle size aggregates stone to stone skeleton	higher than normal	6-12%, 5%/18%	-
Open-graded	no or little percentage of small and middle size aggregates	higher than normal	ca. 20-22%	ca. 15%
Porous	as gap graded	as gap graded	ca. 22-28%	ca. 21-28%

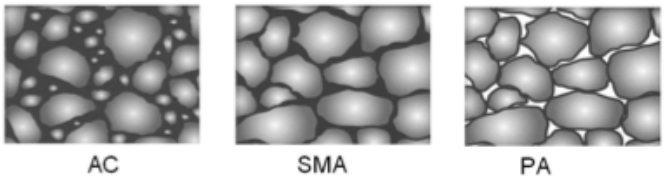

Figure 7 Structure of mixtures with different granulometry, AC (asphaltic concrete) – common dense graded, SMA (stone matrix asphalt) – gap graded, PA (porous asphalt) (source: http://www.eapa.org)

a) *b)* *c)*

Figure 8 a) dense graded b) gap graded SMA c) OGFC (open graded friction course) (source: http://hawaiiasphalt.org)

The findings have shown that a higher void and interconnected void volume content correspond with a higher peak value of absorption coefficient, while the frequency of the peak is inversely proportional to the thickness of the specimen, as shown in Figure 9.

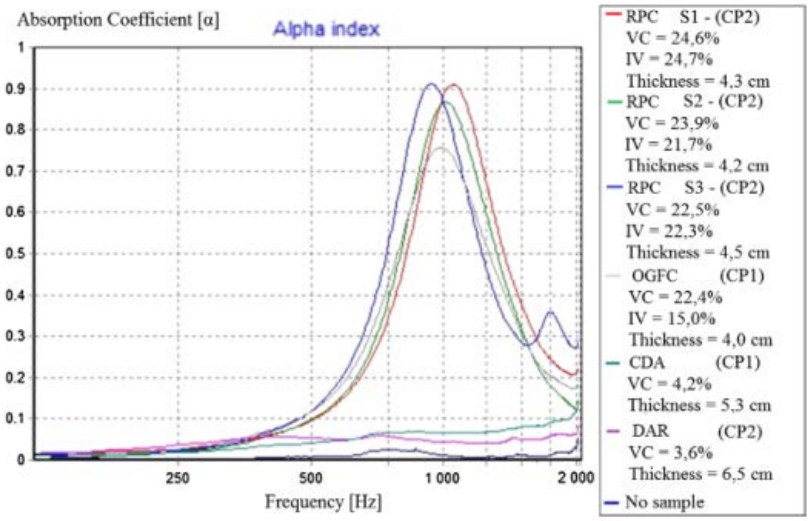

Figure 9 Absorption coefficients of different types of mixtures with various void content (VC): RPC – rubberized porous coat, CDA – common dense-graded asphalt, DAR - Dense-graded rubberized asphalt (source: (Knabben et al. 2016))

A peak in the frequency related absorption coefficients, however, was only detected when the surface was rather porous and not for common dense graded asphalt as shown in Figure 10 and Figure 11.

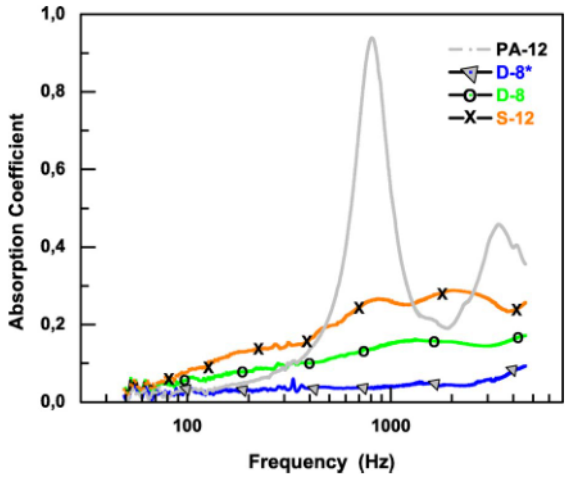

Figure 10 Absorption coefficients determined from impedance tube measurement on specimens retrieved from street pavements: D-8 new dense graded, D-8 old dense graded, S-12 10 month old semi dense graded, PA-12 porous surface (source: (Paje, et al., 2008))*

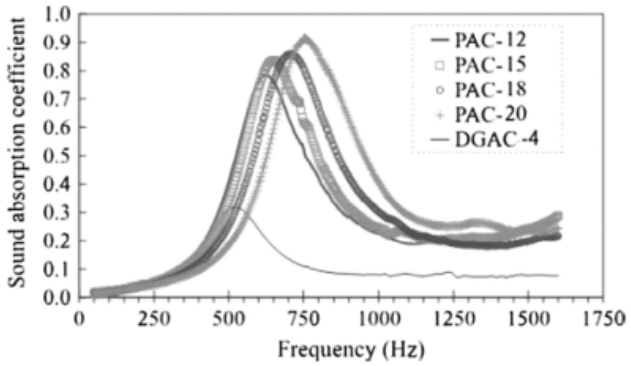

Figure 11 Absorption coefficients with regard to void content: PAC – porous samples and DGAC – dense graded sample (source: (Mun, 2010))

Further research was done on the acoustic performance of wet asphalt (Raimundo, et al., 2010). After a saturation process cores of 30 mm and 80 mm thickness with low porosity have shown the results according to Figure 12 and Figure 13 respectively.

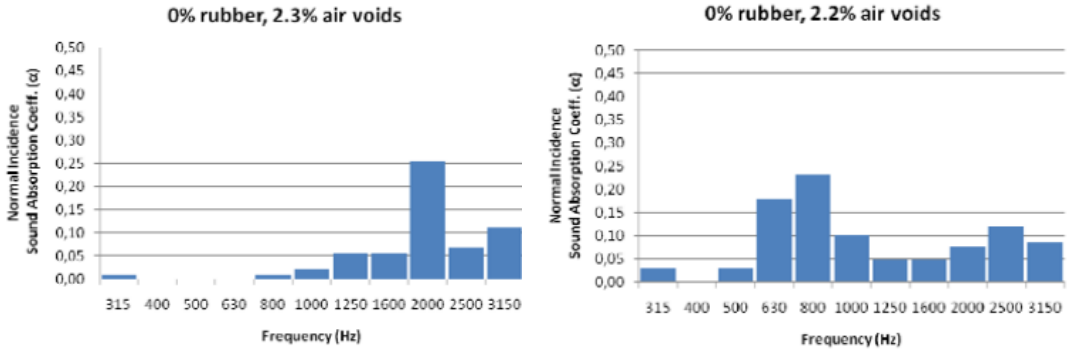

a) *b)*

Figure 12 Absorption coefficients of a) 30 mm and b) 80 mm thick core samples (source: (Raimundo, et al., 2010))

The comparison of wet and dry samples has shown that the water filled pores affect negatively the sound absorption capacity of the surface, see Figure 12 (Raimundo, et al., 2010).

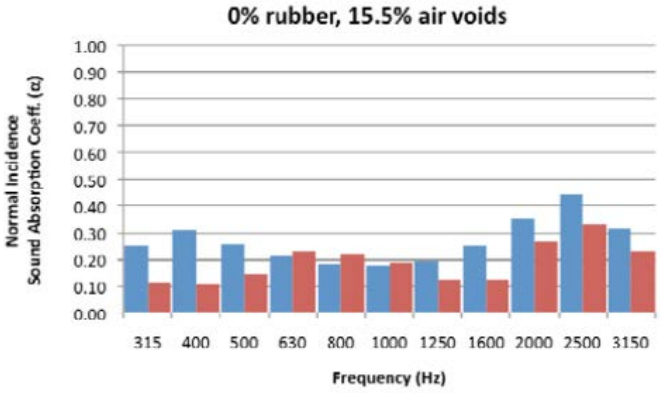

Figure 13 Absorption coefficients of dry (blue) and wet (red) samples of 80 mm thickness (source: (Raimundo, et al., 2010))

Overall, the findings suggest that the sound absorption coefficients depend from a number of parameters and without measurements preferably on in-situ obtained samples it is hard to predict their exact value. Especially in case of porous surfaces that show a peak around a specific frequency. However, in case of dense graded asphalt mixtures with low porosity the results show a rather steady absorption curve without a peak, and therefore a good approximation for the simulation input data is possible. Frequency based absorption datasets based on the reads of curves from introduced researches are presented under chapter *Method / Input data for room acoustic simulation / Absorption* and used as input data for simulation.

1.3.8 Scattering

Scattering is the phenomenon of diffuse reflection of the incident sound. The magnitude of this effect depends of the quality of the surface and the place of incidence on the object. It is characterized by the scattering coefficient that quantifies the diffusely reflected energy over the total reflected energy. It can take a value between 0 and 1, and it is calculated according to Equation 6 (Long, 2014).

$$s_s = \frac{E_{diff}}{E_{spec} + E_{diff}} \qquad 6$$

Where

s_s	surface scattering coefficient,
E_{spec}	specularly reflected part, and
E_{diff}	diffusely reflected part.

The intensity of the direct sound field is reduced by the multiple reflections due to the absorbed and diffusely reflected amount of sound energy (Long, 2014). The scattering due to the surface quality is a frequency dependent variable. In Odeon 11.0 each surface is characterized by its characteristic scattering value at 707 Hz and frequency based values are automatically calculated for the simulation according to Figure 14 (Christensen, 2011).

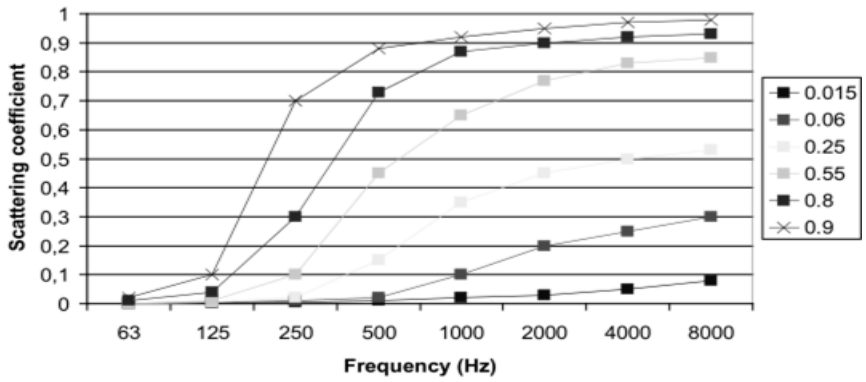

Figure 14 Surface scattering coefficient of materials at different frequency bands with characteristic values at 707 Hz are shown in the legend (source: User Manual Odeon 11.0 (Christensen, 2011))

The User Manual of Odeon 11.0 also suggests some values for the magnitude of various types of surfaces, which is shown in Table 2.

Table 2 Surface scattering coefficients at 707 Hz, source: User Manual Odeon 11.0 (Christensen, 2011)

Material	s_s
Audience area	0.6 – 0.7
Rough building structures, 0.3–0.5 m deep	0.4 – 0.5
Brickwork with open joint	0.1 – 0.2
Brickwork, filled joints but not plastered	0.05 – 0.10
Smooth surfaces, general	0.02 – 0.05
Smooth painted concrete	0.005 – 0.020

It is important to note that the surface scattering coefficients account merely for the scattering due to surface roughness. The additional diffraction due to surface sizes is included in the calculation method called reflection based scattering, already discussed in the calculation process of Odeon. Therefore, in case a curved surface is modelled by many plane sections, and considering it as a regular surface will cause the overestimation of the scattering from diffraction due to the many edges. In this case the surface type 'Fractional' should be applied that ignores the edge effects of these surfaces. However, if small surfaces are replaced by single larger surfaces in the model then the calculation will underestimate the scattering from edge diffraction. Therefore, the estimated value of additional diffraction effects should be included in the surface scattering coefficient.

1.3.9 Diffraction

The value of the scattering coefficient *s* also varies according to the place and angle of incidence on the surface.

At high frequencies incident rays close to the centre of the panel behave as if they hit an infinite panel, which means the reflection is specular. However, close to the edge region diffraction occurs. Consequently, the angle of the incident and reflected rays is not equal and the amplitude of the reflected wave is reduced. In case of low frequency with longer wavelength than the surface size, the rarefactions and compressions go around the object, and therefore the surface does not form an obstacle unlike to short wavelengths. In the edge zone of a surface the attenuation of the reflected sound is higher than in centre zone (Long, 2014).

Odeon 11.0 accounts for the diffraction phenomenon by using the diffraction related scattering factor s_d that is used for the calculation of reflection based scattering coefficient s_r. The derivation of s_d takes into account the dimensions of the surface,

the angle of incidence, the distance of incidence to the edge, the incident and reflected path lengths and the frequency. The scattering effect due to diffraction increases with the angle of incidence, while inversely proportional to the dimensions of the surface and the distance of incidence to the edge. The value of s_d is calculated according to Equation 7 (Christensen, 2011).

$$s_d = 1 - K_w K_l (1 - s_e) \qquad 7$$

Where

s_d scattering coefficient due to diffraction,

K_w attenuation factor derived from the shorter dimension (w) of the surface,

K_l attenuation factor derived from the longer dimension (l) of the surface, and

s_e edge scattering coefficient.

The dimensions of the two sides of the surface determine the cut-off frequencies, f_l and f_w according to Equation 8 (Christensen, 2011).

$$f_w = \frac{c}{\lambda_w}$$

and

$$f_l = \frac{c}{\lambda_l} \qquad 8$$

Where

f_w, (f_l) upper (lower) cut-off frequency, and

λ_w, (λ_w) wavelength that equals to the *w* shorter (*l* longer) dimension of the surface.

The attenuation factors K_w and K_l take into account the frequency of the incident ray. Their value is 1 above the upper cut-off frequency, and therefore, at sufficiently high

frequencies they have no effect. They are calculated according to Equation 9 (Christensen, 2011).

$$K_w = \begin{cases} 1 & for\ f > f_w \\ \dfrac{f}{f_w} & for\ f \leq f_w \end{cases}$$

and

$$K_l = \begin{cases} 1 & for\ f > f_l \\ \dfrac{f}{f_l} & for\ f \leq f_l \end{cases} \qquad 9$$

Where

K_w	attenuation factor derived from the shorter dimension (w) of the surface,
K_l	attenuation factor derived from the longer dimension (l) of the surface,
f_w	upper (lower) cut-off frequency, and
f_l	upper (lower) cut-off frequency.

The concept of the cut-off frequencies is explained in Figure 15. At a specific frequency the field above the thick line stands for the scattered reflections due to diffraction while the area under the line is proportional to the specular reflections. Below the upper cut-off frequency the response falls by 3 dB per octave, and therefore, two octaves below the upper cut-off frequency the specular part of the response is 6 dB smaller than that at the upper cut-off frequency. Furthermore, if the frequency falls below the lower cut-off frequency, the specular part of the response falls by an additional 3 dB.

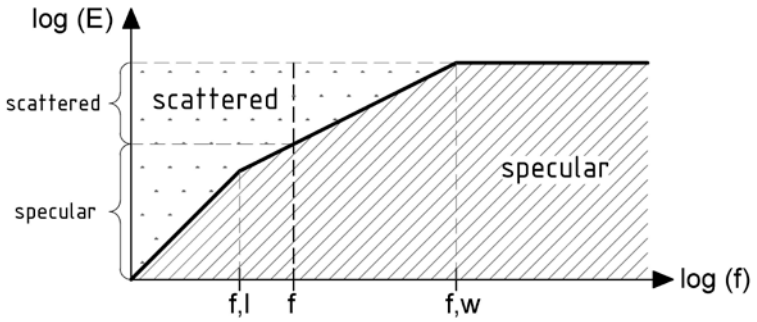

Figure 15 Scattered and specularly reflected energy according to the relation between frequency of incident ray (f) and cut-off frequencies (f_l and f_w) (adapted, based on: User Manual Odeon 11.0 (Christensen, 2011))

Important to note that the diffraction scattering coefficient s_d is calculated only for the so called key diffraction frequency unlike to the surface scattering coefficient s_s, to which frequency dependent values are assigned automatically by Odeon. The key diffraction frequency is set to 707 Hz by default to achieve reliable results in middle frequency range and it should be adjusted if other range is in the focus.

The edge scattering coefficient s_e takes care of the distance of incidence to the edge and the angle of incidence according to Equation 10 (Christensen, 2011).

$$s_e = \begin{cases} 0 & for\ d_{edge} \cos\theta \geq \lambda \\ 0.5\left(1 - \frac{d_{edge} \cos\theta\, f}{c}\right) & for\ d_{edge} \cos\theta < \lambda \end{cases} \qquad 10$$

Where

s_e	edge scattering coefficient,
d_{edge}	the distance of the place of incidence to the edge of the surface,
θ	angle of incidence, and
λ	wavelength of incident ray.

The $d_{edge} \cdot cos\theta$ product is the distance between the incident ray and the edge of the surface and the *c/f* quotient is the wavelength λ of the incident ray. According to the equation above, if the wavelength is smaller than the distance between the incident ray and the edge, no scattering is assigned from edge diffraction effects. Otherwise, if the wavelength of the incident ray is sufficiently large s_e can take a value at most

0.5. This may occur at a very flat incidence angle (*cos90° = 0)* or incidence at the edge (d_{edge} *= 0).* Figure 16 explains the condition of the edge scattering coefficient.

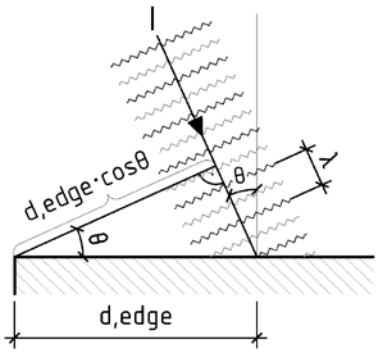

Figure 16 Condition of edge scattering coefficient

Furthermore, there is a setting available in Odeon to distinguish between modest and higher levels of scattering. Below the user defined limit value of the scattering coefficient *s*, derived according to Equation 7, the Lambert oblique algorithm is used. Above the limit, which is usually the case in edge zones due to the additional scattering from diffraction, the scattering is considered as uniform. Best results were achieved at a limit value of scattering coefficient of 0.5 (Christensen, 2011).

1.3.10 Sound sources

The thesis focuses on two urban scenarios with road traffic as the typical source of noise. The room acoustic software Odeon requires sound power levels of the sound source by octave bands between 63 Hz and 8 kHz. The sound pressure level at the receiver is a function of a number of variables – both dependent of the source and the field of propagation. This induced the development of predictive traffic noise models starting from the 1950ies (Quartieri, et al., 2009).

The earliest ones are based on statistical models and characterized the time-varying sound pressure level at the receiver by means of percentile levels. For instance, L_{10} 10 percentile SPL level stands for the SPL exceeded by the signal only 10% during the time of the measurement. They consisted of a single equation that returned a single value SPL at the receiver position, using two input parameters: the distance from source and the level of traffic flow. Later, the models became more sophisticated and they could account for the speed of the flow and the share of different vehicles –

i.e. motorcycles, light vehicles, heavy vehicles – with different noise spectra. The England standard *CoRTN* includes information also about the environment such as gradient of the road, road surface and the weather conditions. Moreover, instead of a single equation a two step method is used, which calculates a base value for reference conditions and correction factors. The latter accounts for deviations in terms of traffic and surrounding. Finally, the base value and correction factors are summed up into a single value indicator of L_{10}. The German standard *RLS 90* and the Italian *C.N.R.* model follow the principles of the CoRTN calculation, but instead of a percentile level they calculate the continuous equivalent sound level at the receiver. Finally, the French model *NMPB – Routes – 98* takes into account the frequency dependent behaviour of the sound propagation too, calculates the sound power level of the source and predicts the A-weighted SPL at the receiver. The methodology of the French model was adopted by the European Commission and formed the basis of the document Common Noise Assessment Methods in Europe (CNOSSOS-EU) in 2012 (Kephalopoulos, et al., 2012). This guideline was developed for the purpose of strategic noise mapping as specified in the END 2002/49/EC (European Commission, 2002) and it was ratified in Annex of Commission Directive (EU) 2015/996 (European Commission, 2015). The free availability, the state of the art approach and the format of the final outputs allow the practical use of the model in this contribution.

A further perspective in the fields of traffic noise prediction is the application of real-time sound emission of single vehicles (De Coensel, et al., 2016). It was found that annoyance due to noise exposure is not only a function of equivalent SPLs but the level and the number of noise events modify the perceived noise situation to a great extent. Therefore, even a distinction between vehicles within the same category would be necessary in order to account for extreme values by cause of vehicle condition, driving style, etc. Consequently, time-related instantaneous sound levels from simulations could form a better ground for validation methods that use real-time on-site measurements. Moreover, it could provide a better understanding of the relation between perceived transient noise levels and the level of annoyance.

2 METHOD

2.1 Overview

The simulation model is set up for two locations in order to check the validity of the method. Both of the two sites are featured by a typical inner city street network, however, they differ in their height-width ratio, the number of lanes, the vegetation and the location of microphones along the street. Nevertheless, the same procedure is used for both.

The methodology of the research includes three main steps. In the first section the derivation of input data is described in terms of geometry, materials, sound sources, receivers and simulation tool settings. In the second step a baseline model is run by using input data that approximates the conditions of the on-site measurements best. Thirdly, a number of scenarios that are changed along one parameter at once are set up and simulated. The sensitivity of simulation results with respect to the changed parameter is analysed and compared.

2.2 Room acoustic simulation

2.2.1 Workflow in Odeon

In this section a compact overview is given in form of instructions about the steps to set up the simulation model in Odeon.

1. Save the edited geometry as *dxf* file, (no later version than Odeon).

2. Import geometry with *full import* option.

3. Run the *3D geometry debugger* to detect overlapping surfaces.

4. Under *Materials* create a local material library for the room *(Toggle between global and local room library)*, add materials (e.g. facade and ground).

5. Assign arbitrary absorption coefficients to all surfaces.

6. Set up the sources and receivers, or import them from a file.

7. Use the *3D investigate rays* option and check if all line sources stay within the model space. Leakages of the model can be detected by this tool as well. If any errors detected, correct it (e.g. lift up a line source, or close a gap in the geometry), and do a check again.

8. Assign the real absorption-, and scattering coefficient to all surfaces.

9. Run the *quick estimate* tool under *Materials.*

10. In *Room Setup* set the *impulse response length* according to the highest Sabine reverberation time from *quick estimate*.

9. Set up jobs, sources (arbitrarily many) – listener (one per job) compositions.

10. Run the jobs (simulation.)

2.2.2 Geometry

The geometry derivation phase consists of the input of facade and ground surfaces, the sky representation, and finally, the receiver and the sound source positions. The latter two are, however, cannot be imported in the Odeon model directly, because the related geometry information is required as numeric data.

The geometry data was retrieved from *Geodatenviewer der Stadtvermessung Wien* that provides the three-dimensional model of buildings without the roof geometry of city Vienna. Under the menu *Geodaten download* - *Baukörpermodell* a part of the 3d model can be downloaded in *.dxf* format. In case of the present study the lack of roof geometry is considered negligible because the sound pressure levels are measured in the street where the main sound sources are located too. However, if the receivers were in an inner courtyard separated from the sound source by a building, the roof geometry would play an important role as the sound rays have to pass above it.

The original 3d data has a high level of details and therefore it needs to be simplified for reasons of better transparency and traceability. The original object of the dxf files are *polyface meshes* (AutoCAD command: PFACE). They have many vertices and can be exploded into *3d faces* (AutoCAD command: 3DFACE) that are defined by 3 or 4 vertices in one plane. These two object types are imported properly in Odeon.

Due to a similar consideration as of rooftops also the building geometry behind the facade is removed from the model. During the downsampling the surfaces in same plane and with same layer name are replaced by single *3d face* triangles. In the original model the changes in street level are taken into consideration by the stepping of the bottom line of the buildings. These steps are smoothed by averaging the height of the adjacent vertices. The upper edge of the facades is left unchanged.

In order to close the bottom and the top of the model the ground and sky surfaces are added as *polyface mesh* objects. With regard to sky representatioin two different

approaches are followed that should theoretically yield the same results. As the sky is assumed to be completely absorbing, all rays that leave the canyon hit a sky surface and therefore instantly absorbed. For this reason there should be no difference in closing the canyon right at the top edge of the facades or put a box with 100 % absorptance above the whole model. The process of editing the geometry is shown on Figure 17 and Figure 18.

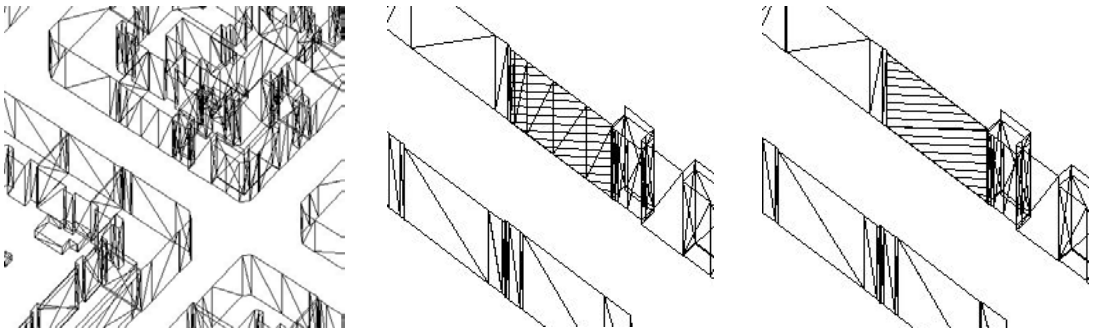

a) *b)* *c)*

Figure 17 a) original 3d data (source: Stadt Wien - data.wien.gv.at) b) facade – before editing c) facade – after editing

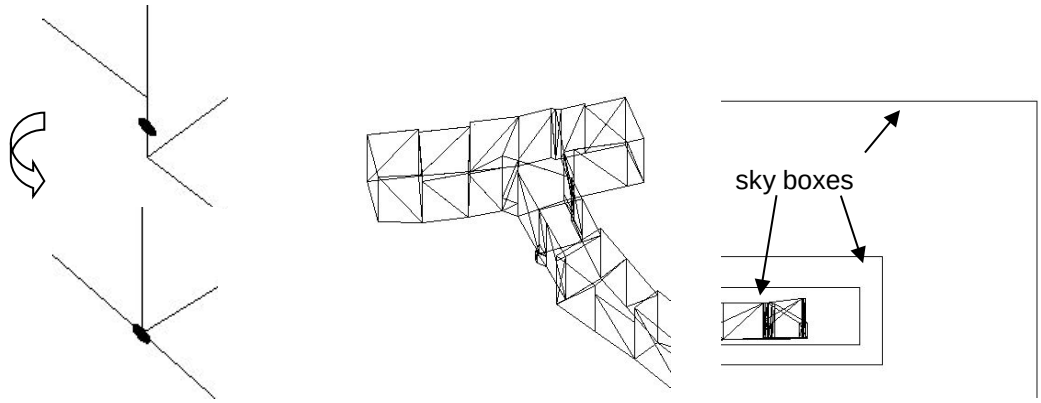

a) *b)* *c)*

Figure 18 a) smoothing bottom vertices of facades b) model with all surfaces c) model with sky boxes

As a final step of the geometry editing the model should be placed close to the origin of the world coordinate system, otherwise extremely big x, y, z numbers may occur in case of receiver and sound source coordinates that may cause problems. The import in Odeon is carried out by the *full import* option. The origin of the coordinate system should be kept as in the *dxf* file, therefore, the location of sources and receivers can

be defined precisely. After importing the *3D geometry debugger* tool of Odeon is run that checks overlaps between the model surfaces.

Finally, the geometry data of sound sources and receivers can be directly set in the *.SouRecScript* file or in the input fields of Odeon. Attention should be paid that azimuth values higher that 180° are not allowed in Odeon, and therefore the *line* (and not *polyline*) objects indicating the line sources should point to a direction which angle to the x axis is less than 180°.

2.2.3 Absorption coefficients

An overview over the size of surface types in Paulanergasse is given in Table 3. Surface types with a high total area, with close proximity to sound sources, or with high reflectivity are of special interest, because a reasonable amount of sound energy will be reflected from them.

Table 3 PA Total area of surface types

Surface	**Total area [m2]**	**[%]**
sky	7208	26
ground	6094	22
facade	12420	44
boundary 1*	1732	6
boundary 2**	484	2
SUM	27938	

*cross street end closing
**street end closing

Ground

Special interest is given to the absorption of the ground surfaces due to their large share and close proximity to the sound sources. Ground surfaces are indicated by green colour on Figure 19.

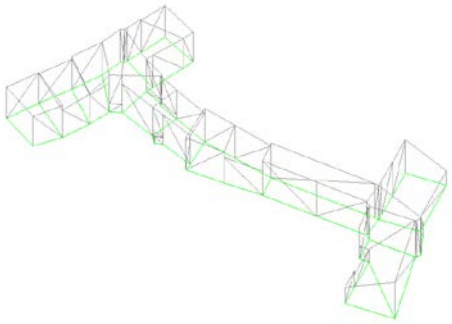

Figure 19 Ground surfaces

A number of datasets on asphalt from various research findings (Raimundo et al. 2010, Paje et al. 2008, Knabben et al. 2016 and Mun, 2010) are collected in Table 4. The arithmetic average of the first three dense graded asphalt data sets, which lack a peak in the sound absorption coefficient curve, is calculated and it is going to be used as a first estimate for the ground surface material. Missing values are extrapolated or estimated and indicated in italic. The same datasets are graphically shown on Figure 20.

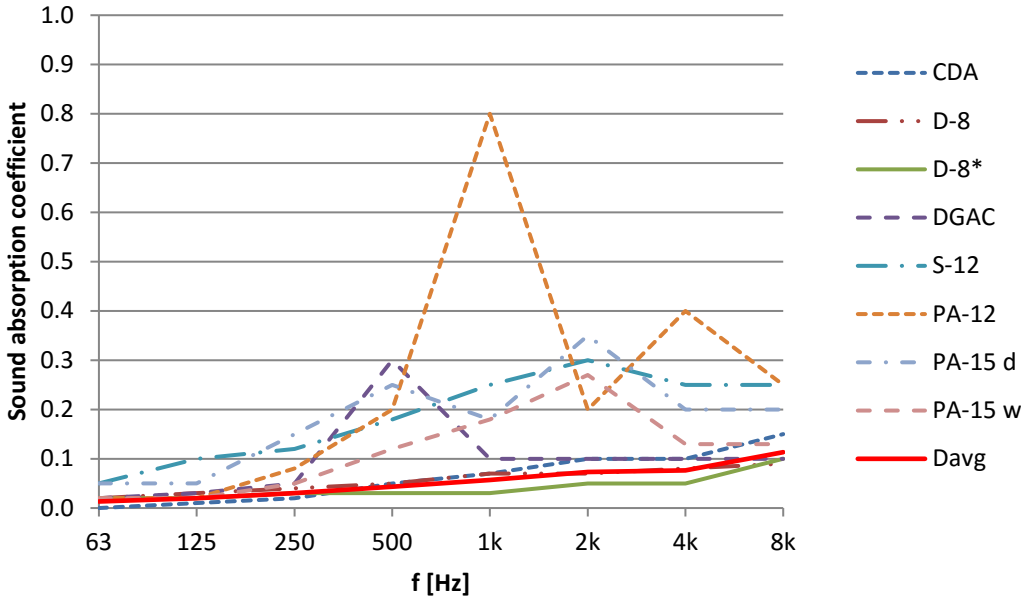

Figure 20 Absorption coefficients based on previous research findings on asphalt (see also Table 4)

Table 4 Absorption coefficients by octave bands based on previous research findings (source: (Raimundo et al. 2010, Paje, et al., 2008, Knabben et al. 2016, Mun 2010))

ID	Description	63	125	250	500	1k	2k	4k	8k
CDA	common dense graded asphalt	0.00	0.01	0.02	0.05	0.07	0.10	0.10	0.15
D-8	new dense graded 2-6% VC	0.02	0.03	0.04	0.05	0.07	0.07	0.08	0.09
D-8*	worn dense graded 2-6% VC	0.02	0.02	0.03	0.03	0.03	0.05	0.05	0.10
DGAC	dense graded asphalt concrete	0.02	0.03	0.05	0.30	0.10	0.10	0.10	0.10
S-12	10 m. old semi dense 12% VC	0.05	0.10	0.12	0.18	0.25	0.30	0.25	0.25
PA-12	porous surface 12% VC	0.02	0.02	0.08	0.20	0.80	0.20	0.40	0.25
PA-15 d	porous surface 15% VC - dry	0.05	0.05	0.15	0.25	0.18	0.35	0.20	0.20
PA-15 w	porous surface 15% VC - wet	0.02	0.02	0.05	0.12	0.18	0.27	0.13	0.13
D_{avg}	avg. value of CDA, D-8, and D-8* dense graded	0.01	0.02	0.03	0.04	0.06	0.07	0.08	0.11

For the reason of comparison some hard surfaces from Odeon database are listed in Table 5 together with D_{avg} dataset and the corresponding absorption curves are drawn in Figure 21.

Table 5 Absorption coefficients by octave bands - hard surfaces from Odeon database

ID	Description	63	125	250	500	1k	2k	4k	8k
Davg	avg. value of CDA, D-8, and D-8* dense graded	0.01	0.02	0.03	0.04	0.06	0.07	0.08	0.11
O 100	Rough concrete	0.02	0.02	0.03	0.03	0.03	0.04	0.07	0.07
O 101	Smooth unpainted concrete	0.01	0.01	0.01	0.02	0.02	0.02	0.05	0.05
O 105	Porous concrete blocks without surface finish	0.05	0.05	0.05	0.05	0.08	0.14	0.2	0.2
O 108	Concrete or terrazzo Ref.	0.01	0.01	0.01	0.01	0.02	0.02	0.02	0.02
O 2001	Marble or glazed tile	0.01	0.01	0.01	0.01	0.01	0.02	0.02	0.02

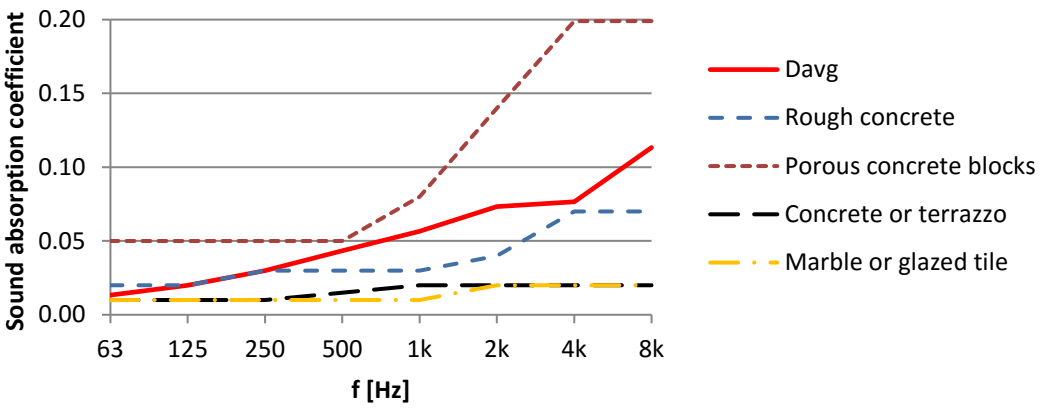

Figure 21 Absorption coefficients of some hard surfaces from Odeon database

Facades

Facades show the highest percentage value among all surface types, see in Figure 22.

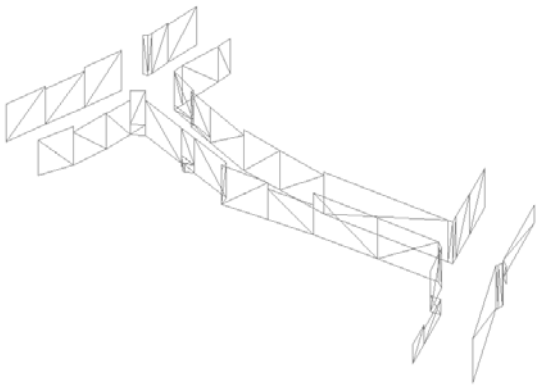

Figure 22 Facade surfaces

Although surfaces further away from sound sources and receivers play a less significant role, a good approximation of their absorption properties is necessary to account for a realistic sound field.

The derivation of absorption data included two steps: the geometrical analysis of the facades and the material assignment with the help of Odeon database. The overall dimensions of the single building facades were retrieved from the 3d data and an orthogonal view of all of them was generated via photomontage. Based on the orthogonal view a material map was drawn and the area of the different materials was

counted. The 2d view of one side of Paulanergasse is shown on Figure 23 both as a photomontage and a material map.

Figure 23 Photomontage and material map of one side of Paulanergasse

An overview of the façade materials is presented both in tabular and graphical form in Table 6 and Figure 24.

Table 6 Absorption coefficients by octave bands - facade materials (source: Odeon database, (Forouharmajd, et al., 2014))

ID	Description	63	125	250	500	1k	2k	4k	8k
O 4002	Painted plaster surface (plaster)	0.02	0.02	0.02	0.02	0.02	0.02	0.02	0.02
O 10003	Double glazing, 2-3 mm glass, 10 mm gap (glass)	0.10	0.10	0.07	0.05	0.03	0.02	0.02	0.02
O 108	Concrete or terrazzo Ref.(stone)	0.01	0.01	0.01	0.02	0.02	0.02	0.02	0.02
-	galvanized steel metal (steel)	0.02	0.07	0.06	0.05	0.04	0.05	0.04	0.04
O 1001	Smooth brickwork with flush pointing (tiles)	0.02	0.02	0.03	0.03	0.04	0.05	0.07	0.07

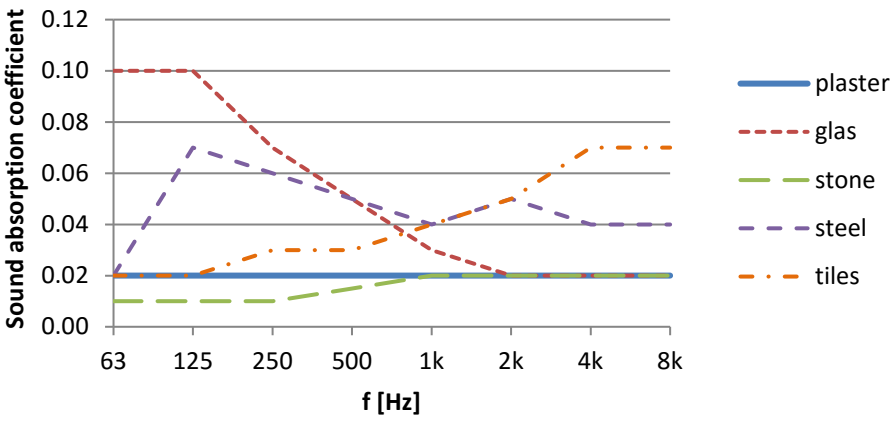

Figure 24 Absorption coefficients of facade materials from Odeon database

However, the selection of materials includes a high level of uncertainty even if a large material library with detailed descriptions is available. In order to illlustrate the wide range of choice in case of a specific material type the absorption properties of available glas materials are listed in Table 7 and shown in Figure 25.

Table 7 Absorption coefficients by octave bands - glas materials from Odeon database

ID	Description	63	125	250	500	1k	2k	4k	8k
10000	Solid glass blocks	0.02	0.02	0.02	0.02	0.02	0.02	0.02	0.02
10001	Single pane of glass	0.18	0.18	0.06	0.04	0.03	0.02	0.02	0.02
10002	Single pane of glass, 3 mm	0.08	0.08	0.04	0.03	0.03	0.02	0.02	0.02
10003	Double glazing, 2-3 mm glass, 10 mm gap	0.10	0.10	0.07	0.05	0.03	0.02	0.02	0.02
10004	Double glazing, 2-3 mm glass, >30 mm gap	0.15	0.15	0.05	0.03	0.03	0.02	0.02	0.02
10005	Glass, large panes of heavy plate glass	0.18	0.18	0.06	0.04	0.03	0.02	0.02	0.02
10006	Glass, ordinary window glass	0.35	0.35	0.25	0.18	0.12	0.07	0.04	0.04
14400	Holzkastenfenster d=0.2 m	0.50	0.25	0.05	0.03	0.02	0.02	0.02	0.02

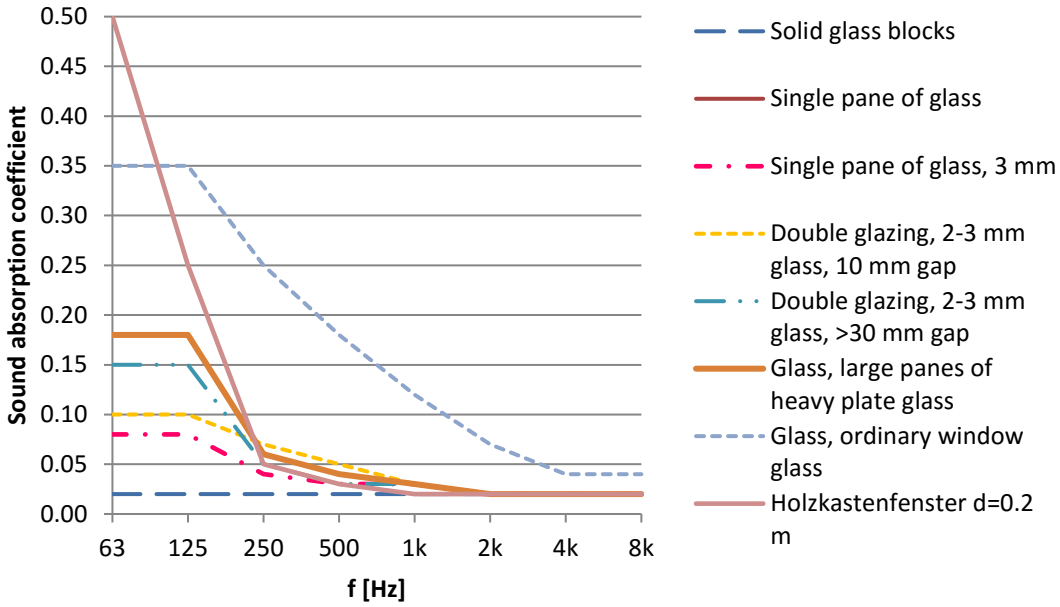

Figure 25 Absorption coefficients of glass materials from Odeon database

For further calculations material *double glazing, 2-3 mm glass, 10 mm gap* was used throughout the whole model. The datasets derive from many different sources, and therefore, the comparability of them is questionable.

In case of each building the façade was divided into regions according to the material pattern of surfaces. Within one region all materials were summed, and based on their ratio the area-weighted avarage sound absorption was calculated. The results were summed up for the whole building according to the ratio of subparts. An example of the division of the façade is shown on Figure 26, and the detailed calculation of the same building is presented in Appendix.

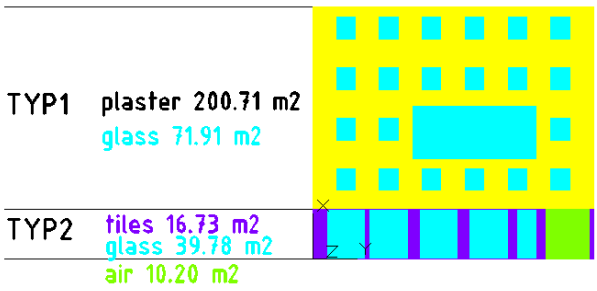

Figure 26 Division of facade and material surfaces – facade 2

The study on facades has shown very little difference between the different buildings in the street. The only outsider is the façade 1 at low frequency range. The reason for that can be easily detected: this building has a high percentage of glazed surfaces that is responsible for increased absorption at low frequencies. The area-weighted average of the facades was calculated based on one side of Paulanergasse and used in the simulations as input data. As the buildings on the other side have similar surface material pattern, no significant deviation is expected from their ignoration. The absorption coefficient values by buildings and the area-weighted dataset for the street are listed in Table 8 and shown in Figure 27.

Table 8 Area-weighted absorption coefficients of facades by octave bands

ID	Surface Name	63	125	250	500	1k	2k	4k	8k
1	106781	0.05	0.05	0.04	0.03	0.02	0.02	0.02	0.02
2	100320	0.04	0.04	0.03	0.03	0.02	0.02	0.02	0.02
3	125992	0.04	0.04	0.03	0.03	0.02	0.02	0.02	0.02
4	007063-007062	0.04	0.04	0.03	0.03	0.02	0.02	0.02	0.02
F_{avg}	-	0.04	0.04	0.03	0.03	0.02	0.02	0.02	0.02

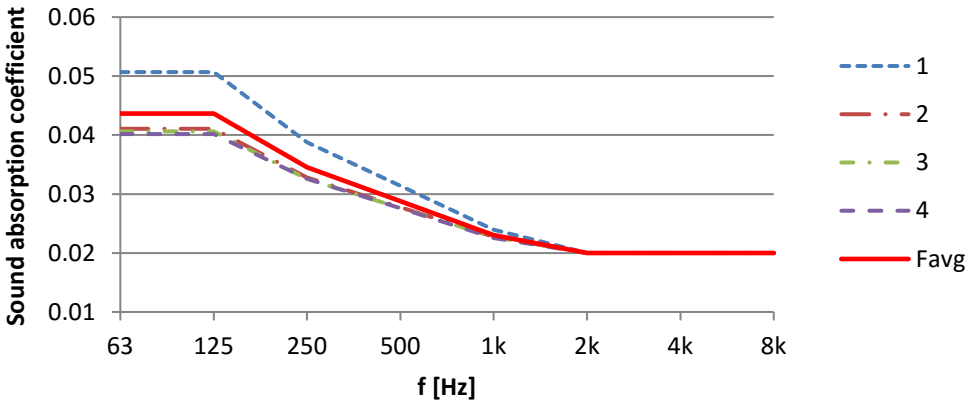

Figure 27 Area-weighted absorption coefficients of facades (see also Table 8)

In the simulations F_{avg} is assigned to all building facades in order to account for realistic absorption characteristics of the street and to keep the number of applied materials in the model as small as possible.

Sky

The sky takes the second largest portion from all surface types. Based on previous considerations 100% absorbent material is assigned to these surfaces. Sky surfaces are outlined in blue colour in Figure 28.

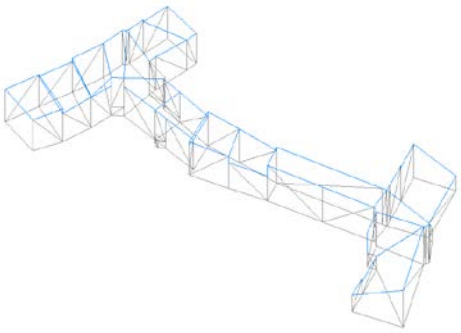

Figure 28 Sky surfaces

In terms of geometry two approaches were used to represent the sky. As Odeon requires a closed geometry the model has to be closed from the top, even though, no physical surface is there in reality. This can be done along the upper edge of the facades that results in a number of sky surfaces and possible errors: overlaps or gaps. Another way is to use a sky box around the entire model, which results in a simple geometry, and therefore, there is a minimal risk of errors. The impact analysis included four different sky types: closed at the facade, small-, medium-, and big sky box as shown in Figure 29.

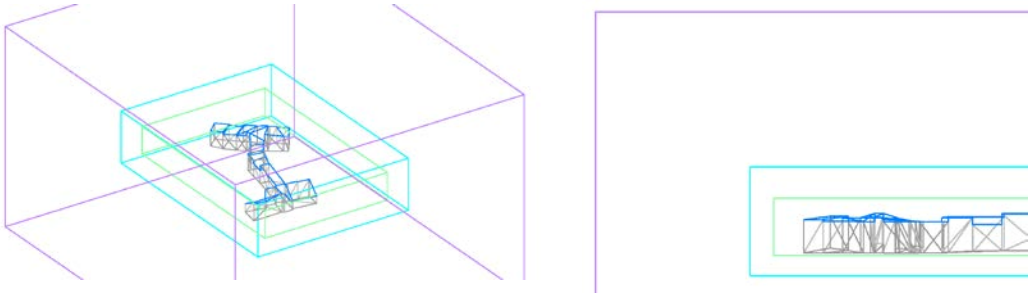

Figure 29 Sky types – closed at facade, small, medium and big sky box – perspective and orthogonal view

Boundary 1 and 2

Boundary 1 (yellow) and boundary 2 (red) are the vertical surfaces that close the cross streets as shown in Figure 30.

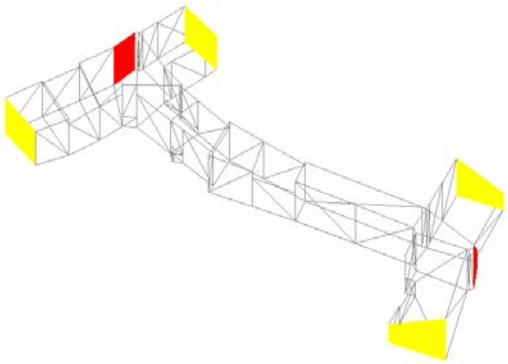

Figure 30 Boundary 1 and 2 surfaces

Regarding the relatively big distance between boundary surfaces and receiver positions their absorption characteristics have presumably little effect on SPLs. The applied absorption coefficients are listed in Table 9.

Table 9 Absorption coefficients by octave bands – sky, boundary 1 and 2 surfaces

ID	Description	63	125	250	500	1k	2k	4k	8k
SKY	sky	1.0	1.0	1.0	1.0	1.0	1.0	1.0	1.0
B1	boundary 1	0.9	0.9	0.9	0.9	0.9	0.9	0.9	0.9
B2	boundary 2	0.5	0.5	0.5	0.5	0.5	0.5	0.5	0.5

As boundary surfaces represent holes, no incident rays are bounced back from them. However, rays may enter into the range of the model form outside in reality. Rays that come from behind B1 surfaces have a very low probability to be bounced to the receivers. As a result, both the incident (i.e. outgoing) and the incoming rays can be ignored, and a high absorption value of 0.9 can be assigned.

In case of B2 surfaces the same consideration stands for the incident rays. However, there is a higher probability that rays coming from outside would be reflected further to the receivers, and thus, they are characterised by a lower absorption of 0.5.

Summary

The material list used in Odeon simulation in the calibration phase of the model is shown in Table 10, Figure 31 and Figure 32. The Sabine area of model surfaces – i.e. equivalent sound absorption area of a perfect absorber – is calculated according to Equation 11.

$$A = \alpha \cdot S \qquad 11$$

Where

A Sabine area [m²],

α sound absorption coefficient, and

S geometric area [m²].

The equivalent Sabine area of the air was obtained from Odeon Quick Estimate of the Material window. The resulting total Sabine area of the model by frequencies is shown in Figure 32.

Table 10 Materials in Odeon model for simulation, Sabine area

Surface	**Area [m²]**	**63**	**125**	**250**	**500**	**1k**	**2k**	**4k**	**8k**
sky	7208	1.00	1.00	1.00	1.00	1.00	1.00	1.00	1.00
ground	6094	0.01	0.02	0.03	0.04	0.06	0.07	0.08	0.11
facade	12420	0.05	0.05	0.04	0.03	0.02	0.02	0.02	0.02
boundary 1	1732	0.90	0.90	0.90	0.90	0.90	0.90	0.90	0.90
boundary 2	484	0.50	0.50	0.50	0.50	0.50	0.50	0.50	0.50
Sabine area [m²]									
Surfaces		9691	9752	9688	9625	9623	9684	9745	9928
air (Odeon)		17	59	170	349	608	1325	4036	14304
Total Sabine area		9707	9811	9858	9974	10231	11009	13781	24232

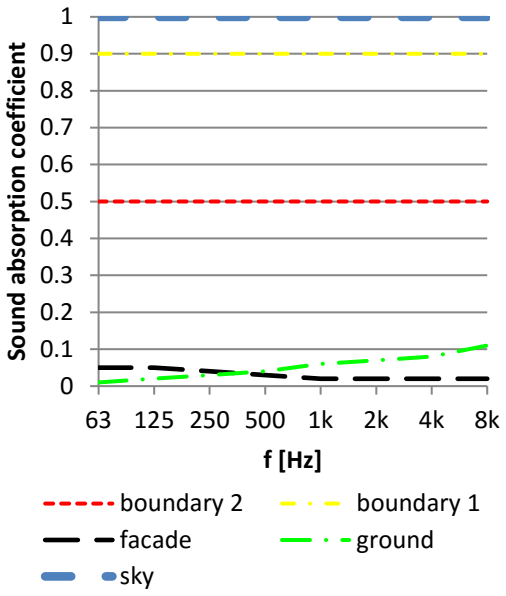

Figure 31 Sound absorption coefficient of materials in Odeon simulation

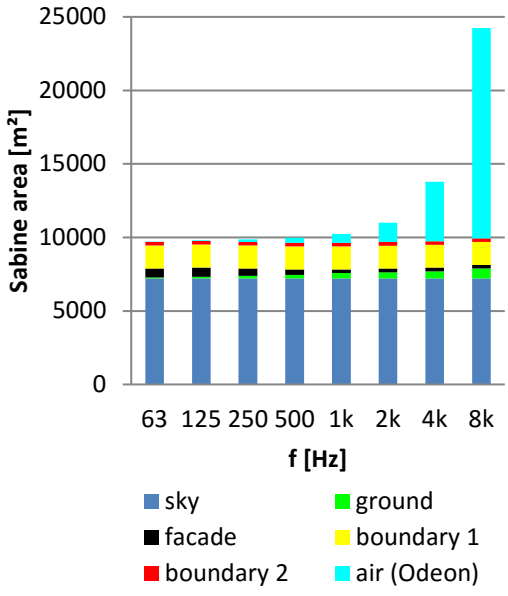

Figure 32 Total Sabine area of the model by frequencies

2.2.4 Scattering coefficients

The scattering coefficients used in the baseline models are presented in Table 11 and derived from recommended values of User Manual Odeon 11.0 (see chapter: *Background / Scattering*).

Table 11 Surface scattering coefficients of baseline model at 707 Hz

Material	s_s
sky	0.05
façade	0.20
ground	0.30
boundary 1, 2	0.50

In case of sky surfaces total sound absorption is assumed, and therefore, the value of surface scattering does not play a role. The coefficient for facade surfaces is based on the consideration that the articulation of facades is rather high. This is either due to the fine decorative elements of historical buildings or the small scale facade finishing elements of buildings from later time periods. Therefore, a value that is dedicated for “brickwork with open joints” is applied for facades. Furthermore, an empty ground surface would get a relatively low surface scattering, however, due to cars and people, the value of rough building structures was assigned here. Finally, as

boundary 1 and 2 surfaces indicate the part of the streets that are out of the model range a high level of scattering is used here.

2.2.5 Sound sources

Overview

The typical sound source for both locations is the road traffic. In order to provide input data for the simulation the CNOSSOS traffic noise prediction model was applied. In this chapter the derivation of sound power from road traffic is described. There are three main steps of the method. The first step is the in-situ traffic flow metering that was carried out at the same hour of the day as the measurements. The second phase is the calculation of frequency based sound power levels based on CNOSSOS. Finally, in the third step the outputs are adjusted to meet the format requirements of the simulation tool.

The road traffic can be represented by *line sources* in Odeon. In each cross-section one line source was placed in the middle of the street to account for the traffic flow regardless to the number of lanes. The sound power of the source is can be either provided to the software as an overall value in dB or in dB/m unit. The one is automatically converted into the other unit based on the length of the line source. Moreover, an equalizer value in dB can be specified for each octave frequency that is arithmetically added to the overall sound power level in dB. Therefore, the frequency dependent nature of the traffic noise is taken into consideration.

The method described above is presented on the example of Paulanergasse. The corresponding tables and figures for Koppstrasse are in the Appendix.

Traffic flow

The traffic flow was observed throughout the range of the model. This includes the section of Paulanergasse between Margaretenstraße and Wiedner Hauptstraße together with the two crossings. The speed limits and the directions of traffic flow are indicated on Figure 33. The numbers in the indices stand for the origin of the traffic flow while the letters indicate the place of arrival. Speed limits are indicated in red circles in km/h unit. The venues of traffic flow metering are indicated by dashed lines.

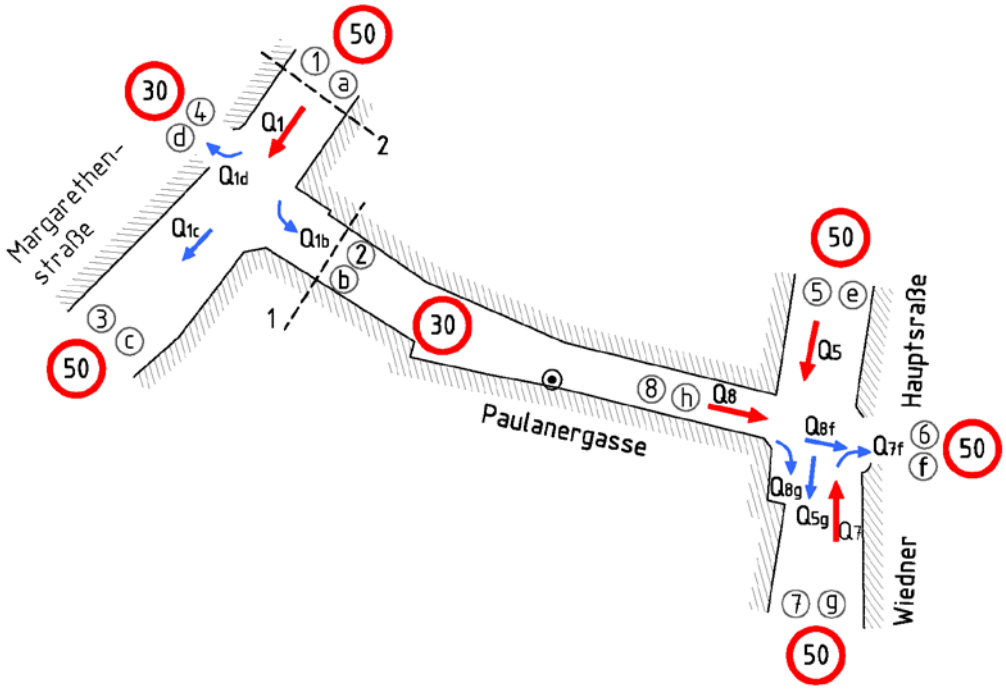

Figure 33 Paulanergasse – Speed limits [km/h], traffic flow directions and positions of traffic flow metering (1, 2)

The corresponding nominations of line sources can be read from Figure 34. For instance, LS9 and LS10 correspond to Q_5, and LS11 to $Q_{5g} + Q_{8g} + Q_7$.

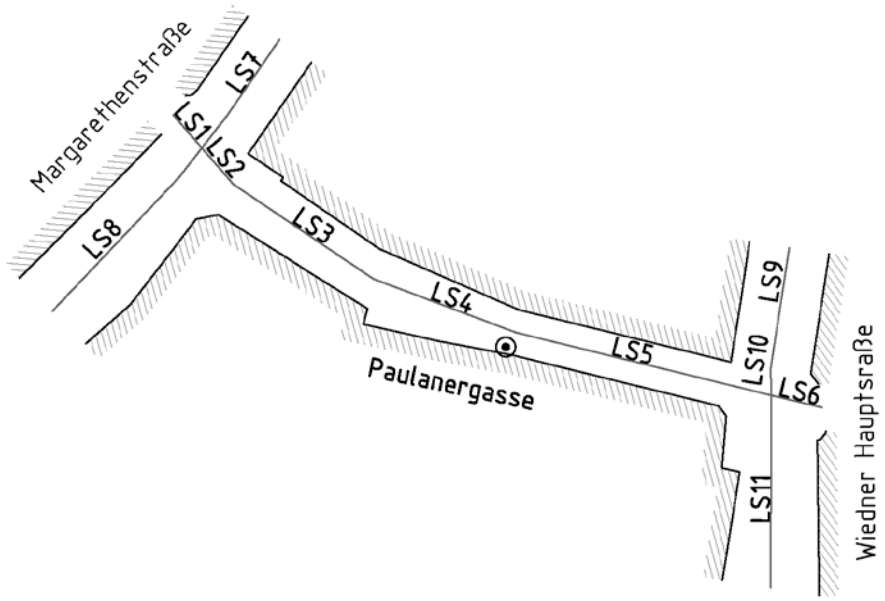

Figure 34 Paulanergasse – Line sources

The correspondence between traffic flows and line sources is shown in Table 12.

Table 12 Components of line sources

Line source	Traffic flow
LS1	Q_{1d}
LS2	$Q_{1b} = Q_8$
LS3	$Q_{1b} = Q_8$
LS4	$Q_{1b} = Q_8$
LS5	$Q_{1b} = Q_8$
LS6	$Q_{8f} + Q_{7f}$
LS7	Q_1
LS8	$Q_{1c} = Q_1 – (Q_{1d} + Q_{1b})$
LS9	Q_5
LS10	Q_5
LS11	$Q_{5g} + Q_{8g} + Q_7$

The results of the traffic flow metering are presented in Table 13.

Table 13 Results of on-site traffic flow metering – Paulanergasse and Margarethenstraße

Paulanergasse				
Date of metering	18 October 2017, Wednesday (weekday)			
Time period	18:05 – 18:25			
Vehicle category	1	2	4a	4b
Number of vehicles	107	2	9	0

Margarethenstraße				
Date of metering	19 October 2017, Thursday (weekday)			
Time period	18:14 – 18:27			
Vehicle category	1	2	4a	4b
Number of vehicles	250	6	19	1

The traffic flow of the other cross sections of the model were estimated as a percentage of the measured flows based on on-site observations. For instance, Q_{1d} flow is almost negligible, while Q_5 approximated as 1/3 of the traffic flow in Paulanergasse. The final input data for sound power simulation is presented in Table 14. The metered data was recalculated to hourly values.

Table 14 Traffic flow of line sources – Q [1/h] – Paulanergasse

Vehicle category	**LS1**	**LS2,3,4,5**	**LS6**	**LS7**	**LS8**	**LS9,10,11**
1	3.0	321.0	107.0	1153.8	829.8	160.5
2	0.0	9.0	3.0	27.7	18.7	4.5
3	0.0	0.0	0.0	0.0	0.0	0.0
4a	3.0	27.0	9.0	87.7	57.7	13.5
4b	0.0	0.0	0.0	4.6	0.0	0.0
Speed limit [km/h]	30	30	50	50	50	50
Data source	metering	metering	1/3xLS2	metering	LS7- (LS1 + LS2)	1/3xLS2

Sound power – CNOSSOS noise prediction model

The methodology of the CNOSSOS noise prediction model is shown in Figure 35. In the flow chart ellipses stand for user defined input data, arrows indicate equations and the boxes stand for sound power levels.

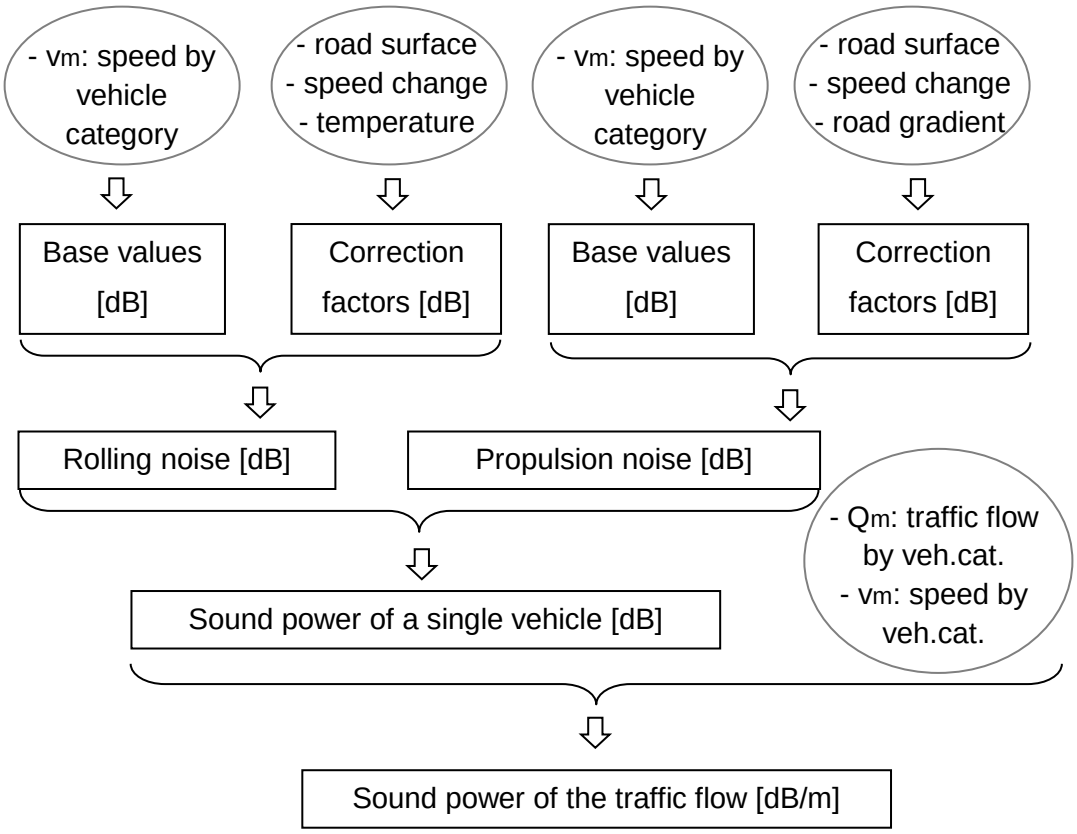

Figure 35 Flow chart of CNOSSOS noise prediction model

The equations of CNOSSOS noise prediction model are listed in the Appendix. The calculation steps and the resulting sound power levels of LS3 are shown by vehicle categories in Figure 36 – Figure 43. The data sets of zero values are not indicated, namely rolling noise base values and correction factors for vehicle category 4a and 4b.

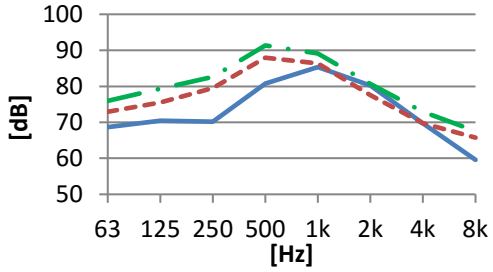

Figure 36 Rolling noise – Base values – LS3

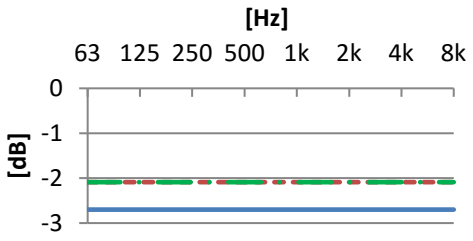

Figure 37 Rolling noise – Correction f. – LS3

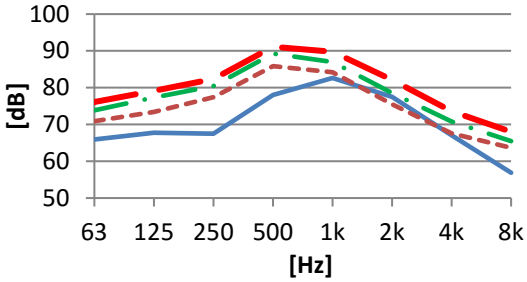

Figure 38 Rolling noise (Base value + correction factors) – LS3

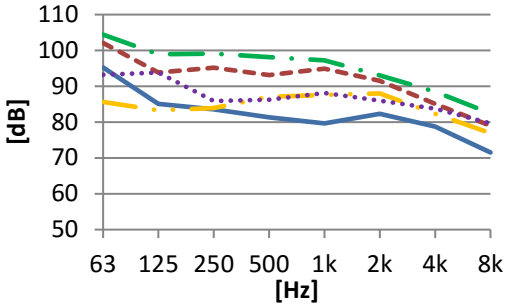

Figure 39 Propulsion noise – Base values– LS3

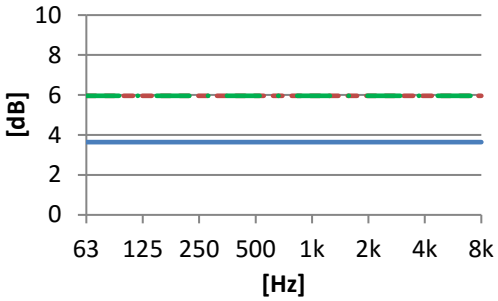

Figure 40 Propulsion noise – Correction f. – LS3

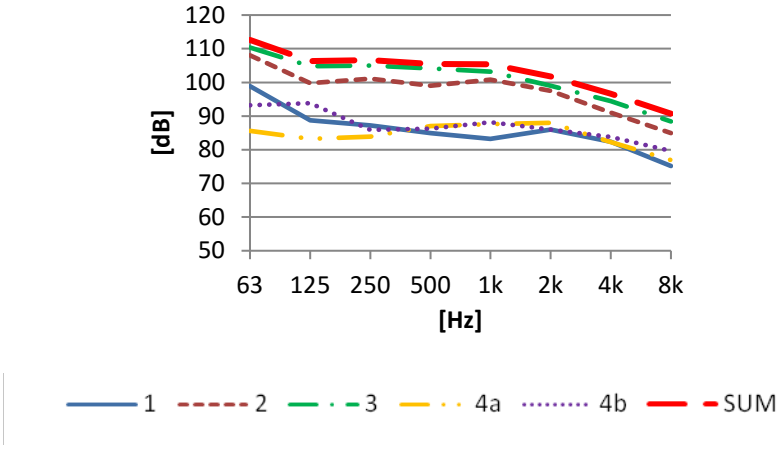

Figure 41 Propulsion noise (Base value + correction factors) – LS3

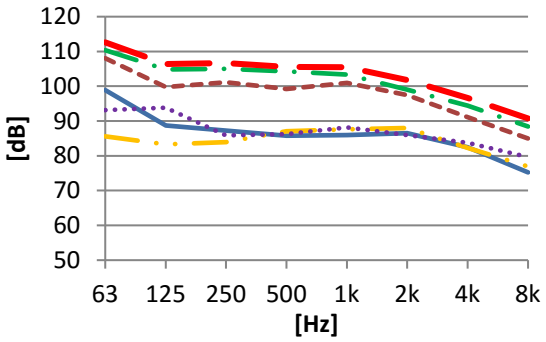

Figure 42 Sound power level of a single vehicle – LS3

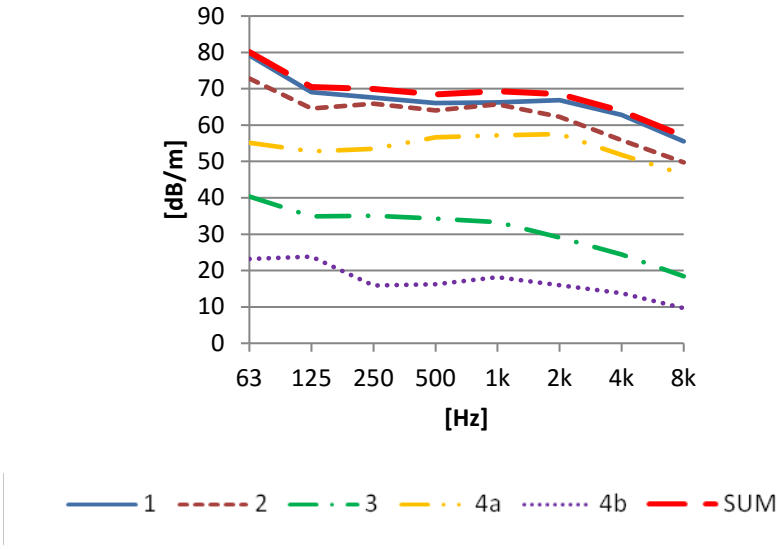

Figure 43 Sound power level of the traffic flow – LS3

The sound power of a single vehicle is given in dB unit, while the sound power of the traffic flow in dB/m. If the traffic flow is negligible, as in case of category 4a, then the power of the traffic flow is small regardless the high emission of a single vehicle.

The energetic sum of the sound power level of all vehicle categories is calculated for all line sources in the model. The results and the length of line sources are listed in Table 15, and shown in Figure 44.

Table 15 Sound power level by octave bands [dB/m] and length [m] of the line sources

LS	63	125	250	500	1k	2k	4k	8k	l [m]
LS1	61.0	51.8	51.1	50.8	51.1	51.3	46.5	40.1	11.9
LS2	80.1	70.5	69.9	68.5	69.3	68.5	63.9	57.0	11.8
LS3	80.1	70.5	69.9	68.5	69.3	68.5	63.9	57.0	43.8
LS4	78.5	68.9	68.3	67.3	68.5	67.4	62.5	55.6	39.5
LS5	79.7	70.0	69.5	68.1	69.0	68.2	63.5	56.6	68.1
LS6	75.0	67.8	67.7	66.2	67.7	66.5	61.5	54.7	13.6
LS7	84.0	76.7	76.3	75.1	76.8	75.7	70.7	63.8	34.8
LS8	82.3	75.0	74.7	73.6	75.5	74.2	69.1	62.1	57.2
LS9	75.3	68.0	67.8	66.7	68.5	67.2	62.1	55.2	31.6
LS10	76.3	69.0	68.9	67.5	69.0	67.8	62.9	56.0	7.0
LS11	75.1	67.9	67.7	66.6	68.4	67.1	62.0	55.1	49.9

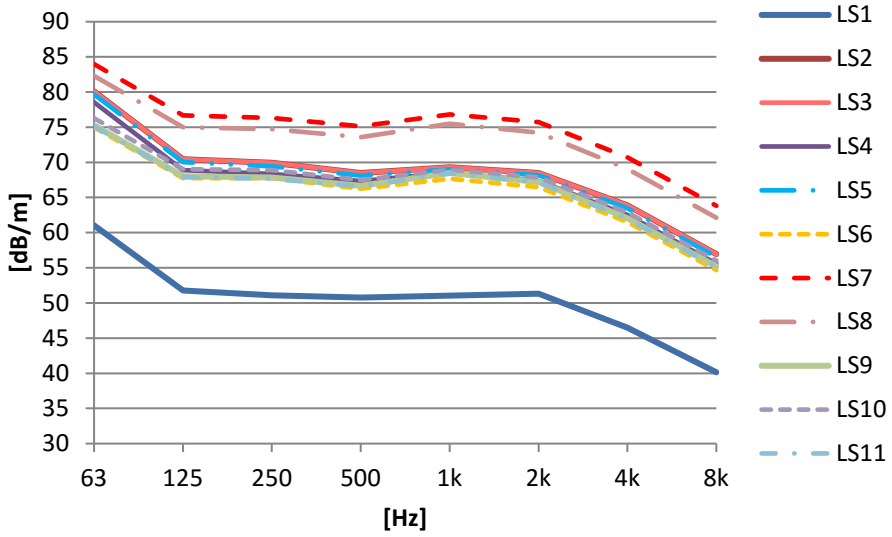

Figure 44 Sound power levels of line sources

The predictions are according to expectation, because the highest sound power levels, namely LS7 and LS8, were found in are in Margarethenstraße, where the highest traffic flow was registered. LS1 is negligible, and all the other sources are rather similar.

Data processing

The output of the CNOSSOS model needs further editing, because the equalizer values in the source input data refer to the overall sound power level, meaning that they are expressed in dB and not in dB/m unit. Therefore, all dB/m values were

converted into an equivalent point source value in dB unit according to the length of the line source. The value in dB/m unit expresses the sound power of a point source that if summed l times will provide the same sound power level as the line source. To this end, the dB/m value must be added up l times by energetic summation according to Equation 12.

$$PS_{eq} = 10 \cdot log_{10}(l \cdot 10^{LS \cdot 0.1}) \qquad 12$$

Where

PS_{eq}	equivalent point source that has the same overall sound power as the line source [dB],
l	length of the line source [m], and
LS	line source (output of CNOSSOS calculation) [dB/m].

The results of the conversion are in Table 16.

Table 16 Sound power level of equivalent point sources [dB]

PSeq	**63**	**125**	**250**	**500**	**1k**	**2k**	**4k**	**8k**
PSeq,1	71.8	62.5	61.9	61.5	61.8	62.1	57.3	50.9
PSeq,2	90.8	81.2	80.7	79.2	80.0	79.2	74.6	67.7
PSeq,3	96.5	86.9	86.3	84.9	85.7	84.9	80.3	73.4
PSeq,4	94.5	84.9	84.3	83.3	84.5	83.3	78.5	71.6
PSeq,5	98.0	88.3	87.8	86.4	87.3	86.5	81.8	74.9
PSeq,6	86.3	79.1	79.1	77.6	79.0	77.8	72.8	66.0
PSeq,7	99.4	92.1	91.7	90.5	92.2	91.1	86.1	79.2
PSeq,8	99.9	92.6	92.3	91.2	93.1	91.8	86.7	79.7
PSeq,9	90.3	83.0	82.8	81.7	83.5	82.2	77.1	70.2
PSeq,10	84.8	77.5	77.4	76.0	77.4	76.3	71.4	64.5
PSeq,11	92.1	84.9	84.7	83.5	85.4	84.1	79.0	72.1

At this point of the data formatting two ways can be followed. The values of Table 16 can be directly set up as equalizer values and in this case the base value of the point source is 0 dB for all sources. Another option could be to select a reference frequency, and define equalizer values with regard to the sound power at this octave band. In the example 1 kHz was taken as reference, and the equalizer values were arithmetically calculated. The equalizer values and the reference overall sound power levels are

listed in Table 17. As both methods return the same overall sound power by frequencies the simulated SPLs are not affected by this choice.

Table 17 Equalizer values [dB] and reference eq. sound power levels at 1 kHz [dB]

EQ	63	125	250	500	1k	2k	4k	8k	PSeq,1kHz [dB]
EQ1	10.0	0.7	0.1	-0.3	0.0	0.2	-4.6	-10.9	61.8
EQ2	10.8	1.2	0.6	-0.8	0.0	-0.8	-5.4	-12.3	80.0
EQ3	10.8	1.2	0.6	-0.8	0.0	-0.8	-5.4	-12.3	85.7
EQ4	10.0	0.4	-0.2	-1.2	0.0	-1.2	-6.0	-13.0	84.5
EQ5	10.7	1.0	0.5	-0.9	0.0	-0.8	-5.5	-12.4	87.3
EQ6	7.3	0.1	0.1	-1.4	0.0	-1.2	-6.2	-13.0	79.0
EQ7	7.2	-0.1	-0.5	-1.7	0.0	-1.1	-6.1	-13.0	92.2
EQ8	6.8	-0.5	-0.8	-1.9	0.0	-1.3	-6.4	-13.4	93.1
EQ9	6.8	-0.5	-0.7	-1.8	0.0	-1.3	-6.4	-13.3	83.5
EQ10	7.3	0.1	-0.1	-1.5	0.0	-1.1	-6.1	-12.9	77.4
EQ11	6.7	-0.5	-0.8	-1.9	0.0	-1.3	-6.5	-13.3	85.4

2.2.6 Receivers

The receivers in the model are defined by their x, y, z coordinates, and their direction is by default the x axis. In case of point sources the receivers could be directed towards the source. Furthermore, there are some geometrical rules that should be considered when placing the listeners. Namely, they should not be too close to any surfaces, otherwise secondary sources may fall too close to the receiver that would generate unrealistically big energy contributions.

The receiver to surface and the source to receiver distances must be sufficiently long according to ISO 3382-1:2009 (ISO, 2009) standard that gives information about the setup of spaces used for the measurements of acoustic parameters. According to the standard any receiver should stay away from surfaces by a quarter of a wavelength. This implies in case of 63 Hz (i.e. the smallest octave band in the simulation) 1.3 m. Based on this consideration the receivers in the model were placed 1.5 m in front of the facade. The minimum source – receiver distance is calculated according to Equation13.

$$d_{min} = 2\sqrt{\frac{V}{c \cdot T}} \qquad 13$$

Where

d_{min}	min. distance between the source and the receiver,
V	volume of the room [m^3],
c	speed of sound [m/s], and
T	expected reverberation time [s].

Taken into account the middle section of the model (i.e. Paulanergasse) the overall dimensions of a 150 x 15 x 25 m cuboid (V = 56250 m^3) and the reverberation times at receiver position of 7 m were used in the calculation. The calculated minimum values for the source – receiver distance are listed in Table 18. The speed of the sound in the calculation was 340 m/s.

Table 18 d_{min} by frequencies

f [Hz]	T30 [s]	d_{min} [m]
63	2.6	15.9
125	2.6	15.9
250	2.8	15.4
500	3.1	14.6
1k	2.9	15.1
2k	2.4	16.6
4k	1.7	19.7
8k	1.0	25.7

The actual source – receiver dimensions are listed in Table 19. The LS4 line source is the closest to the receivers, therefore the distance from all receivers to LS4 is measured. The height of the receivers above ground level is also indicated.

Table 19 LS4 – Receiver dimensions in the model

Source	Receiver	h [m]	d [m]	d > d_{min}
LS4	R1	1.5	6.2	no
	R2	4.0	7.3	no
	R3	7.0	9.3	no
	R4	10.0	11.8	no
	R5	13.0	14.4	no

The source – receiver distances for LS4 are smaller than required but for more distant sources the criterion is easily fulfilled. The bigger the difference between the actual and the required distances, the bigger the chance that unrealistic values will result in the simulation. Nevertheless, the height – width ratio of Paulanergasse is not extreme, and therefore, in case of simulations of urban canyons the same problem will always occur.

2.2.7 Simulation tool settings

The simulation tool settings under *Room setup* are unchanged throughout the baseline and the scenarios. Changes take place only in cases when the scenario focuses on the impact of such settings. The input parameters of room settings are listed in Table 20.

Table 20 Room setup settings

Parameter	Input value		Note
Impulse response length	2500	ms	based on Materials/Quick estimate
Number of late rays	10000		
Max. reflection order	2000		
Impulse response resolution	3 ms		
Transition order	0		in case line sources always 0
Nr. of early scatter ray(/ image source)	100		
Angular absorption	soft materials only		
Screen diffraction	yes		
Surface scattering	actual		based on material settings
Reflection based scatter	enabled		
Key diffraction frequency	707	Hz	
Interior margin	0.10	m	
Scatter coefficients above that handled as uniform scatter	0.50		

2.3 PA – Data processing of on-site measurements

The measurements in 1040 Wien, Paulanergasse 11, Kolpinghaus were taken on 18 April 2011 between 17:57 and 18:12 hours. Five microphones were hanged down in front of the facade from the roof terrace, each of them at different heights, namely at 1.5 m, 4 m, 7 m, 10 m, and 13 m above ground level. The type of measurement device at 1.5 height is called Rion, while the other four had the type Pulse. The duration of measurement captured 15 minutes, i.e. 900 seconds by a recording frequency of 0.1 second. Therefore, 9000 data point is provided for each third-octave frequency between 31.5 and 8000 Hz. The measured quantity was the A-weighted sound pressure level. Based on the frequency dependent A-weighted sound pressure level data over time the following data processing steps were done according to Figure 45.

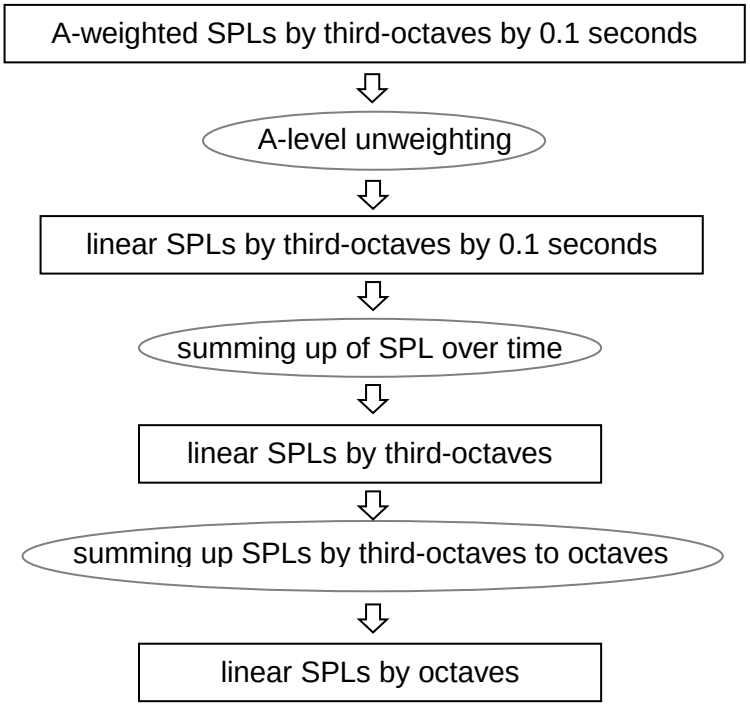

Figure 45 Steps of data processing of measured data

In the first step the A-weighted data set was unweighted, according to the A-weighting correction curve, see in Figure 46. The A-weighting factors by third – octave frequencies are listed in Table 21.

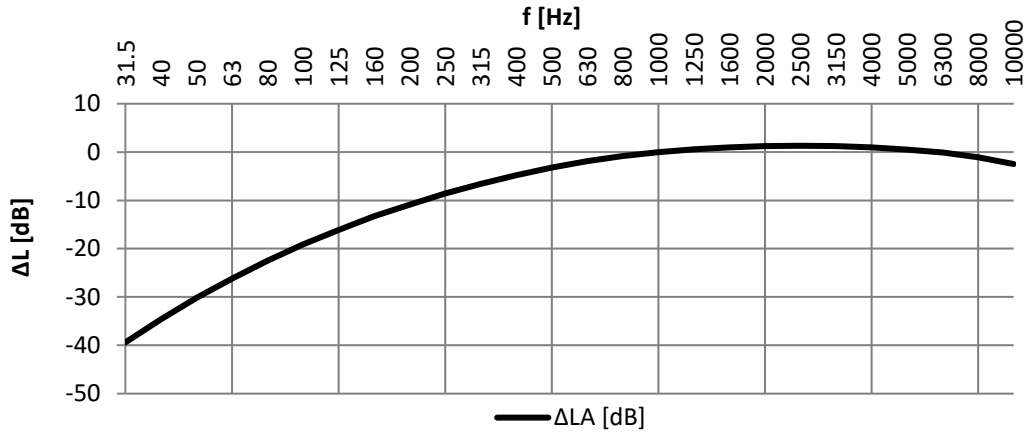

Figure 46 A-weighting curve

Table 21 A-weighting factors by third – octave frequencies

f [Hz]	31.5	40	50	63	80	100	125	160	200	250
ΔLA [dB]	-39.4	-34.6	-30.2	-26.2	-22.5	-19.1	-16.1	-13.3	-10.9	-8.6

f [Hz]	315	400	500	630	800	1000	1250	1600	2000	2500
ΔLA [dB]	-6.6	-4.8	-3.2	-1.9	-0.8	0	0.6	1.0	1.2	1.3

f [Hz]	3150	4000	5000	6300	8000	10000	12500	16000
ΔLA [dB]	1.2	1.0	0.5	-0.1	-1.1	-2.5	-4.3	-6.6

In the second step the continuous equivalent sound level of the dynamically changing noise event (L_{eq}) was calculated to each third-octave frequency, according to Equation 14. The 9000 data points per third-octaves are recorded by a steady frequency, namely 0.1 seconds. Therefore, the equation can be simplified according to Equation 15 (in detail see Appendix).

$$L_{eq} = 10log\left\{\frac{1}{T}\int_0^T 10^{L_i \cdot 0.1}\, dt\right\} = 10log\left\{\frac{1}{T}\sum t(i) \cdot\ 10^{L_i \cdot 0.1}\right\} \qquad 14$$

$$L_{eq} = 10log\left\{\frac{1}{n}\sum\ 10^{L_i \cdot 0.1}\right\} \qquad 15$$

Where

T	total length of time, the sum of $t(i)$ time intervals,
$t(i)$	length of the ith time interval,
t	length of one time interval when all are the same length,
L_i	sound pressure level measured during the ith time interval, and
n	number of time intervals (the number of data points).

In the last step the third-octave band SPLs were summed up into octave band, and thereafter, into single value SPLs. These SPLs are used as reference with regard to simulated data sets. The measured data was processed according to this method and the results for all five microphone positions are presented in the Appendix.

2.4 Performance indicators of SPL analysis

Although the in-situ SPL metering provided SPLs in dB(A) during the analysis of results the linear value of sound pressure will be used (i.e. dB unit). The reason behind is to fully account for the reality and to detect causality between input data and the results easier.

The A-weighting curve is defined in the International standard IEC 61672:200 and it was adjusted to follow the sensitivity of human ear in lower SPL ranges around 40 dB. However, today it is used at louder SPLs as well, which is questionable. The weighting values are arithmetically added to the linear SPLs measured by the instrument to account for the perceived loudness. The unit of the A-weighted SPL is dB(A).

At low frequencies the SPL reduction due to A-weighting is larger, while at middle and slightly high frequencies the correction factors are close to zero or even positive, which accounts for the higher sensitivity of human ear at these bands.

However, the human ear sensitivity increases in the lower frequency range with higher SPLs, and therefore using A-weighting at the SPL of traffic noise would underestimate the perceived loudness of low frequencies. C-weighting accounts for this phenomenon by applying less reduction in low frequencies than A-weighting, and the weighting factors are negligible compared to the precision of the simulations. Due to this consideration the linear SPLs were used throughout the evaluation of the results.

The octave frequency based results allow to make statements about specific frequencies at a certain listener position.

Furthermore, the maximum positive and negative deviations from measured data will be listed together with frequency the occurrence. This two number indicator ($\Delta_{+,max}$, $\Delta_{-,max}$) helps to assess the range of deviation compared to the reference data set. $\Delta_{+,max}$ stands for the maximum positive (or the smallest negative), and $\Delta_{-,max}$ for the maximum negative (or smallest positive) deviation from the reference.

Nevertheless, it is difficult to assess the overall agreement between the reference and the scenario based on frequency based results. Therefore, in order to give a single number indicator per listener another indicator was introduced. This indicator is the root mean square deviation, which is calculated according to Equation 16. This indicator characterizes the spread of a data set from reference values. The deviation of the data from the reference value set is shown on Figure 47. The smaller the RMSD value the better the agreement between any data set and the reference.

$$RMSD = \sqrt{\frac{1}{i}\sum \Delta_i^2} \qquad 16$$

Where

$RMSD$	root mean square deviation of the data set from reference data set,
i	number of data points (index), and
Δ_i	deviation of the data point from reference value (see Figure 47).

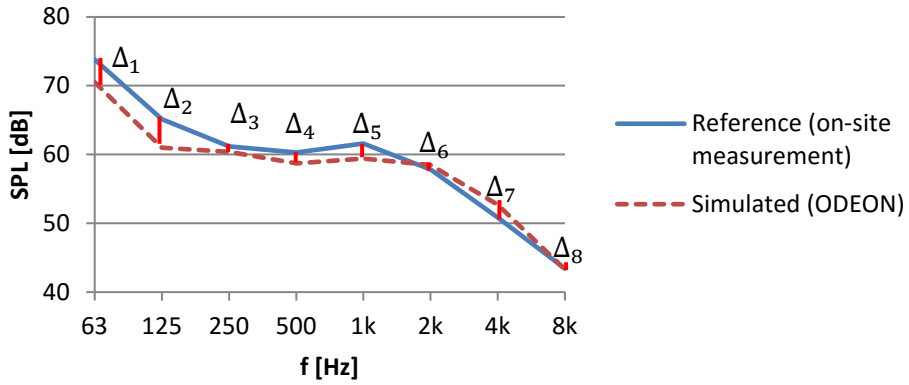

Figure 47 Deviation of data set from reference

In terms of the impact analysis a smaller RMSD indicates that results are less sensitive to the input parameter while a high value implies a more significant impact.

2.5 Comparison of input data of PA and KO

The scope of this chapter is to give a better insight into the similarities and differences between the two locations under investigation. The comparison is carried out both in descriptive, tabular, and graphical form. The main aspects of comparison are the street geometry and the characteristics of traffic flow, but other properties that may influence the results are mentioned and some uncertainties are revealed.

With regard to geometry both PA and KO venues are located in a densely-built area, however, the height – width ratio of their cross-section is different as shown in Figure 48.

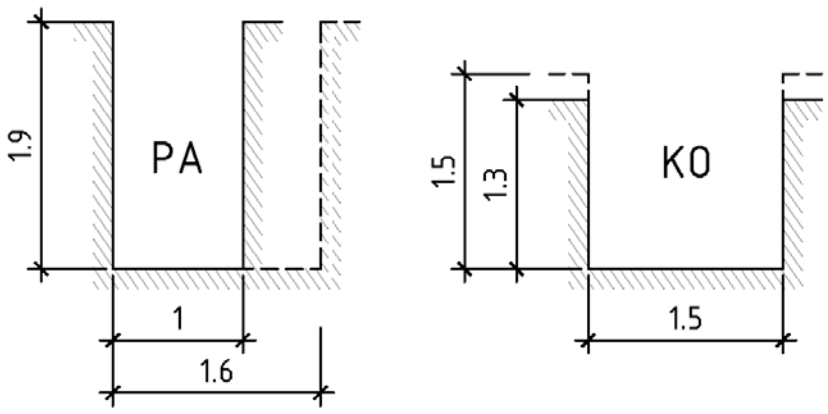

Figure 48 Height – width ratio of Paulanergasse and Koppstraße

Taken the width of PA as the unit, its H/W ratio is between 1.2:1 and 1.9:1. Thus, it is rather narrow and high with a significant variation in the width along the length of the street. On the other hand, KO has a constant width and H/W ratio of 0.85:1 - 1:1 with little deviations in the height of the buildings. Furthermore, while PA has a slightly curved shape and it crosses neighbouring streets in a sharp angle, KO is straight and cross-streets are connected perpendicularly.

With regard to listeners position in PA the measurement location was in the middle along the length of the street, while in KO the microphones were rather close to a corner. Although no traffic noise is expected from the cross-street around the corner due to its very low traffic, its cross section represents a highly absorbing area close to the receivers.

With regard to the spatial distribution of the traffic flow levels the two locations are very different. In case of KO the traffic is remarkable in the street of the receivers but negligible in cross-streets. On the contrary, in PA the street has lower traffic flow and cross-streets are busier. The speed limits follow the pattern of the traffic density. In KO vehicles must not exceed 50 km/h and in cross-streets 30 km/h, while PA it is the other way around. The traffic flows and speed limits are listed in Table 22. The speed limits can be read from Figure 33 as well.

Table 22 Traffic flow of line sources – Q [1/h] of PA and KO

Vehicle category	**PA**	**PA cross-street**	**KO**	**KO cross-street**
1	321.0	1153.8	1864.6	381.5
2	9.0	27.7	9.2	3.1
3	0.0	0.0	0.0	0.0
4a	27.0	87.7	46.2	3.1
4b	0.0	4.6	0.0	0.0
Speed limit [km/h]	30	50	50	30

In KO it was noticed that the level of the traffic flow is highly dependent from the exact time at which the measurements were taken. The metering took place from 17:17 to 17:49, i.e. about 30 minutes. The vehicles both in KO and in one of the cross-streets were counted twice, and therefore, both an earlier and a later data set is available. The difference between them was found to be significant. With reference to the earlier metering the traffic in KO and in the cross-streets dropped by 74% and 39% respectively. The results of the earlier and later traffic metering and the change in percentage are listed in Table 23.

Table 23 Traffic flows of the earlier and later metering in KO [1/h]

	earlier [1/h]		later [1/h]		change [%]	
Vehicle category	**street**	**cross-str.**	**street**	**cross-str.**	**street**	**cross-str.**
1	1864.6	381.5	1144.6	100.0	-39	-74
2	9.2	3.1	9.2	0.0	0	-100
3	0.0	0.0	0.0	0.0	-	-
4a	46.2	3.1	9.2	0.0	-80	-100
4b	0.0	0.0	0.0	0.0	-	-

Furthermore, both locations have one-way traffic flow. However, PA has only one lane, while KO has two. Nevertheless, all parallel lanes are represented by a single line source in the simulation regardless of their real number. The sound power of line sources of PA and KO is shown in Figure 49.

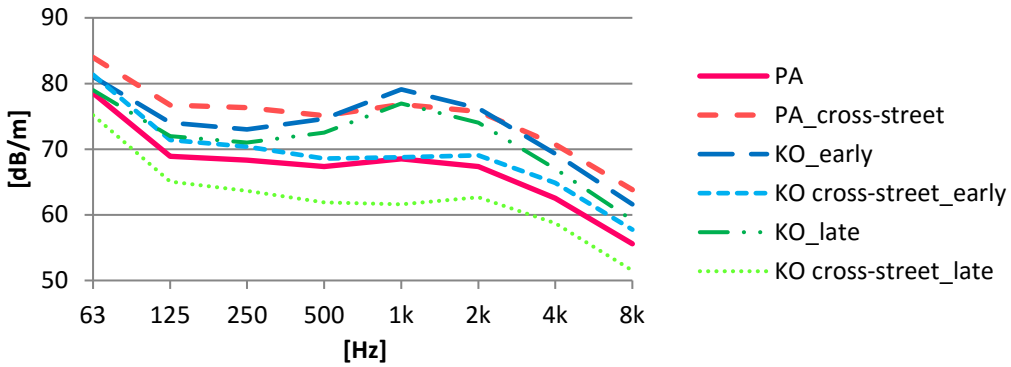

Figure 49 Sound power of source lines in PA and KO

The sound power levels from PA and KO early metering data are rather similar. However, their sound power level curve over frequencies have different shapes. While in case of PA the curve either falls or stays constant, for KO_early and KO_late there is a local peak around 1000 Hz. One explanation could be that in case of higher overall traffic flows the lack of category 2 type vehicles (e.g. buses) is responsible for the drop in sound power level at lower frequencies such like KO_early and KO_late. In comparison, PA_cross-street has a high overall traffic flow with a significant number of heavy vehicles that results in a curve with no drop in lower frequencies. The local peak at around 1000 Hz and the drop at lower frequencies is therefore just two different interpretation of the same curve. In case of an overall low traffic flow, which

is the case in cross-streets of KO, the lack of heavy vehicles does not play a role, namely there is no drop at 125 and 250 Hz frequencies.

With regard to miscellaneous objects the parking cars and vegetation may have an impact on sound propagation, especially on the scattering potential of the surfaces. In both streets there are parking cars on the two sides, in PA parallel and in KO perpendicular to the axis of the street. Furthermore, KO has trees on both sides while in PA there is no vegetation. Although the measurements in KO were taken on 21 March (i.e. at a very early canopy stage) the scattering effect of trees with bare branches may be important.

Finally, the facades of the buildings were found to be very diverse in PA with regard to age and the applied materials, while all were rather the similar in KO. Nevertheless, the same averaged absorption coefficients were used for both locations. The eventual errors due to this simplification are negligible taking into consideration the level of difference in absorption data between different facades as it was shown in Figure 27.

The areas of surface types and the volume of the models are listed in Table 24. These values are derived from a model with sky type closed at the top of the facades. The ratio of each surface type with regard to the sum is also shown on a pie diagram in percentages in Figure 50.

Table 24 Area of surface types and volume in PA and KO

Surface	**PA [m2]**	**KO [m2]**
sky	7208	10372
ground	6094	9891
facade	12420	14361
boundary 1*	1732	1860
boundary 2**	484	973
SUM [m^2]	27938	37457
Volume [m^3]	95162	151689

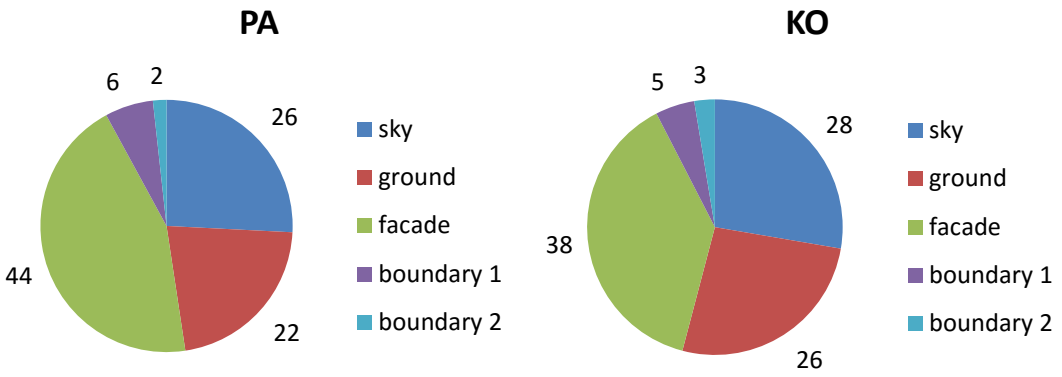

Figure 50 Percentage of surface types in PA and KO model

Although there is a bigger difference in the ratio of facade and ground surfaces between the two model, 44% vs. 38% and 22% vs. 26% respectively, taking the sum of these two types for both models it yields almost the same values, 66% vs. 65% respectively. The deviation can be explained by the difference in H-W ratios. In PA the buildings in general are higher, and therefore the ratio of facade surfaces is bigger.

Moreover, Table 25 gives information about the specific area of each surface type when 1000 m^3 of the model is considered. As expected, due to H-W ratios there is a notable difference between the two model in case of facades and boundary surfaces, the latter of which are also a sort of facade surfaces.

Table 25 Area of model surfaces for 1000 m^3 of the model

Surface	**PA [m^2/m^3]**	**KO [m^2/m^3]**
sky	76	68
ground	64	65
facade	131	95
boundary 1*	18	12
boundary 2**	5	6

Figure 51 shows that most surface types have only very little contribution to the total Sabine area at a specific octave band compared to the sky surfaces and the air. The equivalent Sabine area of the air is calculated by Odeon and has major influence in the highest frequency ranges. The only significant difference between the two model is the share of the sky`s Sabine area that is much higher in PA.

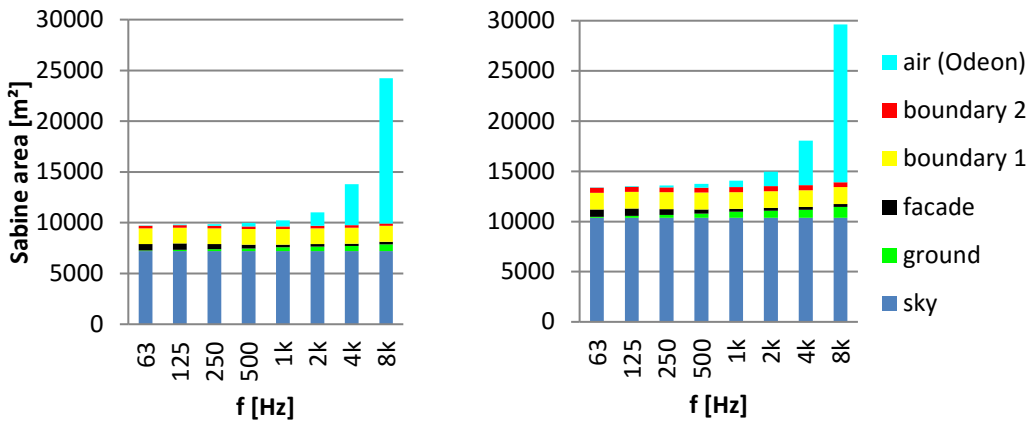

Figure 51 Sabine areas of PA and KO model

The Sabine areas are shown in Figure 52 by octave frequencies for both models including the absorption of the air. The difference between the two data sets is even throughout all frequency ranges and attributed to the deviations in the sky`s Sabine area.

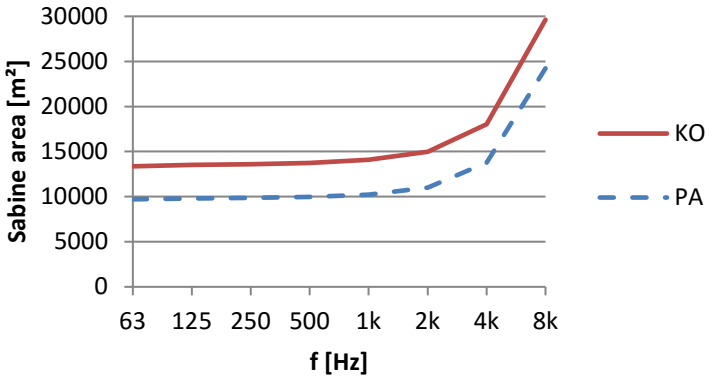

Figure 52 Sabine areas of PA and KO model

Finally, an area-weighted average absorption was calculated for both models, and it was found, that in spite of the differences in the geometry these data sets are very similar. The frequency dependent absorption data sets for both models with and without the absorption of the air are listed in Table 26. As expected, notable difference between the data sets with and without the effect of the air was detected only in 2 kHz – 8 kHz bands, and the two models returned very similar values.

Table 26 Avarage absorption of PA and KO model by frequencies with and without air

	63	**125**	**250**	**500**	**1k**	**2k**	**4k**	**8k**
PA_{avg}	0.35	0.35	0.35	0.34	0.34	0.35	0.35	0.36
$PA_{avg,with\ air}$	0.35	0.35	0.35	0.35	0.36	0.38	0.43	0.57
KO_{avg}	0.36	0.36	0.36	0.36	0.36	0.36	0.36	0.37
$KO_{avg,with\ air}$	0.36	0.36	0.36	0.36	0.37	0.38	0.43	0.56

The findings suggest that urban situations with comparable street geometry, H/W ratio, road type, and building stock have very similar bulk properties in terms of absorption characteristics. Therefore, if no significant alterations in these parameters occur, the input data derivation may be simplified.

3 RESULTS

3.1 PA – Baseline

In the Figure 53 the measured and the simulated SPLs are shown for each receiver position at different heights and the performance indicators are listed in Table 27. In case of the maximum positive and negative deviations the frequency bands are also given.

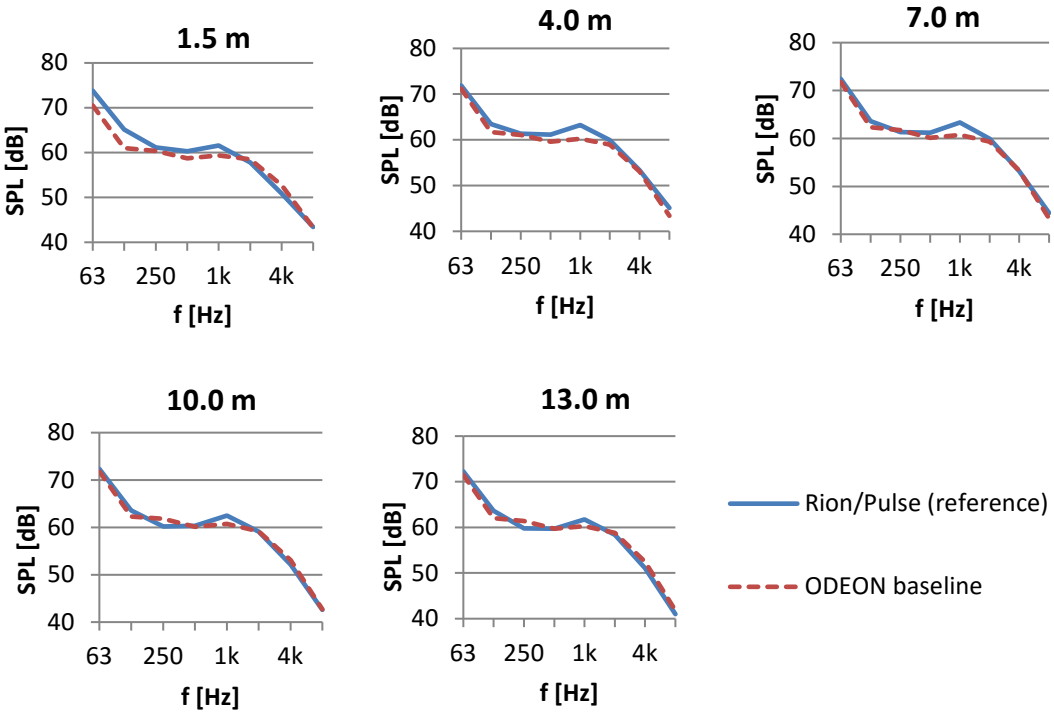

Figure 53 PA Measured (Rion/Pulse) and simulated (Odeon baseline) SPLs [dB]

Table 27 PA Baseline - performance indicators [dB]

Indicator	1.5 m	f [Hz]	4 m	f [Hz]	7 m	f [Hz]	10 m	f [Hz]	13 m	f [Hz]
$\Delta_{+,max}$	1.84	4k	-0.22	250	0.37	250	1.59	250	1.61	250
$\Delta_{-,max}$	-4.13	125	-3.03	1k	-2.63	1k	-1.78	1k	-1.66	125
RMSD	2.23		1.54		1.23		1.04		1.16	

3.2 KO – Baseline

In the Figure 54 the measured and the simulated SPLs are shown for each receiver position at different heights and the performance indicators are listed in Table 28. In case of the maximum positive and negative deviations the frequency bands are also given.

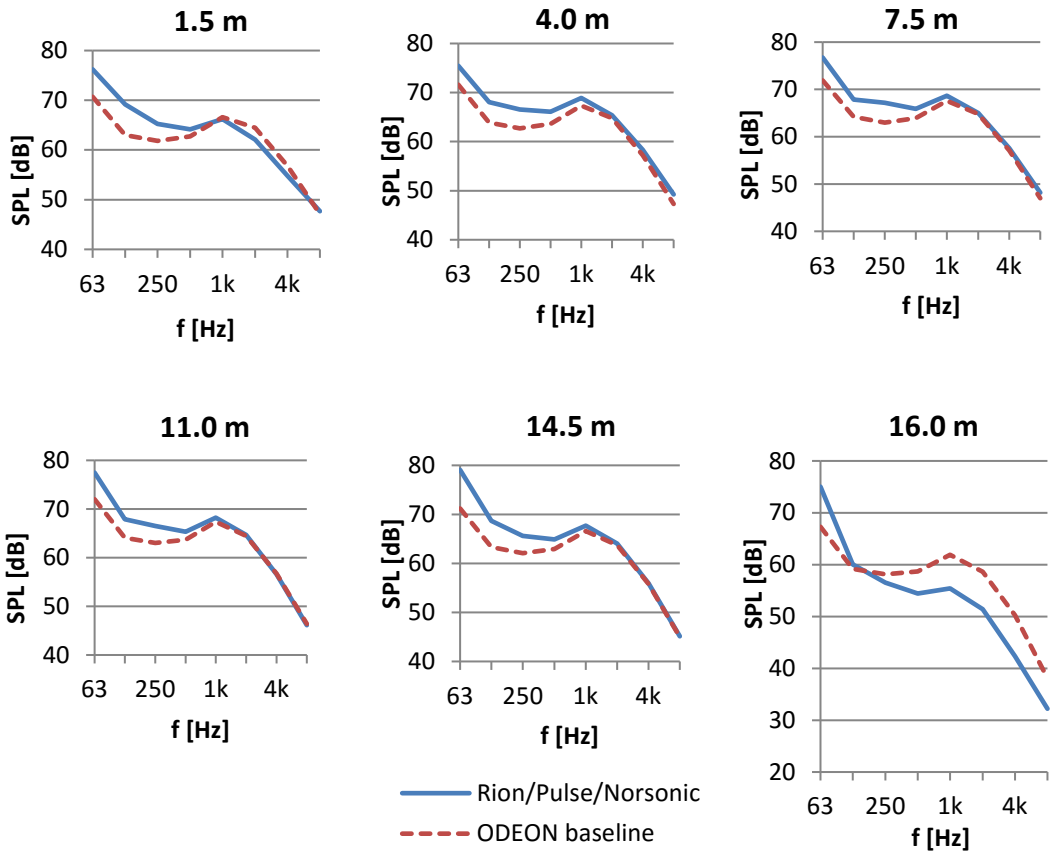

Figure 54 KO Measured (Rion/Pulse/Norsonic) and simulated (Odeon baseline) SPLs [dB]

Table 28 KO Baseline 1 - $\Delta_{+,max}$, $\Delta_{-,max}$, and RMSD [dB]

Indicator	1.5 m	[Hz]	4.0 m	[Hz]	7.5 m	[Hz]
$\Delta_{+,max}$	2.44	2k	-0.57	2k	-0.24	2k
$\Delta_{-,max}$	-6.20	125	-4.14	125	-4.84	63
RMSD	3.41		2.76		2.76	

Indicator	11.0 m	[Hz]	14.5 m	[Hz]	16.0 m	[Hz]
$\Delta_{+,max}$	0.27	8k	-0.13	4k	7.88	4k
$\Delta_{-,max}$	-5.48	63	-7.87	63	-7.73	63
RMSD	2.74		3.68		5.83	

3.3 PA and KO – on-site and baseline

In the next chapters only the results for receiver at 4.0 m height will be provided at frequency level. Table 29 and Figure 55 gives information about the baselines of PA and KO for receiver at 4.0 m and the agreement with on-site measurements.

Table 29 PA and KO, receiver at 4.0 m, on-site, baseline, and ΔSPL [dB]

f [Hz]	PA [dB]			KO [dB]		
	on-site	baseline	ΔSPL	on-site	baseline	ΔSPL
63	71.89	71.50	-0.39	75.46	71.90	-3.56
125	63.43	61.90	-1.53	68.04	64.20	-3.84
250	61.32	61.40	0.08	66.53	62.90	-3.63
500	61.15	59.70	-1.45	66.09	63.80	-2.29
1k	63.23	60.40	-2.83	68.92	67.40	-1.52
2k	59.95	59.10	-0.85	65.37	64.80	-0.57
4k	53.37	53.20	-0.17	58.31	57.10	-1.21
8k	45.11	43.50	-1.61	49.24	47.20	-2.04

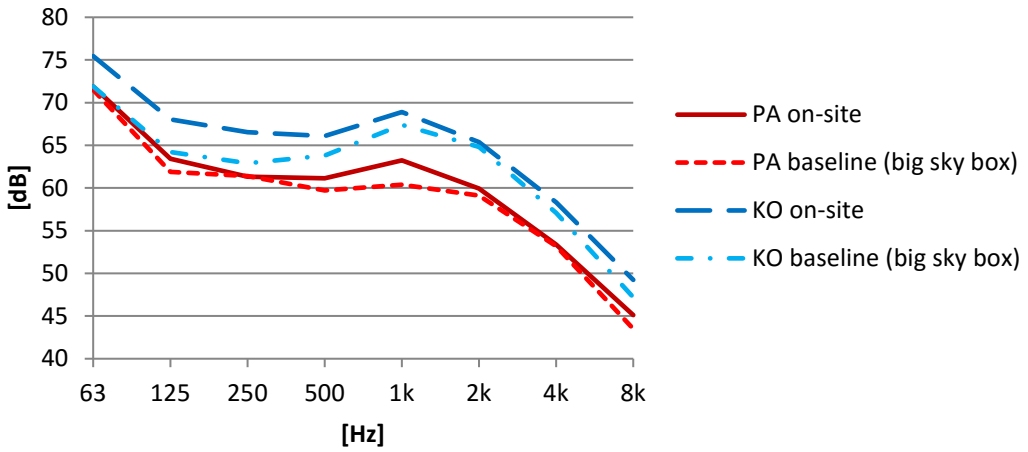

Figure 55 PA and KO - Measured and simulated linear SPL at 4.0m

Both in case of PA and KO the simulated values meet rather precisely the measured data from above 2 kHz. However, PA shows the biggest deviation at 1 kHz, while KO has an even more noticeable error at frequencies below 500 Hz. In both model the

simulation slightly underestimates SPLs throughout the frequency ranges. It is also visible, that KO is a noisier street than PA.

3.4 Impact analysis of input data

The scope of this study is to investigate the impact of input parameters on simulation results. Therefore all scenarios are compared to a baseline that was also simulated by Odeon. Therefore, the findings of the sensitivity analysis are valid within the range of the computer simulation. Possible adjustments on input data in order to reach a better agreement between measured and simulated SPLs are explored in KO where the degree of difference was notable at low frequencies.

In order to get a more compact overview of the findings only the results for the receiver at 4.0 m height are presented with octave frequency resolution. The receiver positions at 7.0, 10.0, and 13.0 m in PA (7.5, 11.0, and 14.5 m in KO respectively) usually have very similar values to that of 4.0 m, however, the results at 1.5 and 16 m are rather outliers due to the close vicinity of ground and sky surfaces.

The data set of the scenario will be compared to both the measured and the baseline dataset for receiver at 4.0 m height, and the RMSD values by listener positions will be presented on line graphs.

3.4.1 PA – Sky types

Theoretically, if a ray leaves the urban canyon it never comes back. Therefore, a sky can be represented by surfaces with 100% absorptance and any sky types should return the same results. However, during the impact analysis study it was found that the different sky type representations do not always result in the same SPLs. Moreover, in case of sky type connected to the top of the facade the model was found to be unstable. That means, although no change was applied in the input data or room settings, a new run of the simulation returned different SPLs as before. The two results simulated by sky type closed at the facades are named as baseline 1 (earlier) and baseline 2 (later). The SPLs of baseline 2 (BL2) were about 1 dB higher than baseline 1 (BL1) and once the shift from BL1 to BL2 occurred, the results did not return to BL1. This phenomenon is attributed to minor deviations in the simulation run that are independent form user settings. Although the difference between BL1 and BL2 is usually not more than 1 dB, which is the JND (just noticeable difference) for the human

ear, this deviation is big enough to compromise the impact analysis. As scenarios are always developed from the baseline model this must be solid in terms of stability of the results. Therefore, throughout the impact analysis the sky will be represented by the big box sky type.

The simulation results of BL1 and BL2, which are derived from a model with sky surfaces connected to the top of the façade, and their difference are listed in Table 30 for the receiver at 4.0 m. Furthermore, Table 31 gives information about the agreement of BL1, BL2, small-, and medium sky types with regard to the baseline with big box sky representation.

Table 30 PA, SPLs at 4.0 m – BL1, BL2, ΔSPL [dB]

f [Hz]	**BL 1**	**BL 2**	**ΔSPL**
63	71.2	72.2	1.0
125	61.7	62.6	0.9
250	61.1	62.1	1.0
500	59.6	60.5	0.9
1k	60.2	61.2	1.0
2k	59.0	60.0	1.0
4k	53.1	54.3	1.2
8k	43.4	45.2	1.8

Table 31 PA, RMSD for BL1, BL2, small-, and medium sky box vs. big sky box [dB]

	BL1	BL2	small	medium
1.5 m	0.2	1.0	1.2	0.0
4.0 m	0.2	1.0	1.0	0.0
7.0 m	0.1	0.9	0.9	0.0
10.0 m	0.1	0.8	0.7	0.1
13.0 m	0.2	0.5	0.6	0.0

The findings on sky types are illustrated on Figure 56. A smaller RMSD value indicates better agreement between the scenario and the baseline, and therefore, it is clear that small sky box results are closer to BL2 while those of medium and big sky boxes are more similar to BL1. This implies that above a certain size of sky box the resulting SPLs are not sensitive to the dimensions of the box.

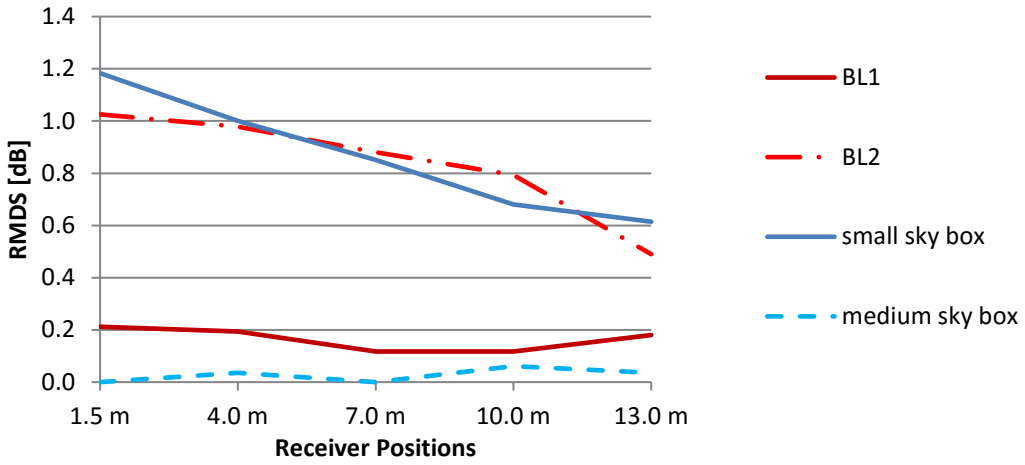

Figure 56 PA – sky types, all receivers, RMSD [dB]

3.4.2 PA – Boundary 1, 2 and scattering coefficient

The following two chapters include the findings of all scenarios where any material properties of surfaces are changed. The modification may affect only a specific surface type (e.g. façade) or influence the whole mode. In terms of absorption coefficients the subjects of the impact analysis are: the glass type, the facades and the boundary 1 and 2 surfaces. Moreover, the impact of scattering coefficients including all surfaces was investigated.

Boundary 1 and 2 are imaginary vertical surfaces that close the cross sections of the streets in the model and therefore represent the rest of the street that is out of the range of the model. The extent of the model should be big enough so that the properties of boundary 1 and 2 surfaces have little effect at the receiver positions. The impact analysis on their absorption coefficient can prove this criterion.

Furthermore, the derivation of scattering coefficients is based on merely recommendations from Odeon manual, i.e. they may differ from real values. Therefore, the impact of their scattering coefficients must be detected taking into account all surfaces.

The input parameters of the baseline and the scenarios are listed in Table 32 and Table 33.

Table 32 Absorption coefficients of boundary 1 and 2 surfaces for 63 – 8k Hz (baseline and scenarios)

surface	baseline	0.01	0.1	0.9
boundary 1	0.90	0.01	0.10	0.90
boundary 2	0.50	0.01	0.10	0.90

Table 33 Scattering coefficients of all model surfaces (baseline and scenarios)

surface	baseline	+ 50 %	full
sky	0.05	0.075	1
façade	0.20	0.30	1
ground	0.30	0.45	1
boundary 1, 2	0.50	0.75	1

Table 34 gives information about the ΔSPLs [dB] and RMSD [dB] at receiver at 4.0 m.

Table 34 PA, receiver at 4.0 m, ΔSPL and RMSD for boundary 1, 2 and scattering scenarios vs. baseline [dB]

f [Hz]	baseline	boundary 1 2_0.01	boundary 1 2_0.1	boundary 1 2_0.9	scattering + 50%	scattering full
63	71.5	0.4	0.3	-0.1	-0.1	1.4
125	61.9	0.6	0.5	-0.1	-0.1	1.3
250	61.4	0.6	0.5	-0.1	-0.2	1.3
500	59.7	0.7	0.6	-0.1	-0.3	1.6
1k	60.4	0.7	0.6	-0.1	-0.1	1.9
2k	59.1	0.6	0.5	0.0	0.9	1.8
4k	53.2	0.3	0.2	0.0	0.8	1.8
8k	43.5	0.1	0.1	0.0	0.6	1.5
RMSD [dB]		0.5	0.4	0.1	0.5	1.6

The absorption coefficient of the street closing boundary surfaces has little effect on simulation results. The maximum difference between the two extreme scenarios - those of highly reflective and very absorbing - was 0.8 dB. The scenario with absorption coefficient of 0.01 yielded a 0.7 dB increase, while the most absorbing scenario resulted in SPLs at most 0.1 dB lower than baseline. Overall, the boundary surfaces have some effect on the SPLs at receiver positions, but the range of fluctuation of the results is within 1 dB, i.e. the JND. The low level of the change can be explained by the small ratio of boundary 1 and 2 type surfaces in the model and by their big distance from the receiver positions. In order to keep the middle road within this 1 dB range the absorptance of street closing boundary surfaces should be less absorbing than it was in the baseline.

With regard to the increase of scattering coefficients the SPLs have shown a rise in most frequency ranges and at all heights. In case of full scattering the level of impact is inversely proportional to the height above the ground, i.e. deviations are more notable at lower levels. However, for + 50% scenario the change is even throughout the different floor levels. As expected, the full scattering scenario affected the results more than the + 50% one. The SPL deviance from the baseline was between - 0.7 and + 3.2 dB for full scattering while the maximum increase was 0.6 - 1.0 dB for + 50% scenario depending from receiver position. The effect of increasing the scattering coefficient at 13 m above the street level remained below 1 dB, and therefore, it is negligible. However, scattering coefficients affect SPLs to a great extent at lower levels, and thus, should not be over (or under) estimated. Figure 57 illustrates the RMSD values of the above mentioned two input parameters in dB for all receiver positions with regard to the baseline.

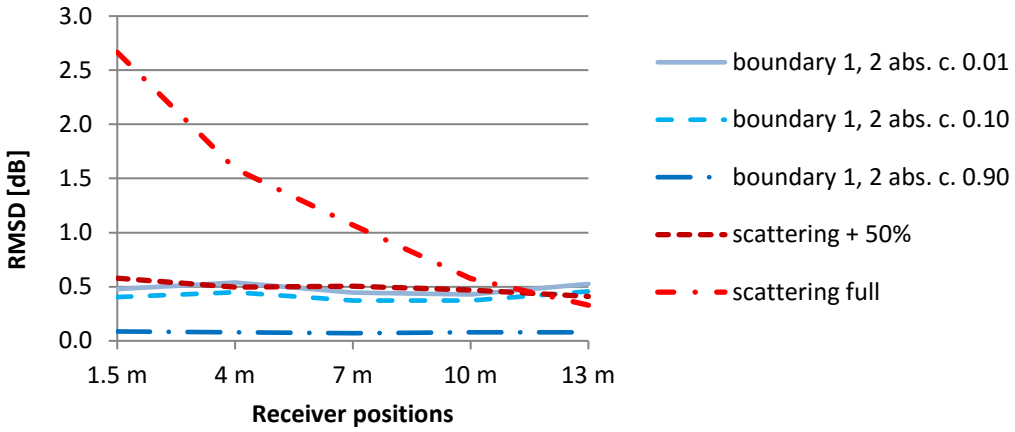

Figure 57 PA - boundary 1 and 2 surfaces and scattering, RMSD [dB]

Overall, it was found that the absorption properties of boundary 1 and 2 surfaces have a minor impact on results that is less that the JND and the level of change is independent from receiver position. On the contrary, a drastic rise in scattering coefficients caused significant increase in SPLs up to 2.5 dB and the level of change is highly dependent from the receiver position.

3.4.3 PA – Glazing type and facade absorption

In this chapter the level of impact of glazing types and the overall absorption properties of facades are investigated with regard to SPLs at receivers.

Regarding to glazing types two different surface materials were used from Odeon database: *double glazed* and *casement window*. The baseline model assumes double glazed glass material to each window, as the majority of windows are indeed double glazed. On the contrary, scenario *casement window* uses casement window (in German: Kastenfenster) material for all glass surfaces, while in scenario *mixed window* the ratio of the two window types is based on estimates of the reality, 65% double glazing and 35% casement window respectively. The absorption coefficients of the two glazing types are shown in Figure 58.

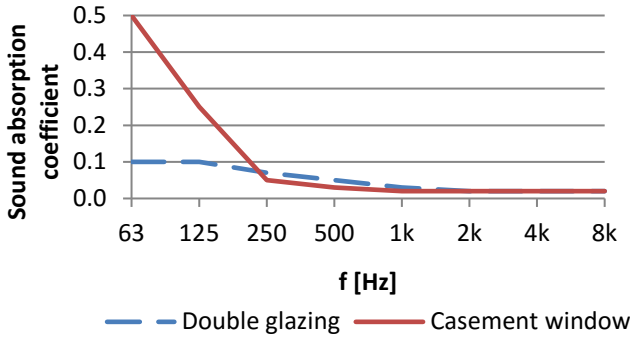

Figure 58 Absorption coefficients of double glazing (O 10003) and casement window (O 14400) materials from Odeon database

The absorption properties of casement window and double glazing are very different in the two lowest octave bands in favour of casement window with a significantly higher absorptance. The effect of glazing type on the level of façade absorption is less, as the facade consists of a number of other surfaces as well. The input data of facade materials according to glazing types is shown on Figure 59. Moreover, other three scenarios with altered absorption data throughout all frequency bands – -50%, +50%, and +100% respectively – are indicated.

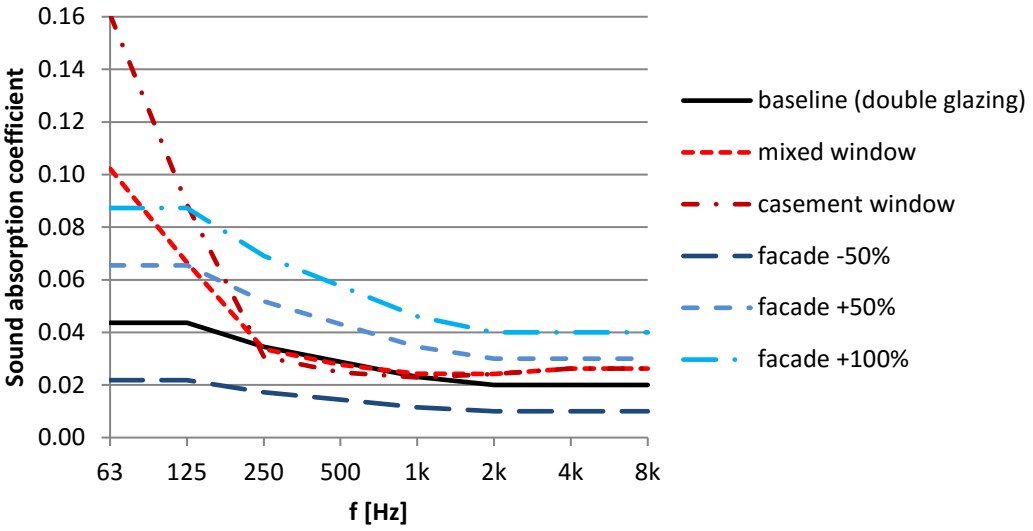

Figure 59 Area-weighted avg. abs. coeff. of facade materials – baseline and scenarios

Furthermore, a scenario with 0.5 absorption at all frequencies was tested in order to detect the potential of highly absorbing surfaces. In case of the baseline low frequencies absorb twice as much as high frequencies and this ratio is the same for *-50%*, *+50%,* and *+100%* scenarios. Although the *mixed window* and *casement window* scenarios have even higher absorption values at low frequencies, at higher octave bands they are rather similar to the baseline. Table 35 gives information about the ΔSPL and RMSD of scenarios with regard to the baseline at receiver position of 4 m.

Table 35 PA, receiver at 4.0 m, ΔSPL and RMSD for surface scenarios vs. baseline [dB]

f [Hz]	BL	casement window	mixed window	façade -50%	façade +50%	façade +100%	façade 0.5
63	71.5	-1.4	-0.7	0.2	-0.4	-0.6	-3.3
125	61.9	-0.6	-0.4	0.3	-0.4	-0.6	-3.2
250	61.4	0.0	0.0	0.1	-0.3	-0.5	-3.9
500	59.7	0.2	0.0	0.3	-0.1	-0.4	-4.2
1k	60.4	0.0	0.0	0.1	-0.2	-0.4	-4.6
2k	59.1	0.0	0.0	0.1	-0.1	-0.2	-4.1
4k	53.2	-0.1	-0.1	0.1	-0.1	-0.2	-3.6
8k	43.5	0.0	0.0	0.1	0.0	-0.1	-2.5
RMSD [dB]		0.5	0.3	0.2	0.2	0.4	3.7

The results show that in case of the *mixed window* scenario the maximum deviation from the baseline was 0.8 dB and as expected it occurred in the lowest frequency

bands. In case of scenario *casement window* the deviation was even greater, the maximum decrease in SPLs compared to baseline amounted to 1.3 - 1.6 dB at 63 Hz.

Overall, the results suggest that in a street with varying window types the use of either double glazing or casement window will cause a negligible effect. However, if a canyon with solely double glazed window is simulated with casement windows then the resulting SPLs will return lower values and therefore underestimate SPLs in low frequencies. Furthermore, it must be noted that a ca. 1.5 dB deviation at the lowest frequencies will not affect significantly the single value A-weighted SPL, as the weighting factor of low frequencies is very low compared to other frequencies.

The 50% reduction in absorption coefficients resulted in a max. 0.3 – 0.4 dB increase in SPLs, and the level of deviation from baseline was even throughout the frequencies. The 50% rise caused a fall in SPLs, and the level of change was very similar to scenario of -50%, namely 0.4 dB. Finally, the +100% absorption has approximately doubled the level of the deviation compared to scenario +50%, SPLs had a maximum drop of 0.6 - 0.7 dB.

A more drastic, however, less realistic scenario with façade absorption of 0.5 in all octave band frequencies yielded a significant fall in SPLs. The maximum decrease throughout the frequency ranges was 4.4 – 5.1 dB and the higher deviances occurred at higher levels above the ground. This meets the expectation that a more absorbing canyon should efficiently reduce the SPLs at higher levels by absorbing sound energy due to multiple reflections.

From the urban noise mitigation point of view the effect of increased absorption was found to be negligible. If the original surface is rather reflective, as it is the case for typical facades, then even doubling of the absorption (i.e. scenario +100%) has little impact on SPLs. However, if the façade finishing is highly absorbing (e.g. scenario 0.5) it can be an efficient means of noise mitigation especially at higher levels. Figure 60 gives information about the RMSD values in terms of glazing and facade absorptance scenarios.

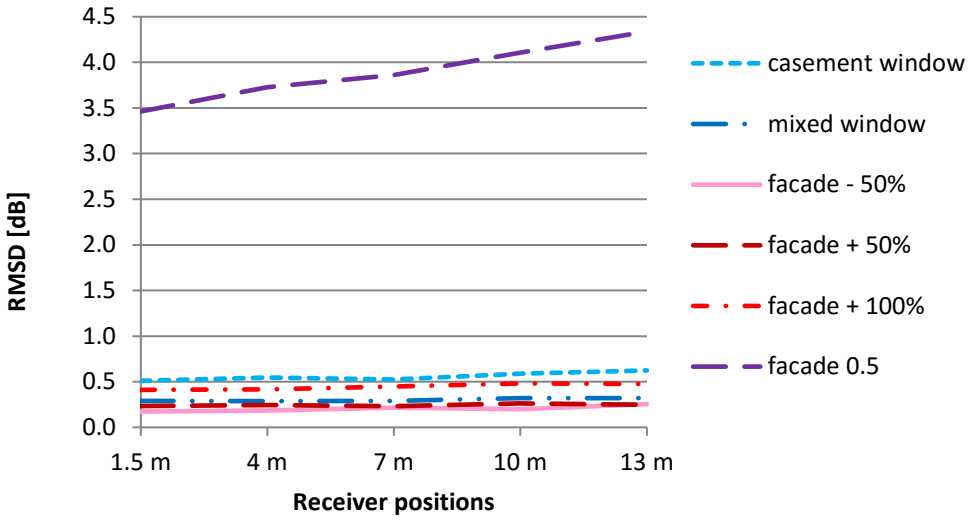

Figure 60 PA – glazing types and facade absorptance, all receivers, RMSD [dB]

3.4.4 PA – Road surface

The modification of road surface type is handled separately from other scenarios with altered material properties. This is due to the fact that a change in the road surface type affects both the absorption of the material in terms of model surfaces and the sound power of the source. The latter is a result of the CNOSSOS calculation method that takes into consideration the road material type. In order to account for the altered absorption properties of the road surface the material must be changed in Odeon. Moreover, in CNOSSOS the early reflections from the road surfaces are characterized with the coefficients $\alpha_{i,m}$ and β_m which describe the surface with regard to a reference road. Although CNOSSOS provides a table for $\alpha_{i,m}$ and β_m values for a number of road surface types, there is no information about the absorption data of those surfaces. As a consequence, absorption data must be investigated and taken from other sources, and thus, the consistency with the chosen surface type in CNOSSOS is questionable.

In the scenario a more porous road surface was assumed compared to the baseline. The changes of the input parameters in terms of absorption coefficients for Odeon and $\alpha_{i,m}$, β_m values for CNOSSOS are shown in Table 36 and Table 37.

Table 36 PA, surface types in Odeon – absorption coefficients of baseline and scenario

ID	Description	63	125	250	500	1k	2k	4k	8k
D_{avg}	dense graded asphalt (baseline)	0.01	0.02	0.03	0.04	0.06	0.07	0.08	0.11
S-12	10 month old semi dense 12% VC (scenario)	0.05	0.1	0.12	0.18	0.25	0.3	0.25	0.25

Table 37 PA, surface types in CNOSSOS – $\alpha_{i,m}$, β_m coefficients of baseline and scenario

Description	Veh. cat.	$\alpha_{i,m}$ 63	125	250	500	1k	2k	4k	8k	$\beta_{i,m}$
reference road surface (baseline)	1	0.0	0.0	0.0	0.0	0.0	0.0	0.0	0.0	0.0
1-layer ZOAB (scenario)	1	0.5	3.3	2.4	3.2	-1.3	-3.5	-2.6	0.5	-6.5

In order to track the impact of these two changes three scenarios were set up. In case of scenario *road surface* only the material properties were changed in Odeon, while in scenario *sound power* only the $\alpha_{i,m}$, β_m coefficients were modified. Finally, in scenario *r. surf. + s. p.* both changes took place. The SPLs for the baseline and the deviation of the three scenarios in dB are presented in Table 38 for receiver position at 4 m.

Table 38 PA, receiver at 4.0 m, ΔSPL and RMSD for road surface scenarios vs. baseline [dB]

f [Hz]	baseline	road surface	sound power	r. surf. + s. p.
63	71.5	-0.1	0.0	-0.1
125	61.9	-0.1	0.1	0.0
250	61.4	-0.2	0.1	-0.1
500	59.7	-0.3	1.2	0.9
1k	60.4	-0.4	-1.3	-1.7
2k	59.1	-0.2	-2.9	-3.1
4k	53.2	-0.4	-2.3	-2.7
8k	43.5	-0.3	-0.2	-0.5
RMSD [dB]		0.3	1.5	1.6

The results show a frequency dependent response of the altered input parameters. In all scenarios SPLs at low frequencies stayed rather unchanged, while between 500 and 4 kHz there is a perceivable sound reduction for *sound power* and *r. surf. + s. p.* scenarios. However, in case of *road surface* scenario the deviation stayed below the JND for all frequencies. Figure 61 gives information about the RMSD values in terms of road surface scenarios with regard to baseline.

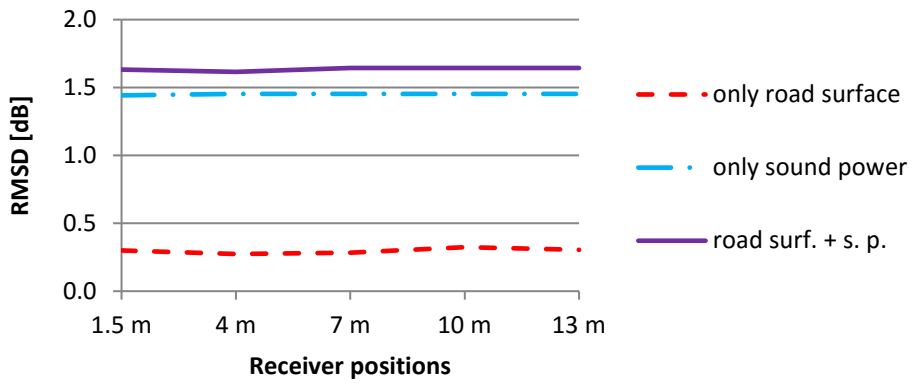

Figure 61 PA – road surface, all receivers, RMSD [dB]

Overall, it was found that even a significant rise in the absorption of road surfaces will not affect SPLs without the alteration of the sound power level. Consequently, the *sound power* and the *r. surf. + s. p. scenarios* resulted in very similar SPLs with a difference of 0.2 – 0.4 dB between them.

In Figure 62 the sound power level of LS4 is shown for both the baseline and the scenarios with modified sound power. In the Figure 63 the SPLs of the baseline model and the *r. surf. + s. p.* scenario can be seen. The SPLs curves follow the shape of sound power levels. Furthermore, at each octave band the difference in SPLs between baseline and scenario equals to that of the sound power levels (i.e. sound power levels and SPLs are highly correlated).

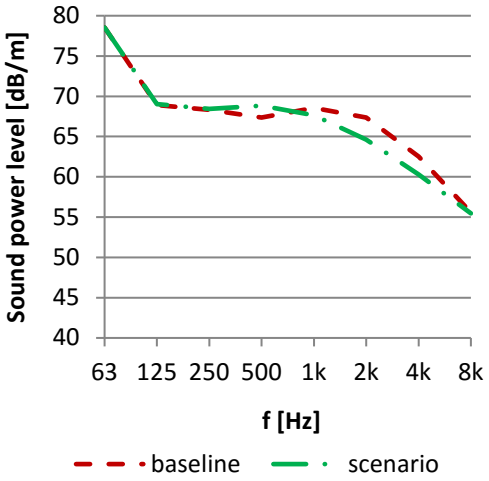

Figure 62 Sound power level of LS4 [dB/m] – baseline and scenario

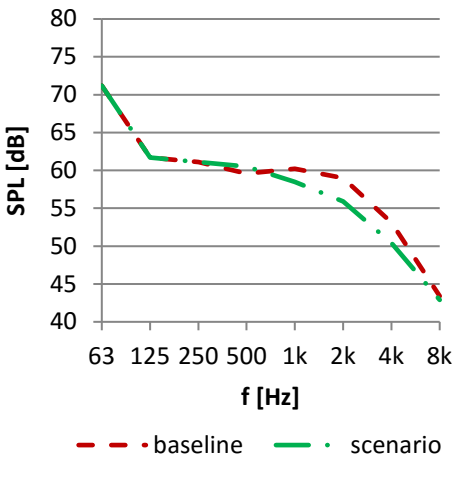

Figure 63 SPLs [dB] at receiver position 4.0 m – baseline and scenario

The derivation of reliable and consistent input data with regard to the categorization of the road surface material, the assignment of absorption data for Odeon and the selection of relevant road surface type in CNOSSOS remain an open question of this section.

3.4.5 PA – Road traffic

In this section the impact of traffic flow and vehicle speed input parameters are tested. With regard to the level of the traffic flow two scenarios were investigated: - 50% and + 50% flow in all vehicle categories. In case of vehicle speed the speed limit was altered by 10 km/h both as a rise and a drop. Both traffic flow and vehicle speed are input parameters for the sound power calculation and the deviation from baseline is shown with the example of LS4 on Figure 64.

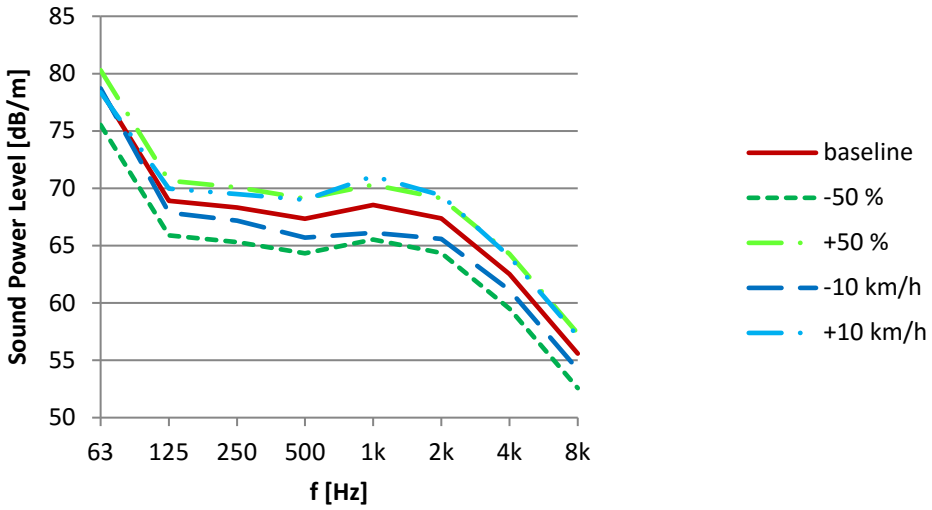

Figure 64 Sound power level of LS4 [dB/m] – baseline and scenarios

As expected, the rise in traffic flow and vehicle speed increased sound power level, and the + 50% and + 10 km/h scenarios give almost the same values. In the meanwhile, the - 50% drop in traffic flow has a bigger impact on sound power level than the - 10 km/h reduction of vehicle speed. Nevertheless, due to the logarithm scale of dB it is not obvious at this step which scenario would have higher level of impact in terms of SPLs. The SPLs of the baseline and the deviation of the 4 traffic scenarios in dB are presented in Table 39 for receiver position at 4 m.

Table 39 PA, receiver at 4.0 m, ΔSPL and RMSD for traffic scenarios vs. baseline [dB]

f [Hz]	Baseline	- 50%	+ 50%	- 10 km/h	+ 10 km/h
63	71.5	-3.1	1.8	0.1	-0.2
125	61.9	-3.1	1.9	-1.0	1.1
250	61.4	-3.1	1.9	-1.2	1.1
500	59.7	-3.1	1.9	-1.5	1.6
1k	60.4	-3.2	1.9	-2.2	2.3
2k	59.1	-3.1	1.9	-1.6	1.9
4k	53.2	-2.9	1.8	-1.3	1.5
8k	43.5	-2.9	1.8	-1.4	1.5
RMSD [dB]		3.1	1.9	1.4	1.5

Figure 65 gives information about the RMSD values in terms of traffic scenarios with regard to baseline.

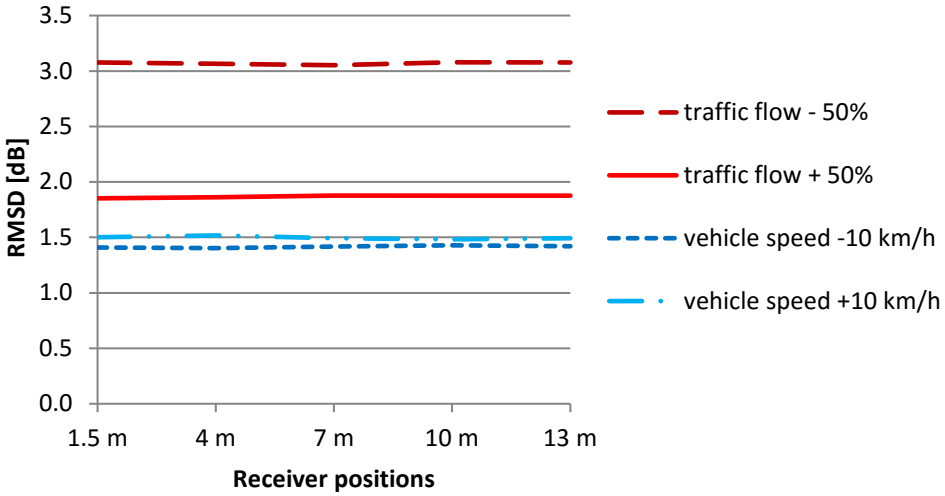

Figure 65 PA – traffic flow and vehicle speed, all receivers, RMSD [dB]

The -50% change in traffic flow resulted in a maximum reduction of the SPL by 3.2 dB including all receivers and the level of change is independent from the level above the ground or frequency. The +50% traffic flow yielded a maximum SPL increase of 2 dB and the deviation from the baseline is rather unchanged throughout all octave bands and receiver positions.

The increase of speed by 10 km/h caused a maximum rise in SPLs by 2.3 dB and the same level of reduction caused a maximum fall of 2.2 dB of SPLs. Both the maximum reduction and increase occurred at 1 kHz independent from receiver position. Overall, a 20 km/h speed difference (-10 km/h and +10 km/h scenarios) caused ca. 4.4 dB

difference at 1 kHz that is one of the most audible frequencies. (Note: 10 dB perceived as the doubling of loudness.) The reduction of the speed has a reverse effect at 63 Hz, it yielded higher SPLs than the baseline by ca. 0.2 dB. This is due to the increased propulsion noise at 63 Hz that is considered by a negative B_p coefficient in the CNOSSOS calculation method. To sum up, the 10 km/h reduction of speed limit has a perceivable impact around 1 – 2.2 dB fall in SPLs, and therefore, this can be an effective means of noise abatement.

Vehicle speed scenarios – method

The first vehicle speed scenario that had a reduction of vehicle speed of 10 km/h for all line sources surprisingly resulted in higher SPLs than the baseline. This is an anomaly, and therefore, the underlying reason was investigated. The SPLs of scenario -10 km/h and baseline 1 are plotted in Figure 66.

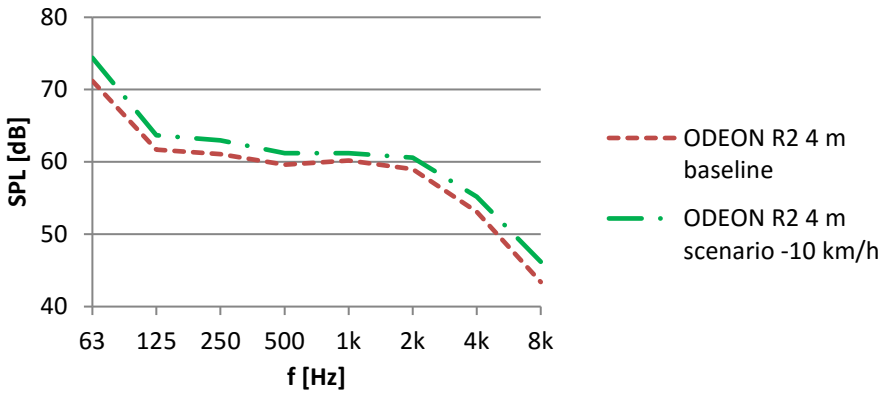

Figure 66 PA – SPLs [dB] of baseline and -10 km/h scenario without Q_m adjustment

It was found that the reason of this unexpected behaviour is a result of the last step of the CNOSSOS sound power calculation. The method calculates through multiple steps the sound emission of a single vehicle first, and in the last step based on the traffic flow and the vehicle speed ratio it is converted to the emission of the total traffic flow. The formula of this step is given in Equation 17.

$$L_{W',eq,line,i,m} = L_{W,i,m} + 10 \cdot lg\left(\frac{Q_m}{1000 \cdot v_m}\right) \qquad 17$$

Where

$L_{W',eq,line,i,m}$	sound power of traffic flow at i[th] frequency band, vehicle category m [dB],
$L_{W,i,m}$	sound power of single vehicle at i[th] frequency band, vehicle category m [dB],
$\mathrm{Q_m}$	traffic flow of vehicle category m [1/hr], and
$\mathrm{v_m}$	vehicle speed of vehicle category m [km/h].

The ratio of Q_m traffic flow [1/hr] and v_m vehicle speed [km/h] returns the number of vehicles in 1 metre. Therefore, if Q_m = 1000 and v_m = 50 km/h, then cars with 50 km/h follow each other by 50 metres. However, if v_m = 30 km/h, then the cars with 30 km/h follow each other only by 30 metres. Although the speed of the vehicles decreased from 50 km/h to 30 km/h, however, their density increased from 50 m to 30 m distance, and therefore, it is possible that the 30 km/h scenario returns higher SPLs than the baseline. In order to keep the density of the traffic flow constant, the Q_m value needs to be adjusted in accordance with the change in vehicle speed as it is shown in Equation 18.

$$Q_{m,2} = Q_{m,1} \cdot \left(\frac{v_{m,2}}{v_{m,1}}\right) \qquad 18$$

Where

$Q_{m,2}$	traffic flow of vehicle category m adjusted according to the change of vehicle speed [1/hr],
$\mathrm{Q_{m,1}}$	traffic flow of vehicle category m relating to $v_{m,1}$ [1/hr],
$\mathrm{v_{m,1}}$	vehicle speed of baseline, vehicle category m [km/h], and
$\mathrm{v_{m,2}}$	vehicle speed of scenario, vehicle category m [km/h].

With this adjustment of the traffic flow the density of cars stays constant by changing vehicle speed. On the other hand, in case of changes in traffic flow there is no such adjustment needed, because the Q_m/v_m ratio in the last step of the calculation is responsible for the density of vehicles, and the effect of speed is taken into account at the level of a single vehicle.

3.4.6 PA – Room setup

In the impact analysis of room setup settings two parameters were studied: the impulse response length and the number of late rays. Their impact on SPLs was found to be negligible and under the JND. As the transition order (i.e. the number of reflections after that the sound rays are considered as late rays) is zero in case of line sources, the number of late rays equals to the total amount of rays in the simulation. The room setup settings of the baseline and the scenarios are listed in Table 40.

Table 40 PA, room setup settings of baseline and scenarios

	impulse response length [ms]	number of late rays
baseline	2500	10000
-1500 ms	1500	10000
+1500 ms	3500	10000
x0.1 late rays	2500	1000
x10 late rays	2500	100000

The SPLs for the baseline and the deviation of the 4 room setup scenarios are presented in Table 41 for receiver position of 4 m.

Table 41 PA, receiver at 4.0 m, ΔSPL and RMSD [dB] for room setup scenarios vs. baseline [dB]

f [Hz]	baseline	-1000 ms	+1000 ms	x0.1 late rays	x10 late rays
63	71.5	-0.2	0.0	0.1	-0.2
125	61.9	-0.1	0.0	0.2	-0.2
250	61.4	-0.1	0.0	0.1	-0.2
500	59.7	-0.1	0.0	0.3	-0.2
1k	60.4	-0.2	0.0	0.3	-0.3
2k	59.1	-0.1	0.0	0.3	-0.2
4k	53.2	-0.1	0.0	0.3	-0.2
8k	43.5	0.0	0.0	0.6	-0.1
RMSD [dB]		0.1	0.0	0.3	0.2

Figure 67 gives information about the RMSD values in terms of room setup scenarios.

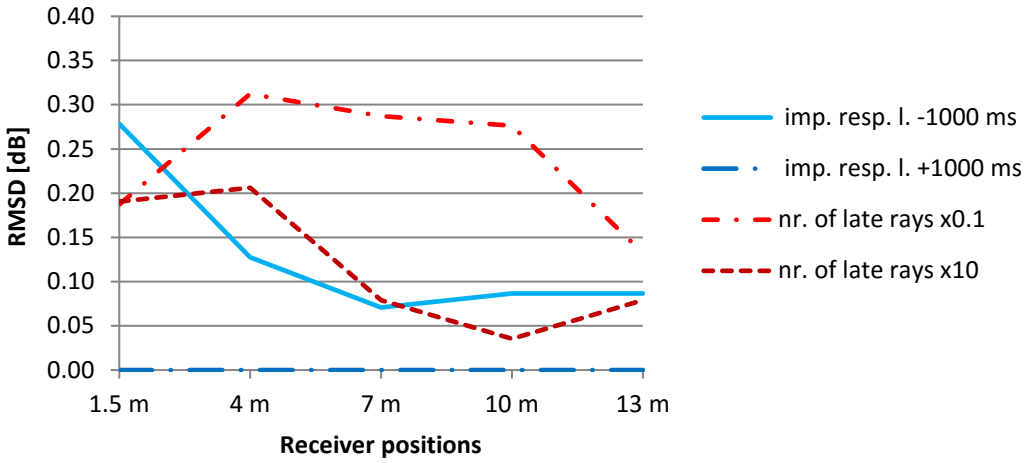

Figure 67 PA – impulse response length and number of late rays, all receivers, RMSD [dB]

The decrease of impulse response length of 1000 ms caused a fall in SPL in the lowest two receiver position, however, the level of change is much below 1 dB. On the other hand, the increase of impulse response length of 1000 ms had no impact on the results. Furthermore, a decrease of late rays to the 1/10 of that of the baseline had the biggest impact at receivers at 4, 7 and 10 m height of about +0.3 dB. However, the increase of the same parameter by a factor of 10, as expected, caused a fall of the SPL and the extent of the change was even less noticeable. Overall, it was found that the SPL results are very stable with respect to the changes of the tested room setup parameters in this section.

3.4.7 PA – Receiver position

With regard to the microphone positions of the on-site measurement information was available alone in terms of height above the street level. Moreover, receivers have to keep a minimal distance from the boundary surfaces and from the sound sources that may induce an alteration of the position of listeners. Therefore, the placement of receivers in Odeon model may not fully agree with those of the microphones in the on-site measurement. For this reason, a sensitivity analysis of the SPL results was done with respect to the receiver positions. Three scenarios were investigated: once the receiver was shifted along the street by 8 m (scenario 1), while in the scenario 2 and 3 it was pushed by 1.5 m and 4.5 m towards the middle axis of the street as is illustrated on Figure 68.

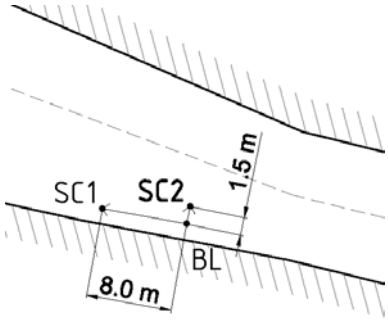

Figure 68 PA – receiver position of baseline and scenarios

The SPLs for the baseline and the deviation of the two scenarios are presented in Table 42 for receiver position of 4 m.

Table 42 PA, receiver at 4.0 m, ΔSPL and RMSD for rec. pos. scenarios vs. baseline [dB]

f [Hz]	baseline	|| 8.0 m	|_ 1.5 m	|_ 4.5 m
63	71.5	-0.7	-0.2	0.0
125	61.9	-0.6	-0.2	0.0
250	61.4	-0.7	-0.3	-0.1
500	59.7	-0.6	-0.2	-0.1
1k	60.4	-0.7	-0.3	-0.2
2k	59.1	-0.7	-0.3	-0.2
4k	53.2	-0.9	-0.3	-0.2
8k	43.5	-1.1	-0.2	0.2
RMSD [dB]		0.8	0.3	0.2

Figure 69 gives information about the RMSD values in terms of receiver position scenarios.

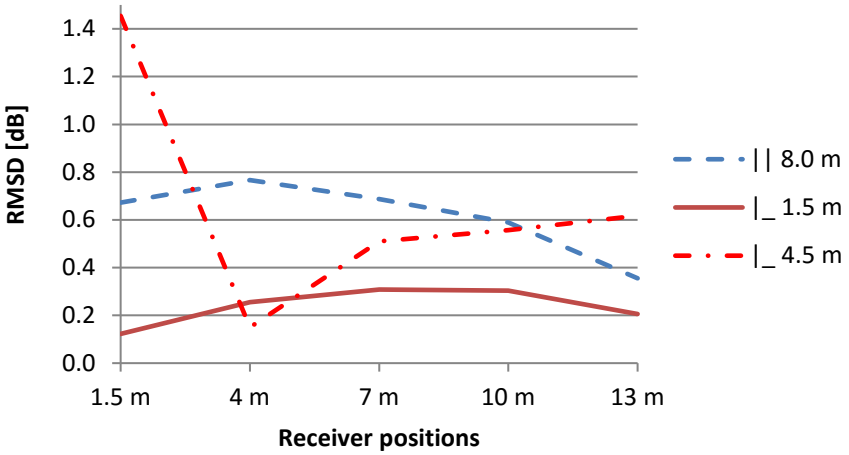

Figure 69 PA – receiver position scenarios, all receivers, RMSD [dB]

Overall, the replacement of the receivers by 1.5 m towards the centre axis of the road affected the SPLs only to a small extent, however, the 8 m change parallel to the facade caused a perceivable change. Interestingly, the shift towards to the centre of the street by 1.5 m caused a fall in SPLs, although receivers get closer to the source. Even a shift by 4.5 m towards the centreline resulted in a rise of SPLs at the receiver positions of 1.5 m, and interestingly at 13 m.

3.4.8 PA – Weather conditions

Sound propagation is affected by the weather conditions such as temperature, relative humidity and wind. Temperature and relative humidity are available input parameters in Odeon, and therefore, an impact analysis was performed on them. The season of the on-site measurements (i.e. April) was not taken into consideration in the baseline. However, the default values, namely 20°C and 50% relative humidity, do not differ much from the actual weather indicators of the month. Three of the scenarios affected the temperature, other too the relative humidity. The input parameters were set according to Table 43.

Table 43 Temperature and relative humidity input data of baseline and scenarios

	Θ [°C]	**RH [%]**
baseline	20	50
3°C	3	50
13°C	13	50
33°C	33	50
30%	20	30
85%	20	85

The SPLs of the baseline and the deviation of the scenarios for the receiver at 4.0 m. are presented in Table 44. Furthermore, Figure 70 gives information about the RMSD values of weather condition scenarios.

Table 44 PA, receiver at 4.0 m, ΔSPL and RMSD for weather conditionsscenarios vs. baseline [dB]

f [Hz]	**baseline**	**3°C**	**13°C**	**33°C**	**30%**	**85%**
63	71.5	-0.2	-0.1	-0.3	0.0	0.0
125	61.9	-0.1	-0.1	-0.2	0.0	0.0
250	61.4	-0.1	-0.1	-0.3	0.0	0.0
500	59.7	-0.1	0.0	-0.3	0.0	0.0
1k	60.4	-0.3	-0.1	-0.5	-0.1	-0.1
2k	59.1	-0.7	-0.1	-0.4	-0.2	0.1
4k	53.2	-1.5	-0.5	0.0	-0.8	0.5
8k	43.5	-1.2	-0.8	0.9	-1.4	1.2
RMSD [dB]		0.7	0.3	0.4	0.6	0.5

From the frequency based results it is visible that the changes were notable only at the highest frequencies. The maximum negative deviation occurred at 8 kHz at 13 m in case scenario 3°C, while the most significant rise amounted to 1.7 dB and took place in case of RH 85%. A fall in the temperature and a smaller level of relative humidity reduced SPLs, while a rise in the same parameters resulted in higher SPLs.

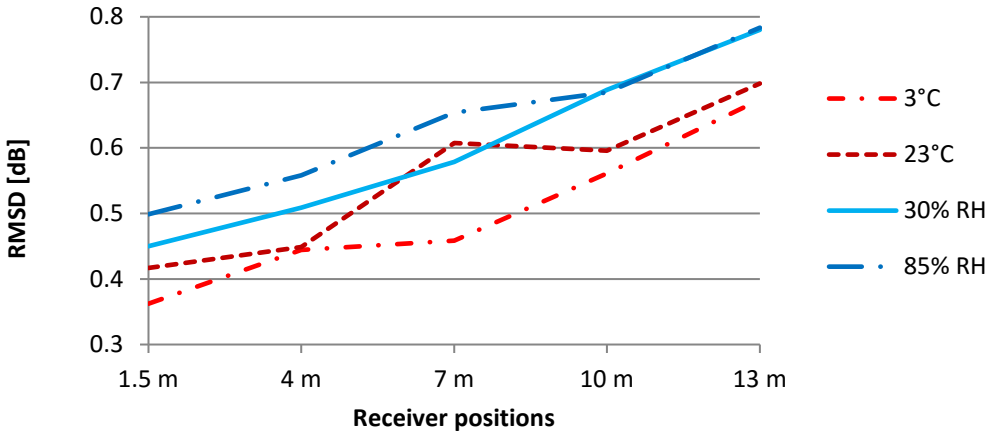

Figure 70 PA – weather condition scenarios, all receivers, RMSD [dB]

The line graph suggests that both in case of the temperature and the relative humidity the SPLs were much more affected at higher floor levels. An explanation for this may be that the longer a ray travels in the medium, the higher the impact of weather condition parameters grows. Overall, the decrease of the temperature by 7°C (i.e. 13°C) had the lowest impact while the 35% increase in RH (i.e. 85%) had the most remarkable effect on SPLs. Moreover, the 20-35% change in relative humidity had a bigger impact than the -7°C (i.e. 13°C) and +13°C (i.e. 33°C) change in temperature. Nevertheless, the RSMD value exceeded or get close to 1 dB in case of a more drastic change in temperature or relative humidity, and therefore, the results are regarded to be moderately sensitive to weather condition parameters.

The CNOSSOS sound power calculation method also requires the input of the air temperature as an input parameter. Thereby new sound power levels were calculated and simulations were run with the temperature scenarios as before, but there was no noticeable change in the SPLs. The reason for this was explored by tracking down the calculation steps for LS 4 that is right in front of the receivers and therefore has the highest potential to affect the results. It was found that weather conditions in the CNOSSOS calculation method affect only the rolling noise that has usually a much lower SPL than the propulsion noise. The rolling noise is affected through the correction factor for temperature that results in higher values in case of lower temperatures as it is shown on Figure 71. It is visible that 10 K difference results in 0.4 dB in case of vehicle category 1 that is the most typical.

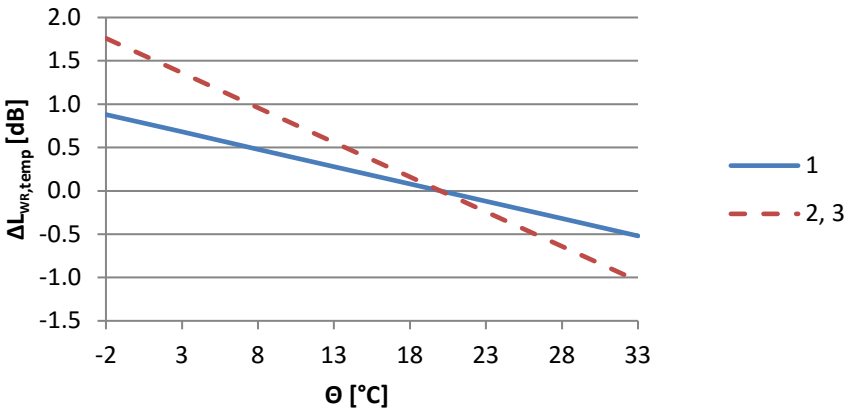

Figure 71 $\Delta L_{WR,temp}$ [dB] – correction factor for temperature, vehicle category 1, 2 and 3

On the level of the sum of the correction factors for rolling noise, 10 K difference still yields about 0.4 dB difference due to the lower magnitude of other correction factors such as road surface and speed change. The results in case of LS4 are shown on Figure 72 for vehicle category 1.

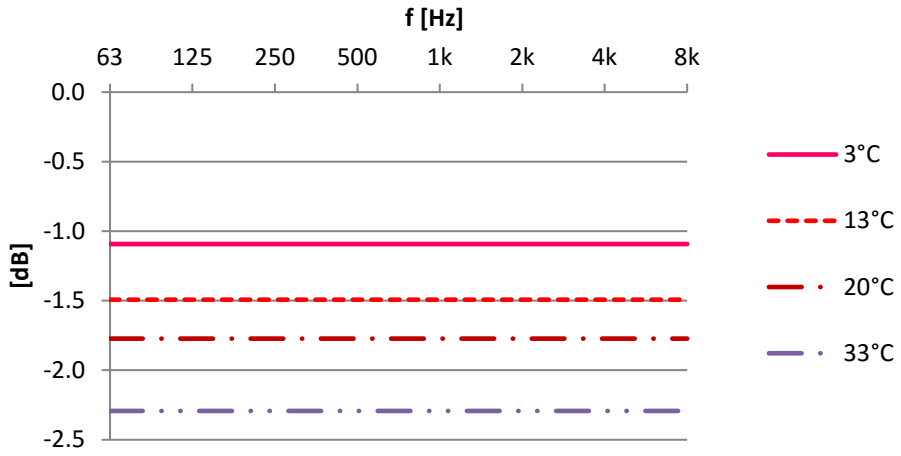

Figure 72 $\Delta L_{WR,i,1}$ [dB] – correction factor of rolling noise for vehicle category 1 by temperatures

The difference in the correction factors due to the deviation in temperature yields small alteration in the total sum of rolling (i.e. base value and correction factor) and it has significantly lower values than propulsion noise throughout all frequencies, as it is shown on Figure 73.

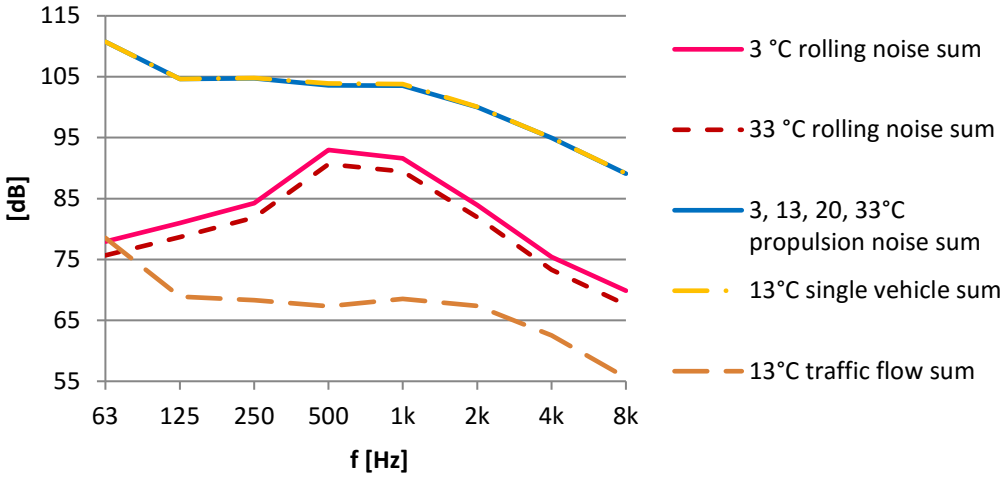

Figure 73 Sound power of rolling noise (3°C, 33°C), propulsion noise (3°C, 13°C, 20°C, 33°C), single vehicle (13°C) and traffic flow (13°C)

The min. difference between propulsion noise and rolling noise is ca. 10.5 dB at 500 Hz frequency in case of the 3°C scenario, while the biggest deviation is ca. 34 dB at 63 Hz in case of the 23°C scenario. Therefore, due to the logarithmic nature of the dB unit the sum of the rolling noise and the propulsion noise, equals to the level of propulsion noise in most frequencies. The biggest deviation between the propulsion noise and the emission of a single vehicle amounts to 0.36 dB in case of the 3°C scenario at 500 Hz. Taken into consideration that at the given vehicle speed and traffic flow the sound power of a single vehicle in dB unit is always higher than the sound power of the traffic in dB/m unit, the maximum difference in sound power levels between the three scenarios are even less than 0.35 dB. This is a negligible change in the sound power input data in Odeon and therefore no perceivable difference in SPLs occurs.

The weather condition parameters of Odeon affect the propagation of the sound, and therefore, receivers further from the sound source are more sensitive to these parameters. The impact is perceivable only at high frequencies, and thus, the frequency independent RMSD index suggests a moderate overall impact of these input values. On the contrary, the effect of temperature on sound power in CNOSSOS was found to be negligible. Moreover, an increase of temperature reduces the rolling noise, i.e. its effect is opposite compared to the same input parameters in Odeon.

3.4.9 KO – Sky types

The simulation results of BL1 and BL2, which are derived from a model with sky surfaces connected to the top of the façade, are listed in Table 45 for the receiver at 4.0 m. Furthermore, Table 46 gives information about the agreement of BL1, BL2, small-, and medium sky types with regard to the baseline with big box sky representation. The same results are presented on Figure 74.

Table 45 KO, SPLs at 4.0 m – BL1, BL2, ΔSPL [dB]

f [Hz]	BL 1	BL 2	ΔSPL
63	71.6	72.6	1.0
125	63.9	65.0	1.1
250	62.7	63.8	1.1
500	63.6	64.8	1.2
1k	67.3	68.7	1.4
2k	64.8	66.1	1.3
4k	57.2	58.6	1.4
8k	47.3	49.0	1.7

Table 46 KO, RMSD for BL1, BL2, small-, and medium sky box vs. big sky box [dB]

	BL1	BL2	small	medium
1.5 m	0.3	1.4	0.0	0.0
4.0 m	0.2	1.2	0.0	0.0
7.5 m	0.2	0.9	0.0	0.0
11.0 m	0.1	1.0	0.0	0.2
14.5 m	0.1	1.0	0.0	0.0

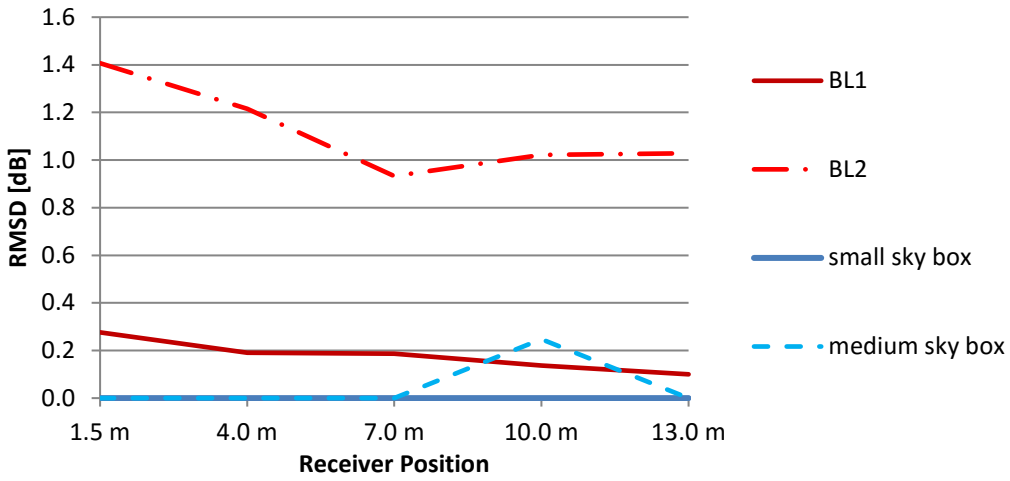

Figure 74 KO – sky types, all receivers, RMSD [dB]

In contrast to PA results where the small sky box had better agreement with BL2 in case of KO all sky boxes return the same SPLs and these values match well with BL1. This difference between PA and KO model may be explained by the different height of the buildings at the two locations. Due to the smaller façade heights even the small sky box might count as relatively big in KO. Further in the impact analysis the sky is represented by a big sky box.

3.4.10 KO – Boundary 1, 2 and scattering coefficient

Due to the findings in PA an impact analysis on the absorption of boundary 1 and 2 surfaces, furthermore, on scattering coefficients was carried out. The assignment of boundary 1 and 2 surfaces is based on the consideration whether reflections from behind these surfaces may reach the receivers or not. Boundary 1 surfaces are indicated with yellow, at a bigger distance from listeners and more absorbent. In the meanwhile, the red surfaces are closer to the receivers and more reflective. The distribution of the two surface types is indicated on Figure 75.

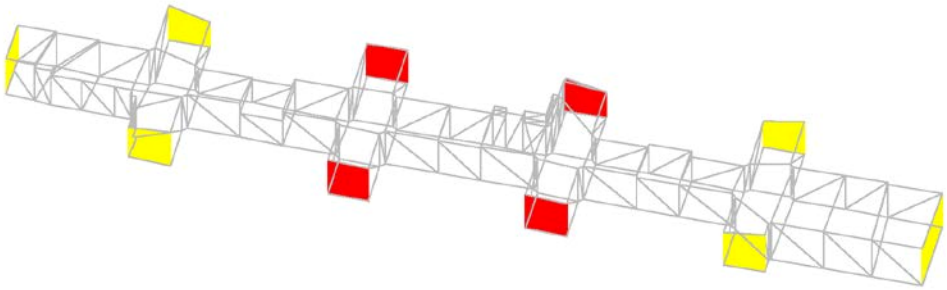

Figure 75 KO, Boundary 1 (yellow) and 2 (red) surfaces

Three scenarios with 0.01, 0.10 and 0.90 absorption coefficient on all boundary surfaces were tested. In case of scattering + 50% and full scattering scenarios were investigated. The input values are the same as for PA. The deviance of the scenarios from the baseline is shown for receiver at 4.0 m throughout the frequency ranges in Table 47.

Table 47 KO, receiver at 4.0 m, ΔSPL and RMSD for boundary 1, 2 and scattering scenarios vs. baseline [dB]

f [Hz]	baseline	boundary surf. 0.01	boundary surf. 0.1	boundary surf. 0.9	scattering + 50%	scattering full
63	71.9	0.3	0.3	-0.3	-0.2	2.7
125	64.2	0.2	0.2	-0.3	-0.2	2.9
250	62.9	0.3	0.3	-0.2	-0.2	3.0
500	63.8	0.2	0.2	-0.2	-0.5	3.5
1k	67.4	0.3	0.3	-0.1	0.2	4.1
2k	64.8	0.2	0.2	-0.2	0.9	3.7
4k	57.1	0.1	0.1	-0.1	1.0	3.9
8k	47.2	0.1	0.1	0.0	0.9	4.0
RMSD [dB]		0.3	0.2	0.2	0.6	3.5

The maximum difference between the two extreme scenarios - those of highly reflective and very absorbing - was 0.7 dB looking at all receivers and frequency bands. The scenario with absorptance of 0.01 yielded a maximum increase of 0.6 dB, while the most absorbing scenario resulted in SPLs up to 0.5 dB lower compared to baseline. Overall, the absorption of boundary surfaces have some effect on the SPLs, but the range of fluctuation of SPLs is within 1 dB, and thus, it is negligible.

On the other hand, the change of the scattering coefficients throughout the model brings a more significant deviation of the results. Figure 76 gives information about the RMSD values of the above mentioned two input parameters in dB for all receiver positions.

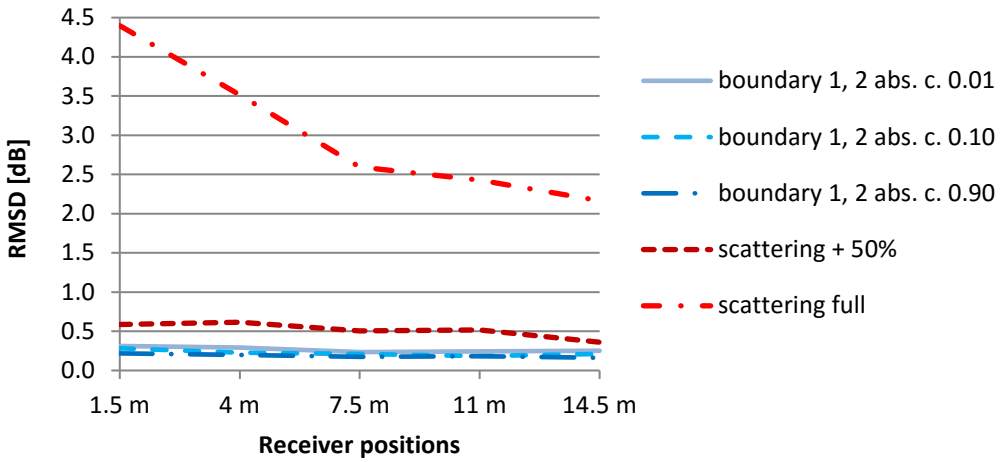

Figure 76 KO - boundary 1 and 2 surfaces and scattering, RMSD [dB]

Overall, both in case of PA and KO it was found that the absorption properties of boundary 1 and 2 surfaces and a moderate increase in scattering of all surfaces have

a minor impact on results and the level of change is independent from receiver position. On the contrary, a drastic rise in scattering coefficients of all surfaces caused significant increase in SPLs up to 4.5 dB and the level of change is highly dependent from the receiver position.

3.4.11 KO – Traffic flow

The traffic flow was found to be one of the most important factors during the impact analysis of PA. Therefore, the three scenarios were investigated. Firstly, the flow of all vehicle categories (VC) was increased by 50%, in the second scenario only the number of vehicles in category 2 (medium heavy) was multiplied by 5, and finally, in the third scenario VC 1 was reduced by 30 % and VC 2 was multiplied by 10. Being the original values rather small for VC 2, the factor of 5 or 10 will not cause unrealistic values. This last scenario gives an impression how results are affected by eventual wrong classification of vehicles during the traffic flow metering. Table 48 and Figure 77 give information about the change of SPLs regarding the scenarios.

Table 48 KO, receiver at 4.0 m, on-site, baseline, ΔSPL and RMSD for traffic flow scenarios vs. baseline [dB]

f [Hz]	on-site	baseline	+ 50% all vehicles	+ 400% VC 2	- 30% VC 1 and + 900% VC 2
63	75.5	71.9	3.5	0.7	0.4
125	68.0	64.2	3.4	0.7	0.5
250	66.5	62.9	3.6	1.4	1.9
500	66.1	63.8	3.7	0.8	0.7
1k	68.9	67.4	4.1	0.5	-0.2
2k	65.4	64.8	4.0	0.3	-0.5
4k	58.3	57.1	4.1	0.3	-0.5
8k	49.2	47.2	4.6	0.5	-0.1
	RMSD [dB]		3.9	0.7	0.8

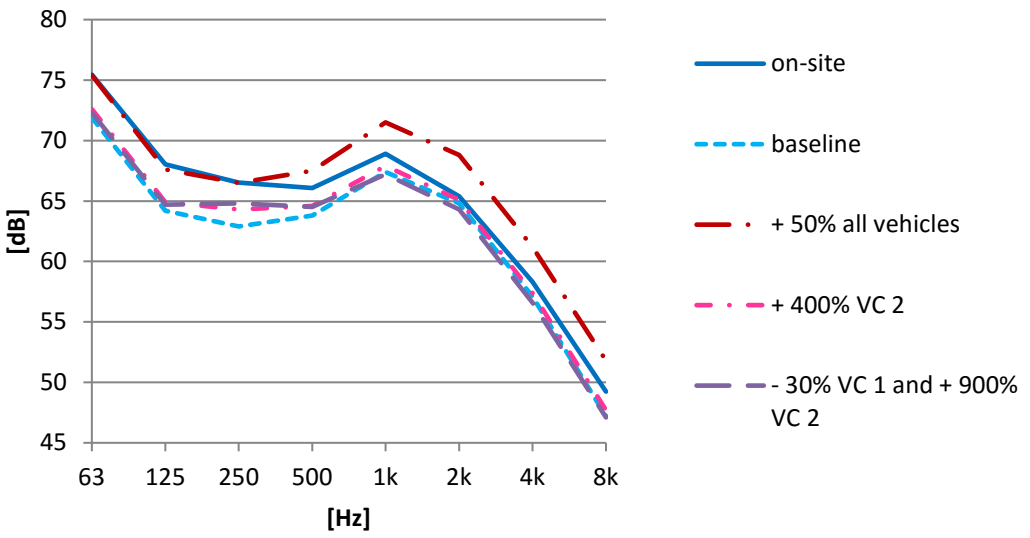

Figure 77 Measured and simulated SPL at receiver at 4.0 m

The results show, that the overall increase of the traffic causes a significant rise in the SPLs and the level of change is even throughout all frequency bands. On the other hand, a higher number of VC 2 resulted in noticeable difference only at 250 Hz and the low level of deviation can be explained by the overall low number of this vehicle category. Moreover, in the third scenario low frequencies have shown increasing SPLs while higher frequencies have slightly fallen. Therefore, a wrong classification of vehicles can be a possible reason of both positive and negative deviation according to frequencies in comparison with the on-site measurements. In case of KO both the overall traffic flow and the rate of medium heavy vehicles seem to be underestimated in the simulation.

4 DISCUSSION

This contribution consisted of two main parts. The first section included the acquisition of input data for room acoustic simulations, furthermore, a methodology on the derivation of such models was presented. The second part of the work comprises the comparison of measured and simulated results, moreover, an impact analysis on the input parameters.

The goal of the data acquisition was on one hand to gain state of the art information on the necessary input parameters such as relevant material properties and sound power of sources. Besides, input values for the baseline model were assigned based on these available data sets and in-situ observations. As the findings on material properties derive from a number of sources and different measurement methods the comparability of the data sets is questionable. However, the built-in material library of Odeon is also based on different sources. The CNOSSOS sound power calculation method gives a state of the art approach to estimate the noise emission from road traffic. The method takes into consideration many parameters such as the flow and speed of the traffic by vehicle categories and it also accounts for the road conditions in terms of its surface characteristics and gradient. It was found that the sound power level of the source and the resulting SPLs have a strong correlation, and therefore, a realistic estimate of the power of the source is essential. The results have shown a good agreement between the measured and simulated data sets for PA that suggest sound power levels were specified correctly. Nevertheless, the deviation of simulated results from the measured data was significant at the lower frequencies. While in case PA the deviation from the measured values stayed below 3 dB, for KO the differences amounted to 4 – 8.5 dB (see: Table 29 and Figure 55). As simulated SPLs are strongly correlated to sound power levels, a remarkable deviation to the reference indicates inaccuracy of the traffic flow input parameters.

The second part of the work consisted of the impact analysis of the input parameters, and a compact overview of the findings is given in Table 51. The table includes the range of ΔSPLs and RMSD values in dB unit by reporting the minimum and maximum values based on all receivers and octave bands. While min. and max. ΔSPL values give a hint on the positive and negative extremes, the RMSD values are less sensitive to outliers of ΔSPLs, and therefore, characterize the overall level of the change at a certain receiver. The RMSD indicator is calculated for each receiver positions based on ΔSPLs of the full frequency range. Therefore, RMSD extreme values give an impression about the level of change in vertical terms. If the minimum and maximum

of the RMSD values are close, the results are not sensitive to receiver positions. On the contrary, a notable difference indicates a major impact of the floor levels on SPLs.

The column with the header “receiver” reports about the *receiver positions* at which the scenario has ΔSPL values significantly different than other receivers. Thus, it is not the absolute ΔSPL values that matter, but the receivers with outlying values. If at a certain receiver the absolute ΔSPL values tend to be higher at least by 0.5 dB compared to others, the position of that receiver is listed in the table. Otherwise, the cell remains empty. Although a scenario may have a remarkable effect on SPLs, if the change is even at all receivers, the cell is not filled.

Similarly to the previous consideration, the level of effect by *frequency ranges* was studied too. Under the column “frequency” the bands with absolute ΔSPLs at least by 0.5 dB different from those of most common ones are listed. Therefore, it is not the absolute ΔSPLs that count, but frequencies that are affected to a greater extent than others. If no such octave band is detected, the cell stays empty.

Furthermore, a descriptive overall assessment of the level of impact was developed and listed in the last column. The method of classification into three categories is described in Table 49, and includes the test of two conditions listed in Table 50.

Table 49 Classification method for impact categories

Impact category	**Condition 1**	**Condition 2**
high	true	true
moderate	true	false
moderate	false	true
low	false	false

Table 50 Condition 1 and 2 of classification algorithm of impact categories

Condition 1	**Condition 2**
$\lvert\Delta SPL_{min}\rvert$ >1 dB or $\lvert\Delta SPL_{max}\rvert$ >1 dB or $\lvert\Delta SPL_{max} - \Delta SPL_{min}\rvert$ > 1 dB	$RMSD_{max}$ > 1 dB

On one hand, condition 1 tests whether the there is any absolute ΔSPLs that are at least by 1 dB above or below the baseline data set, or the interval of minimum and maximum levels exceed 1 dB. On the other hand the condition 2 with regard to RMSD checks if the scenario has a reasonable impact at least for one receiver position. The value of 1 dB was chosen because it is considered as the just noticeable difference

(JND) for the human ear. The conditions are found to be appropriate to differentiate between scenarios because all categories have a number of representatives.

Table 51 Overview of the impact of scenarios

ID	ΔSPL [dB]		RMSD [dB]		rec.	fr [Hz]	impact
	min.	max.	min.	max.			
PA_sky to facades_BL1	-0.3	0.2	0.1	0.2	-	-	low
PA_sky to facades_BL2	0.2	1.8	0.5	1	-	8k	moderate
PA_sky box_small	0.4	1.9	0.6	1.2	-	8k	high
PA_sky box_medium	-0.1	0.0	0.0	0.1	-	-	low
PA_boundary 1,2_abs.c._0.01	0.1	0.7	0.4	0.5	-	500 - 1k	low
PA_boundary 1,2_abs.c._0.1	0.1	0.6	0.4	0.5	-	500 - 1k	low
PA_boundary 1,2_abs.c._0.9	-0.1	0.0	0.1	0.1	-	-	low
PA_all surfaces_+ 50% scattering	-0.3	0.9	0.4	0.6	-	2k - 8k	moderate
PA_all surfaces_full scattering	1.3	1.8	0.3	2.7	low	-	high
PA_win_casement	-1.6	0.2	0.5	0.6	-	63 -125	moderate
PA_win_mixed	-0.8	0.0	0.3	0.3	-	63 -125	low
PA_facade_abs.c._-50%	0.0	0.4	0.2	0.3	-	63-250	low
PA_facade_abs.c._+50%	-0.4	0.0	0.2	0.3	-	63-250	low
PA_facade_abs.c._+100%	-0.7	-0.1	0.4	0.5	-	63-250	low
PA_facade_abs.c._0.5	-5.1	-2.1	3.5	4.3	at high level	63-250	high
PA_road surface_abs.c.	-0.5	0.0	0.3	0.3	-	-	low
PA_road surface_sound power	-2.9	1.2	1.4	1.5	-	1k - 4k	high
PA_road surface_abs.c. and s. p.	-3.2	0.9	1.6	1.6	-	1k - 4k	high

ID	ΔSPL [dB] min.	ΔSPL [dB] max.	RMSD [dB] min.	RMSD [dB] max.	rec.	fr [Hz]	impact
PA_road traffic_- 50% flow	-3.2	-2.8	3.1	3.1	-	-	high
PA_road traffic_+ 50% flow	1.7	2.0	1.9	1.9	-	-	high
PA_road traffic_- 10 km/h speed	-2.2	0.2	1.4	1.4	-	1k	high
PA_road traffic_+ 10 km/h speed	-0.2	2.3	1.5	1.5	-	1k	high
PA_room setup_imp. res._-1000 ms	-0.3	0.1	0.1	0.3	-	-	low
PA_room setup_imp. res._+1000 ms	0.0	0.0	0.0	0.0	-	-	low
PA_room setup_late rays_x0.1	-0.2	0.6	0.1	0.3	-	-	low
PA_room setup_late rays_x10	-0.3	0.0	0.0	0.2	-	-	low
PA_receiver position_|| 8 m	-1.2	-0.4	0.6	0.8	-	-	moderate
PA_receiver position_|_ 1.5 m	-0.4	0.3	0.1	0.3	-	-	low
PA_receiver position_|_ 4.5 m	-0.7	2.4	0.2	1.5	low	-	high
PA_weather conditions_3°C	-2.1	0.1	0.7	1.1	-	4k - 8k	high
PA_weather conditions_13°C	-1.3	0.2	0.3	0.5	-	8k	moderate
PA_weather conditions_33°C	-0.5	1.4	0.4	0.5	-	8k	moderate
PA_weather conditions_RH 30%	-2.1	0.0	0.5	0.9	-	4k -8k	moderate
PA_weather conditions_RH 85%	-0.1	1.7	0.4	0.6	-	4k - 8k	moderate
KO_sky to facades_BL1	-0.5	0.2	0.1	0.3	-	-	low
KO_sky to facades_BL2	0.0	1.9	0.9	1.4	-	8k	high
KO_sky box_small	0.0	0.0	0.0	0.0	-	-	low
KO_sky box_medium	-0.7	0.0	0.0	0.2	-	-	low
KO_boundary 1,2_abs.c._0.01	0.0	0.5	0.2	0.3	-	-	low
KO_boundary 1,2_abs.c._0.1	0.0	0.4	0.2	0.3	-	-	low
KO_boundary 1,2_abs.c._0.9	-0.3	0.0	0.2	0.2	-	-	low
KO_all surfaces_+ 50% scattering	-0.7	1.0	0.4	0.6	-	4k - 8k	moderate
KO_all surfaces_full scattering	1.1	5.2	2.2	4.4	low	4k - 8k	high

Firstly, the scenarios with low impact are discussed. The study on sky boxes was important from modelling point of view. The findings have shown that a sky representation with sky surfaces sufficiently far from the urban canyon returns stable results, and therefore, a big sky box is recommended to model the sky. Another theoretical consideration with regard to boundary surface properties were investigated, and their impact was found to be little. In terms of the room setup settings of Odeon, it was found that results are not sensitive neither to impulse response length nor to the number of late rays using a difference of +/- 1000 ms and a factor of 0.1 and 10 respectively. Moreover, the influence of the absorption data proved to be less remarkable if the amount of affected surfaces was rather small as it was the case for windows or road surfaces. Also, the change in material properties caused less dramatic change in absolute values, as it was shown in +/- 50% and + 100% facade absorption scenarios. However, a significant rise in the absolute value of façade absorption caused a notable shift of SPLs. Furthermore, the results were less sensitive to the replacement of the receiver along the facade by 8 m and towards the centreline of the street by 1.5 m. On the other hand, a more significant shift towards the sound source caused a perceivable change in SPLs. Surprisingly, the deviation from the baseline was positive in case of the lower-, and uppermost receivers, while at all other levels the scenario returned lower SPLs. The extremes of the weather condition parameters returned ΔSPLs up to 2 dB but their overall impact was found to be moderate unless there was a more significant change in the temperature. Interestingly, a change of all window materials also had moderate effect due to the significant difference at low frequencies between the two glass types. The scenarios with *high* impact are shown on Figure 78 and Figure 79 and visualise the ΔSPL and RMSD values respectively.

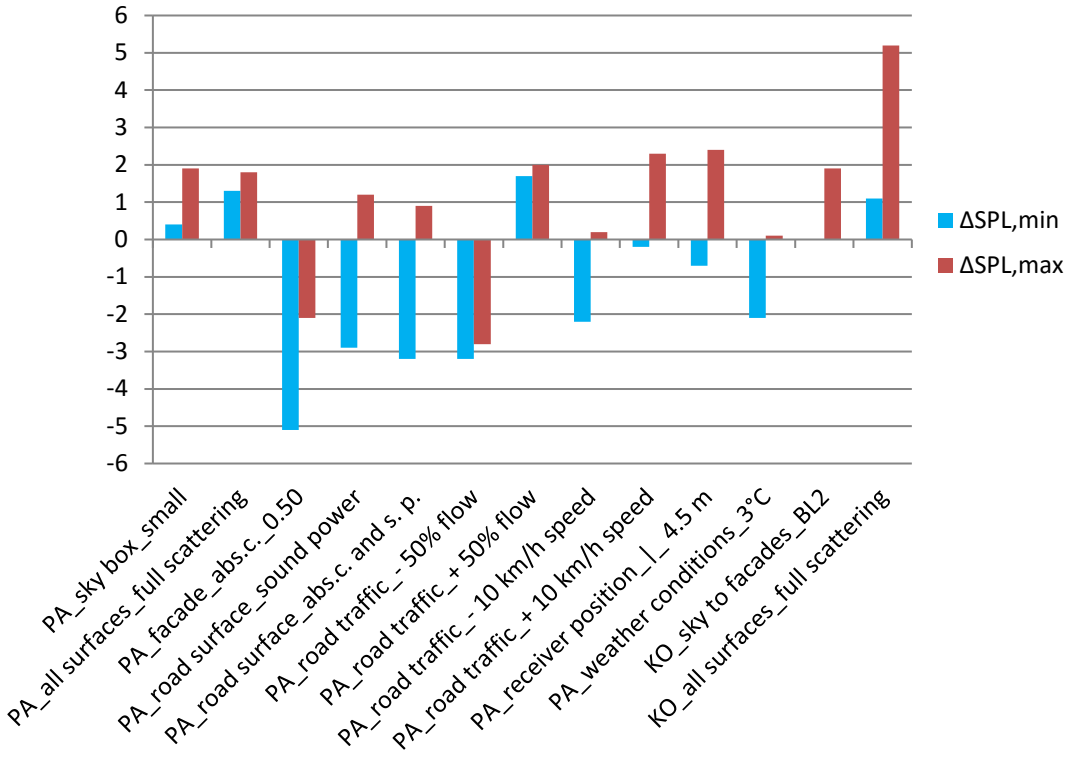

Figure 78 ΔSPL [dB] min. and max. of scenarios with high impact

The ΔSPLs on a bar chart give a quick overview on the positive or negative nature of the change and inform about the level of extreme deviations. Some scenarios are important from simulation model point of view (e.g. small sky box), while others assess the impact of extreme input parameters (e.g. facade absorption of 0.5 and full scattering). Finally, some of them could be realistic scenarios, such as changes in the traffic flow, vehicle speed and road surface. Furthermore, the bar chart shows if the alteration of the input parameter returns either solely positive or negative deviation of SPLs (e.g. scattering, facade absorption, and traffic flow), or causes both positive and negative alterations according to the frequency band (e.g. road surface and vehicle speed). For instance, the lowering of the speed limit implies a fall of SPLs at most frequencies, however, at the lowest octave band it has a reverse effect and slightly increases SPL. Moreover, if the minimum and maximum ΔSPLs are close (e.g. traffic flow scenarios), this indicates a rather constant change throughout the frequencies and floor levels. On the contrary, a big difference here implies frequency dependency (e.g. facade absorption of 0.5 and full scattering). Nevertheless, the minimum and maximum ΔSPLs do not necessarily give reliable information about the overall impact of the parameter, as certain frequencies and receiver positions may produce outlier ΔSPL values that are not typical for the rest of the data set.

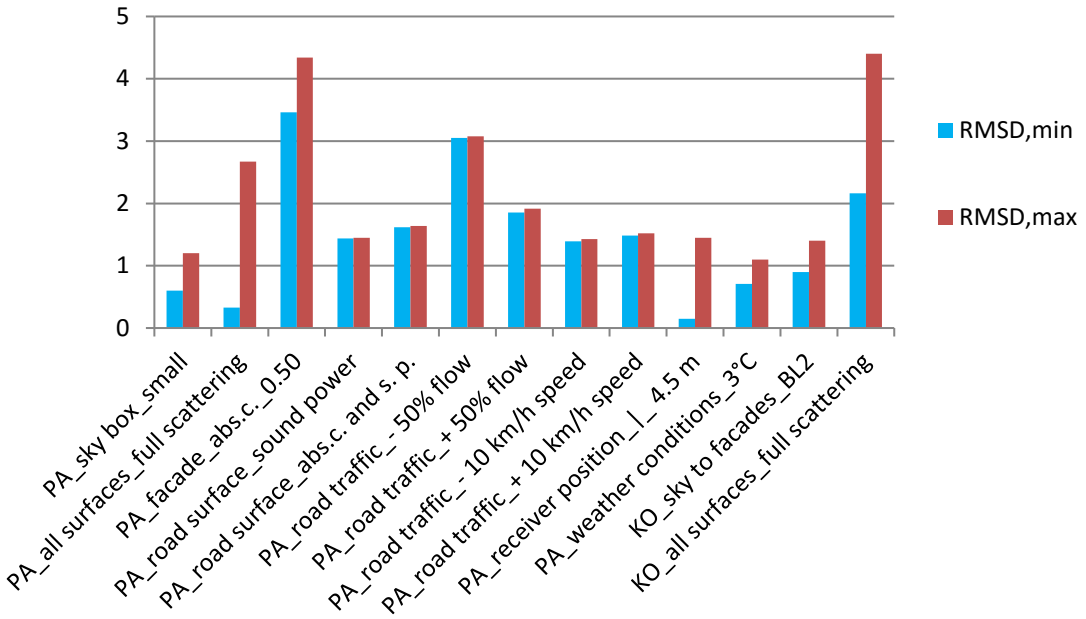

Figure 79 RMSD [dB] min. and max. of scenarios with high impact

Therefore, in order to gain information about the level of impact of each measure the bar chart of RMSD values should be looked at. The difference between the minimum and maximum values usually stays below 0.5 dB, indicating a constant nature of the change in vertical sense. However, the RMSD values reveal that scattering affects bottom floors more than higher ones up to a difference of 2.4 dB in case PA. The same scenario for KO yielded in even higher RMSDs, but the difference between minimum and maximum values is similar to PA. By ranking among those of realistic measures, the graph suggest that the most efficient way of noise mitigation is the reduction of traffic flow by 50%, which may cause up to 3 dB reduction in SPLs, but changing the road surface material would also bring a moderate change about 1.5 dB. Finally, the lowering of the speed limit by 10 km/h in the entire range of the model might result in a noticeable improvement of 1 dB as well.

Furthermore, a remarkable improvement of absorption capability of facades could succeed in up to 3.4 – 4.4 dB drop in SPLs, while, in turn an overall rise in the scattering of all materials seems to have a serious reverse effect. However, taking into consideration the facade finishing materials of building industry and modest knowledge about scattering coefficients – these two measures are less reliable from practical point of view.

5 CONCLUSION

The main goal of this work was on one hand the validation of a methodology to set up room acoustic simulation model for urban scenarios, while, on the other hand the impact of input parameters on SPLs was investigated. The implementation of the baseline model relied on carefully chosen input values. These parameters were based on findings of previous research contributions and in-situ observations in order to best represent the given location. The comparative analysis of the simulation results and the outputs of on-site measurements returned satisfactory agreement at all octave bands in case of Paluanergasse. However, SPLs below 1 kHz were underestimated for Koppstraße location that is most probably a result of imprecise input data on the level and the composition of the traffic flow.

The parametric study on input data revealed the level of impact of changes in model geometry, material properties, road traffic, receiver positions, weather conditions and simulation tool settings. Overall, the findings have shown that little changes have small impact. Therefore, if the order of magnitude of the input data is appropriate, then the simulation results in reliable outputs. Furthermore, the ranking of scenarios gave information about the most promising measures in terms of noise mitigation. Not surprisingly most of them are in connection with the road traffic itself that suggest noise abatement measures directly at the sound source. Besides, a change in absorption and scattering properties of the surfaces (i.e. alterations of the propagation field) might have some effect, however, to this end these parameters need to be altered significantly.

In addition, with regard to the methodology it was found that the geometry can be simplified to a great extent without the risk of harm the results and room setups. Also, the impulse response length and the number of late rays had a small impact. Altogether, it was found, that closed urban situations can be modelled by a room acoustic software with good precision and at a low computational cost. On the other hand, the results suggest that a more sophisticated situation yields inaccuracy of the input parameters, and therefore, the simulation results are less reliable. For instance, in case of Koppstraße the parking cars and the trees introduce uncertainty in the material properties of the ground surfaces. Moreover, the smaller height to width ratio and the corner situation decreases the compactness of the model.

Overall, the presented methodology of deriving the input data can be a future tool to assess existing urban situations and to rank between potential noise abatement measures.

A further goal of this section to shed light on aspects of the research that were not discussed within the framework of this thesis. In the fields of urban noise mitigation firstly the sound source and secondly the field of sound propagation should be targeted. In practical terms the impact of share of vehicle categories at constant traffic flow and vehicle speed could be tested that would provide a better understanding of the influence of traffic composition. As a long term goal, instead of constant sound power levels the fluctuating real time data of traffic flow emissions should be used as the level and the number of peak events have a better correlation with reported disturbance compared to equivalent sound levels. Furthermore, the influence of cross-streets' traffic, and therefore, the geometrical extent of the model could be checked by running scenarios without sound sources here. Besides, electric cars, which have presumably much lower sound power levels than combustion vehicles represent a very promising perspective, and thus, their emission needs to be researched. With regard to facade surfaces, indoor acoustic solutions could be looked at in detail to gain inspiration for the development of new facade constructions. Thereafter, their potential could be explored by means of simulation. Likewise, the impact of placing miscellaneous objects in the sound field should be tested with regard to their potential of absorbing and scattering sound energy. From the theory point of view more information should be gathered on weather conditions in order to detect the extreme potentials of noise mitigation measures. In terms of sound power calculation methods other frequency based standards should be researched and compared. Finally, the impact of the level of detail both in terms of the geometry and the surface characteristics should be studied thoroughly.

6 INDEX

6.1 List of Figures

6.2 List of Tables

6.3 List of Equations

7 LITERATURE

Aspöck, L., Opdam, R., Behler, G. and Vorländer, M., 2016. *Acquisition of boundary conditions for a room acoustics simulation comparison.* In: International Symposium on Musical and Room Acoustics (ISMRA2016), 11-13 September 2016, La Plata, Argentina.

Christensen, C. L., 2011. *Odeon User Manual.* Lyngby: Industrial, Auditorium and Combined Editions.

Christensen, C. L., Koutsouris, G. and Rindel, J. H., 2014. *Estimating absorption of materials to match room model against existing room using a genetic algorithm.* In: Forum Acusticum, 7-12 September 2014, Krakow. DOI: 10.13140/2.1.1588.8647.

De Coensel, B., Brow, A. L. and Tomerini, D., 2016. *A road traffic noise pattern simulation model that includes distributions of vehicle sound power levels.* Applied Acoustics 111, pp. 170-178. DOI: 10.1016/j.apacoust.2016.04.010.

Environmental Noise Directive 2002/49/EC of the European parliament and of the council of 25 June 2002 relating to the assessment and management of environmental noise. Official Journal of the European Communities, 2002. Available from http://eur-lex.europa.eu/legal-content/EN/TXT/PDF/?uri= CELEX:32002L0049&from=EN; accessed 15 January 2018.

Directive 2015/996/EC of 19 May 2015, establishing common noise assessment methods according to Directive 2002/9/EC of the European Parliament and of the Council. Official Journal of the European Union, 2015. Available from http://eur-lex.europa.eu/legal-content/EN/TXT/PDF/?uri= CELEX:32015L0996&from=EN; accessed 15 January 2018.

Forouharmajd, F., Nassiri, P., Monazzam, M.R. and Yazdchi, M., 2014. *Predicted sound absorption coefficients of absorber materials lined in a chamber.* Int J Env Health Eng 2014;3:13.

Hornikx, M., 2009. *Numerical modeling of sound propagation to closed urban courtyards.* Thesis for the degree of doctor of philosophy: Chalmers University of Technology.

Hornikx, M., 2016. *Ten questions concerning computational urban acoustics*. Building and Environment 106 (6), pp. 409-421. DOI: 10.1016/j.buildenv.2016.06.028

ISO, 1998. *International Standard ISO-10534: Acoustics – Determination of sound absorption coefficient and impedance in impedance tubes.*

ISO, 2003. *International Standard ISO-354: Acoustics – Measurement of sound absorption in a reverberation room.*

ISO, 2009. *International Standard ISO-3382-1: Acoustics – Measurement of room acoustic parameters – Part 1: Performance spaces.*

Kephalopoulos, S., Paviotti, M., Anfosso Lédée, F., 2012. *Common Noise Assessment Methods in Europe (CNOSSOS EU), EUR 25379 EN.* Luxembourg: Publications Office of the European Union, 2012. Available from http://publications.jrc.ec.europa.eu/repository/bitstream/JRC72550/cnossos-eu%20jrc%20reference%20report_final_on%20line%20version_10%20august%202012.pdf, accessed 15 January 2018.

Knabben, R. M., Trichês, G., Gerges, S. N.Y. and Vergara, E. F., 2016. *Evaluation of sound absorption capacity of asphalt mixtures.* Applied Acoustics 114, pp. 266-274. DOI:10.1016/j.apacoust.2016.08.008

Long, M., 2014. *Architectural Acoustics.* Oxford: Academic Press.

Mun, S., 2010. *Sound absorption characteristics of porous asphalt concrete pavements.* Canadian Journal of Civil Engineering 37(2), pp. 273-278. DOI: 10.1139/L09-142.

Naylor, G., 1992. *Treatment of Early and Late Reflections in a Hybrid Computer Model for Room Acoustics*. In: 124th ASA meeting, November 1992, New Orleans.

Naylor, G. and Rindel, J.H., 1992. *Predicting Room Acoustical Behaviour with the Odeon Computer Model.* In: 124th ASA meeting, November 1992, New Orleans.

Odeon, 2017. *Traffic noise in atrium courtyard.* Available from http://www.Odeon.dk/traffic-noise-atrium-courtyard; accessed 5 January 2017.

Paje, S. E., Bueno, M., Terán, F., Viñuela, U. and Luong, J., 2008. *Assessment of asphalt concrete acoustic performance in urban streets.* The Journal of the Acoustical Society of America 123(1439). DOI: 10.1121/1.2828068.

Quartieri, J., Mastorakis, N. E., Iannone, G., Guarnaccia, C., D'Ambrosio, S., Troisi, A. and Lenza, T.L.L., 2009. *A review of traffic noise predictive noise models.* In: 5th WSEAS Int. Conf. on Applied and Theoretical

Mechanics" (MECHANICS'09), 14-16 December 2009, Puerto De La Cruz, Tenerife, Spain.

Raimundo, I., Freitas, E., Inácio, O. and Pereira, P., 2010. *Sound absorption coefficient of wet gap graded asphalt mixtures.* In: 39th International Congress and Exposition on Noise Control Engineering (INTER-NOISE 2010), 13-16 June 2010, Lisbon.

Savioja, L., 1999. *Modeling techniques for virtual acoustics.* Ph.D. dissertation: Helsinki University of Technology, Espoo, Finland.

Savioja, L., Huopaniemi, J., Lokki, T. and Väänänen, R., 1999. *Creating interactive virtual acoustic environments.* Journal of the Audio Engineering Engineering Society 47(9), pp. 675-705.

Siltanen, S., Lokki, T., Savioja, L. and Claus Lynge, C., 2008. *Geometry reduction in room acoustics.* Acta Acustica united with Acustica 94(3), pp. 410–418. DOI: 10.3813/AAA.918049.

WHO-JRC, 2011. *Burden of disease from environmental noise - Quantification of healthy life years lost in Europe.* Available from http://www.euro.who.int/__data/assets/pdf_file/0008/136466/e94888.pdf; accessed 15 January 2018.

8 APPENDIX

A. Figures

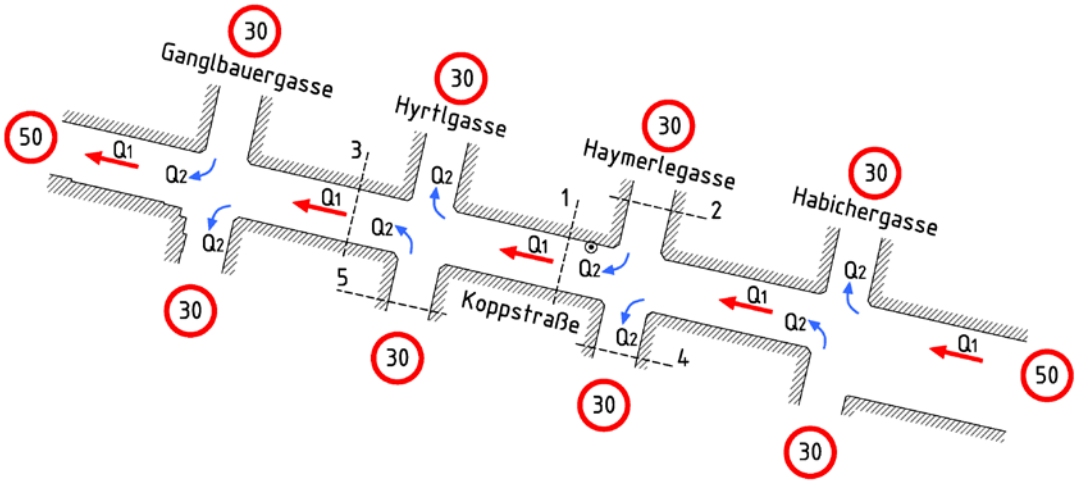

Figure 80 Koppstraße – Speed limits [km/h], traffic flow directions and locations of traffic flow metering (1-5)

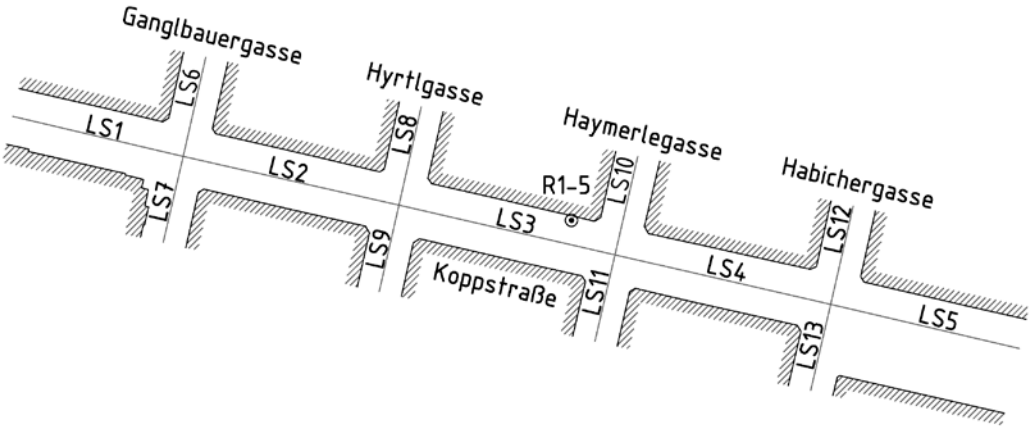

Figure 81 Koppstraße – Line sources

B. Tables

B.1 PA, KO – On-site SPL measurement data

Table 52 On-site SPL measurement data [dB] – Paulanergasse, 18.4.2011 17:57 to18:12

f [Hz]	1.5 m Rion	4 m Pulse	7 m Pulse	10 m Pulse	13 m Pulse
63	73.80	71.89	72.43	72.34	72.26
125	65.13	63.43	63.61	63.58	63.66
250	61.18	61.32	61.33	60.21	59.79
500	60.27	61.15	61.22	60.35	59.68
1k	61.58	63.23	63.33	62.48	61.73
2k	57.82	59.95	59.94	59.12	58.36
4k	50.86	53.37	53.19	52.13	51.08
8k	43.42	45.11	44.45	42.59	41.01

Table 53 On-site SPL measurement data [dB]– Koppstraße, 21.3.2011, 17:00 to17:45

f [Hz]	1.5 m Rion	4 m Pulse	7.5 m Pulse	11 m Pulse	14.5 m Pulse	16 m Norsonic
63	76.21	75.46	76.74	77.48	79.07	75.03
125	69.20	68.04	67.88	67.88	68.65	60.07
250	65.25	66.53	67.15	66.48	65.61	56.55
500	64.12	66.09	65.88	65.34	64.91	54.42
1k	66.19	68.92	68.64	68.24	67.69	55.43
2k	62.06	65.37	65.04	64.67	64.03	51.40
4k	54.80	58.31	57.53	56.57	55.93	42.32
8k	47.68	49.24	48.18	46.13	45.14	32.21

B.2 KO – Traffic flow metering data and traffic flow of line sources

Table 54 Results of on-site traffic flow metering – Koppstraße

Location	Koppstraße (location 1)			
Date of metering	10 November 2017, Friday (weekday)			
Time period	17:17 – 17:27			
Vehicle category	1	2	4a	4b
Number of vehicles	202	1	5	0

Location	Haymerlegasse (locations 2,4 – in cross street)			
Date of metering	10 November 2017, Friday (weekday)			
Time period	17:28 – 17:35			
Vehicle category	1	2	4a	4b
Number of vehicles	19	6	1	0

Location 3 and 5 metering occurred slightly later and the results suggest that the traffic flow became slightly smaller. In simulations the earlier (higher) traffic scenario was considered. The traffic flow of line sources is listed in Table 55.

Table 55 Traffic flow of line sources – Q [1/h] – Koppstraße

Vehicle category	**LS1 – LS5**	**LS6 – LS13**
1	1864.6	381.5
2	9.2	3.1
3	0.0	0.0
4a	46.2	3.1
4b	0.0	0.0
Speed limit [km/h]	50	30
Data source	metering	LS 10, LS 11 metering, all other considered as same

C. Equations

C.1 Continuous equivalent sound level

The calculation of continuous equivalent sound level of the dynamically changing noise event when all t(i) time intervals are equal is shown in Equation 19.

$$L_{eq} = 10 \cdot log\left\{\frac{1}{T}\int_0^T 10^{L_i(t)\cdot 0.1}\,dt\right\} = \\ = 10 \cdot log\left\{\frac{1}{T}\sum t(i) \cdot 10^{L_i(t)\cdot 0.1}\right\} = \\ = 10 \cdot log\left\{\frac{1}{n \cdot t}\sum t \cdot 10^{L_i(t)\cdot 0.1}\right\} = \\ = 10 \cdot log\left\{\frac{1}{n}\sum 10^{L_i(t)\cdot 0.1}\right\} \qquad 19$$

Where

L_{eq}	continuous equivalent sound level,
T	total length of metering in time, the sum of $t(i)$ time intervals,
$L_i(t)$	sound pressure level of the ith time interval,
$t(i)$	length of the ith time interval,
n	number of time intervals (the number of data points), and
t	length of one time interval when all are the same length.

C.2 CNOSSOS – Rolling noise

The calculation of rolling noise according to CNOSSOS is shown in Equation 20.

$$L_{WR,i,m} = A_{R,i,m} + B_{R,i,m} \cdot lg\left(\frac{v_m}{v_{ref}}\right) + \Delta L_{WR,i,m}(v_m) \qquad 20$$

Where

$L_{WR,i,m}$	rolling noise for i[th] frequency band, vehicle category m [dB],
$A_{R,i,m}$	coefficient for rolling noise for i[th] frequency band, vehicle category m [dB],
$B_{R,i,m}$	coefficient for rolling noise for i[th] frequency band, vehicle category m [dB],
v_m	speed of vehicle category m [km/h],
v_{ref}	reference speed: 70 km/h, and
$\Delta L_{WR,i,m}(v_m)$	sum of correction coefficients for rolling noise (function of road surface, speed, speed change, and temperature) [dB].

C.3 CNOSSOS – Correction factors for rolling noise

The calculation of the sum of correction factors for rolling noise according to CNOSSOS is shown in Equation 21.

$$\Delta L_{WR,i,m}(v_m) = \Delta L_{WR,road,i,m}(v_m) + \Delta L_{WR,acc.i,m} + \Delta L_{W,temp} \qquad 21$$

Where

$\Delta L_{WR,i,m}(v_m)$	sum of correction factors for rolling noise for i[th] frequency band, vehicle category m [dB],
$\Delta L_{WR,road,i,m}(v_m)$	correction factor for road surface [dB],
$\Delta L_{WR,acc,i,m}$	correction factor for speed change [dB], and
$\Delta L_{W,temp}(\tau)$	correction factor for temperature [dB].

C.4 CNOSSOS – Propulsion noise

The calculation of propulsion noise according to CNOSSOS is shown in Equation 22.

$$L_{WP,i,m} = A_{P,i,m} + B_{P,i,m} \cdot \left(\frac{v_m - v_{ref}}{v_{ref}}\right) + \Delta L_{WP,i,m}(v_m) \qquad 22$$

Where

$L_{WP,i,m}$	propulsion noise for ith frequency band, vehicle category m [dB],
$A_{P,i,m}$	coefficient for propulsion noise for ith frequency band, vehicle category m [dB],
$B_{P,i,m}$	coefficient for propulsion noise for ith frequency band, vehicle category m [dB],
v_m	speed of vehicle category m [km/h],
v_{ref}	reference speed: 70 km/h, and
$\Delta L_{WP,i,m}(v_m)$	sum of correction coefficients for propulsion noise (function of road surface, speed, speed change, and temperature) [dB].

C.5 CNOSSOS – Correction factors for propulsion noise

The calculation of the sum of correction factors for propulsion noise according to CNOSSOS is shown in Equation 23.

$$\Delta L_{WP,i,m}(v_m) = \Delta L_{WP,road,i,m}(v_m) + \Delta L_{WP,acc.i,m} + \Delta L_{WP,grad,i,m}(v_m) \qquad 23$$

Where

$\Delta L_{WP,i,m}(v_m)$	sum of correction factors for propulsion noise for ith frequency band, vehicle category m [dB],
$\Delta L_{WP,road,i,m}(v_m)$	correction factor for road surface [dB],
$\Delta L_{WP,acc,i,m}$	correction factor for speed change [dB], and
$\Delta L_{WP,grad,i,m}(v_m)$	correction factor for road gradient [dB].

C.6 CNOSSOS – Sound power of a single vehicle

The calculation of the sound power of a single vehicle according to CNOSSOS is shown in Equation 24.

$$L_{W,i,m} = 10 \cdot lg(10^{L_{WR,i,m} \cdot 0.1} + 10^{L_{WP,i,m} \cdot 0.1}) \quad 24$$

Where

$L_{W,i,m}$ sound power of a single vehicle (energetic sum of rolling noise and propulsion noise) for i[th] frequency band, vehicle category m [dB],

$L_{WR,i,m}$ rolling noise for i[th] frequency band, vehicle category m [dB], and

$L_{WP,i,m}$ propulsion noise for i[th] frequency band, vehicle category m [dB].

C.7 CNOSSOS – Sound power of the traffic flow of a single vehicle category

The calculation of the sound power of the traffic flow of a single vehicle category according to CNOSSOS is shown in Equation 25.

$$L_{W',eq,line,i,m} = L_{W,i,m} + 10 \cdot lg\left(\frac{Q_m}{1000 \cdot v_m}\right) \quad 25$$

Where

$L_{W',eq,line,i,m}$ sound power of the traffic flow for i[th] frequency band, vehicle category m [dB/m],

$L_{W,i,m}$ sound power of a single vehicle for i[th] frequency band, vehicle category m [dB],

Q_m traffic flow of vehicle category m [1/h], and

v_m speed of vehicle category m [km/h].

C.8 CNOSSOS – Sound power of the traffic flow

The calculation of the sound power of the traffic flow according to CNOSSOS is shown in Equation 26.

$$L_{\Sigma} = 10 \cdot lg\left[\Sigma\left(10^{L_{W',eq,line,i,m} \cdot 0.1}\right)\right] \qquad 26$$

Where

$L_{W',eq,line,i,m}$ sound power of the traffic flow for i[th] frequency band, vehicle category m [dB/m],

$L_{W,i,m}$ sound power of a single vehicle for i[th] frequency band, vehicle category m [dB],

Q_m traffic flow of vehicle category m [1/h], and

v_m speed of vehicle category m [km/h].

C.9 Area weighted average sound absorption coefficients

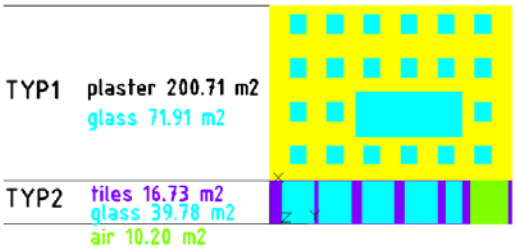

Figure 82 Material map of 2_125992 facade

Table 56 Area of materials – type 1

Material	area [m²]	[%]
plaster	200.71	74
glass	71.91	26
SUM	272.62	100

Table 57 Area of materials – type 2

Material	area [m²]	[%]
tiles	16.73	25
glass	39.78	60
air	10.2	15
SUM	66.71	

The area weighted sound absorption coefficients are calculated according to Equation 27.

$$a = \frac{1}{100}\sum m_i p_i \qquad 27$$

Where

a area weighted sound absorption coefficient at the given octave band frequency,

m_i sound absorption coefficient of a material at the given octave band frequency, and

p_i percentage of the given material surface.

Table 58 Area weighted sound absorption coefficients of facade 2_125992

Material	63	125	250	500	1k	2k	4k	8k	Source of data
plaster	0.02	0.02	0.02	0.02	0.02	0.02	0.02	0.02	Odeon 4002
glass	0.10	0.10	0.07	0.05	0.03	0.02	0.02	0.02	Odeon 10003
tiles	0.02	0.02	0.03	0.03	0.04	0.05	0.07	0.07	Odeon 1001
air	1.00	1.00	1.00	1.00	1.00	1.00	1.00	1.00	-
TYP1	0.04	0.04	0.03	0.03	0.02	0.02	0.02	0.02	
TYP2	0.06	0.06	0.04	0.03	0.03	0.02	0.02	0.02	
SUM	0.04	0.04	0.03	0.03	0.02	0.02	0.02	0.02	